

# Design and construction of a portable whole-cell living bacterial biosensor for the detection of arsenic in water

THÈSE N° 5690 (2013)

PRÉSENTÉE LE 19 AVRIL 2013

À LA FACULTÉ DES SCIENCES ET TECHNIQUES DE L'INGÉNIEUR  
LABORATOIRE DE MICROSYSTÈMES 4  
PROGRAMME DOCTORAL EN MICROSYSTÈMES ET MICROÉLECTRONIQUE

ÉCOLE POLYTECHNIQUE FÉDÉRALE DE LAUSANNE

POUR L'OBTENTION DU GRADE DE DOCTEUR ÈS SCIENCES

PAR

**Nina BUFFI**

acceptée sur proposition du jury:

Prof. M. Gijs, président du jury  
Prof. Ph. Renaud, directeur de thèse  
Prof. J. McKinney, rapporteur  
Dr C. Valsangiacomo, rapporteur  
Prof. J. R. van der Meer, rapporteur



ÉCOLE POLYTECHNIQUE  
FÉDÉRALE DE LAUSANNE

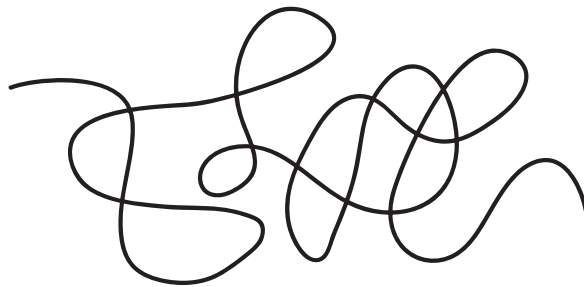
Suisse  
2013



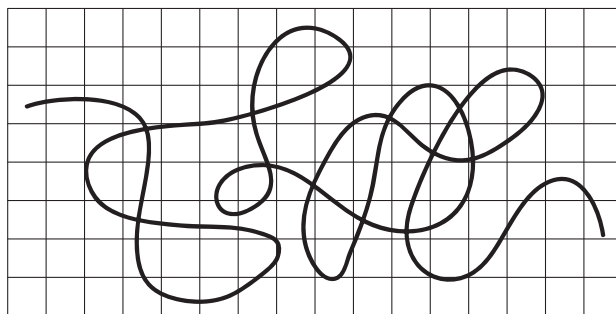


*A mia mamma.*

On the blackboard of a high school in Paris, during a discussion about the philosopher Sartre, a teacher made this drawing [Maksik, 2011]:



What is.



What we insist it is.



# Abstract

Contamination of drinking water with arsenic is a recurring problem in both industrialized and developing countries. Supplies for large populations can have concentrations much higher than the permissible levels, set by the World Health Organization (WHO) to 10  $\mu\text{g As/L}$  for most European countries and the United States and to 50  $\mu\text{g As/L}$  elsewhere. As arsenic analysis requires high-end instruments, which are largely unavailable in developing countries, bioassays based on genetically engineered bacteria have been proposed as suitable alternatives. Yet, such tests would profit from better standardization and direct incorporation into sensing devices.

The final objective of this work was to develop a microfluidic device in which bacterial bioreporters could be embedded, actively maintained for at least one week, exposed to arsenic and which allowed direct detection of the reporter signal produced, as a further step towards a complete miniaturized bacterial biosensor. The signal element in the biosensor is a nonpathogenic laboratory strain of *Escherichia coli*, which produces a variant of the green fluorescent protein after contact to arsenite and arsenate. To reach the stated objective, we proposed two different solutions. The first one consists in the encapsulation of *E. coli* bioreporter cells in agarose beads and in their incorporation into a microfluidic device, where they are captured in 500 x 500  $\mu\text{m}^2$  cage and exposed to aqueous samples containing arsenic. Cells in beads frozen at  $-20^\circ\text{C}$  in the microfluidic chip retained inducibility for up to a month and arsenic samples with 10 or 50  $\mu\text{g As/L}$  could be reproducibly discriminated from the blank in less than 200 minutes. In the second approach, we directly captured free cells against a filter wall and for their active maintenance we integrated a microchemostat on chip. Because of a lack of robustness of the microfluidic device, we could not maintain cells on chip for more than one week, but we showed that it is possible to have a biosensor in which the sensitive element is continuously renewed and, when needed, exposed to the target chemical.

## Abstract

---

In the last part of this thesis, we studied the relation between arsenite transport and reporter signal production. We observed the formation of extensive gradients of reporter signal intensity as a function of distance to the inflowing sample, arsenite concentration and flow rate, and we attempted to explain their nature by a modeling approach.

We think that the devices proposed in this work constitute a crucial step forward in the direction of an inexpensive and robust in-field arsenic detection system.

**Keywords:** *bacterial biosensors, microfluidics, arsenic, Escherichia coli, ArsR, green fluorescent protein, GFP, chemostat on chip, microfabrication.*

## Version abrégée

La contamination de l'eau potable par l'arsenic est un problème aussi récurrent dans les pays industrialisés que dans les pays en voie de développement. En effet, les réserves d'eau peuvent contenir des concentrations beaucoup plus grandes que les limites permises, qui ont été fixées par l'Organisation mondiale de la Santé (OMS) à 10 µg As/L en Europe et à 50 µg As/L ailleurs. Puisque l'analyse de l'arsenic requiert des instruments de haute gamme, qui ne sont pas disponibles dans les pays en voie de développement, des solutions alternatives ont été proposées. Une des plus prometteuses utilise des tests biologiques basés sur l'utilisation de bactéries génétiquement modifiées, lesquels bénéficieraient d'une meilleure standardisation et de l'incorporation dans des dispositifs microfluidiques.

Dans l'optique de marquer une nouvelle étape vers la conception d'un biocapteur bactérien complètement miniaturisé, l'objectif principal de ce travail était de développer un système microfluidique dans lequel les bactéries sensibles à l'arsenic pourraient être incorporées, maintenues en vie pendant au moins une semaine, exposées à l'arsenic et qui permettrait la détection directe du signal rapporteur produit. L'élément sensible est une souche de laboratoire non-pathogène de *Escherichia coli* qui, au contact avec l'arsenite et l'arsenate, produit une variante de la protéine GFP. Pour atteindre le but que nous nous étions fixés, nous avons développé deux solutions différentes. La première consiste en l'encapsulation des cellules sensibles dans des billes d'agarose et dans l'incorporation de ces dernières dans un système microfluidique où elles sont capturées dans une cage de 500 x 500 µm<sup>2</sup> et exposées à l'échantillon aqueux à analyser. En les congelant à -20°C dans le chip, nous avons réussi à maintenir l'inductibilité des cellules pendant un mois et nous avons pu discriminer des échantillons avec 10 ou 50 µg/L d'arsenic en moins de 200 minutes de manière reproductible. Dans la seconde approche, nous avons directement accumulé les cellules contre un filtre et pour les maintenir en vie dans le système, nous avons intégré un chemostat. À cause d'un manque de

robustesse du dispositif, nous n'avons pas pu maintenir les cellules sur la puce pendant plus d'une semaine ; néanmoins nous avons démontré qu'il est possible d'avoir un biocapteur dans lequel l'élément sensible est continuellement renouvelé et, au moment voulu, exposé à la substance chimique cible.

Dans la dernière partie de ce travail, nous avons étudié la relation entre le transport d'arsenic et la production du signal rapporteur. Nous avons observé que le signal rapporteur produit par les cellules accumulées contre le filtre présente des gradients en fonction de la distance du point où l'échantillon entre en contact avec les cellules, la concentration d'arsenic et le débit, et nous avons réussi à expliquer leur nature grâce à une approche de modélisation.

Nous sommes convaincus que les systèmes proposés dans le cadre de ce travail représentent une étape essentielle dans le développement d'un système de détection de l'arsenic bon marché, robuste et utilisable sur le terrain.

**Mots-clés :** *biocapteur bactérien, microfluidique, arsenic, Escherichia coli, ArsR, protéine GFP, chemostat sur chip, microfabrication.*

## Riassunto

La contaminazione dell'acqua potabile da parte dell'arsenico è un problema ricorrente sia nei paesi industrializzati sia in quelli in via di sviluppo. Le riserve idriche possono infatti contenere delle concentrazioni di arsenico sensibilmente superiori alla soglia di tolleranza, fissata dall'Organizzazione mondiale della Sanità a 10 µg As/L in Europa e negli Stati Uniti e a 50 µg As/L nel resto del mondo. Siccome l'analisi dell'arsenico richiede strumenti di alta gamma, i quali non sono disponibili nei paesi in via di sviluppo, sono state proposte diverse soluzioni alternative. Una delle più promettenti è quella delle analisi biologiche basate sull'utilizzo di batteri geneticamente modificati, le quali trarrebbero beneficio da una maggiore standardizzazione e dall'incorporazione in dispositivi microfluidici.

Nell'ottica di compiere un primo importante passo verso la concezione di un biosensore batterico completamente miniaturizzato, l'obiettivo principale di questo lavoro era quello di sviluppare un sistema microfluidico nel quale i batteri sensibili all'arsenico avrebbero potuto essere incorporati, mantenuti in vita per almeno una settimana, esposti all'arsenico e che avrebbe permesso il rilevamento diretto del segnale reporter prodotto. Come elemento sensibile abbiamo utilizzato un ceppo di laboratorio non patogeno di *Escherichia coli* che, a contatto con l'arsenito e l'arsenato, produce una variante della proteina GFP. Per raggiungere l'obiettivo fissato, abbiamo sviluppato due diverse soluzioni. La prima consiste nell'incapsulamento delle cellule sensibili in biglie di agarosio e nell'incorporazione di queste ultime in un sistema microfluidico, dove vengono catturate in una gabbia di 500 x 500 µm<sup>2</sup> ed esposte al campione acquoso da analizzare. Congelando le biglie a -20°C nel chip siamo riusciti a mantenere l'inducibilità durante un mese e siamo stati in grado di discriminare concentrazioni di 10 e 50 µg/L di arsenico in meno di 200 minuti e in maniera riproducibile.

Il secondo approccio consiste nell'accumulare direttamente le singole cellule contro un filtro. Per poterle mantenere in vita abbiamo integrato un chemostato nel chip. Il sistema non

## Riassunto

---

si è rivelato sufficientemente robusto per permetterci di andare oltre una settimana di funzionamento, tuttavia abbiamo mostrato che è possibile realizzare un biosensore nel quale l'elemento sensibile si rinnova continuamente e, quando è necessario, viene esposto alla sostanza chimica da analizzare.

Nell'ultima parte di questo lavoro abbiamo analizzato la relazione tra il trasporto dell'arsenico e la produzione del segnale reporter. Abbiamo osservato che il segnale reporter prodotto dalle cellule accumulate contro il filtro presenta dei gradienti in funzione della distanza dal punto in cui il campione entra in contatto con le cellule, la concentrazione di arsenico e la sua portata, e siamo riusciti a spiegare la loro natura grazie a un approccio di modellazione.

Siamo convinti che i sistemi proposti in questo lavoro rappresentino una tappa fondamentale per lo sviluppo di un sistema di rilevamento dell'arsenico poco costoso, robusto e utilizzabile sul campo.

**Parole chiave:** *biosensore batterico, microfluidica, arsenico, Escherichia coli, ArsR, proteina GFP, chemostato su chip, microfabbricazione.*



# Acknowledgements

I would like to express my gratitude to a lot of people who took part in one way or the other in this thesis.

First of all, I would like to thank Prof. Philippe Renaud for accepting me in his lab, providing financial support and scientific advice, and Prof. Jan Roelof van der Meer from University of Lausanne for his guidance in a field that was new to me.

Thank you also to the members of the jury, Prof. John McKinney and Dr. Claudio Valsangiacomo, for acting as my jury, and Prof. Martin Gijs for presiding this jury.

I had the opportunity to work with people from different backgrounds and this was a very enriching experience. In particular, I would like to thank Siham, Davide and Frederic.

For proofreading my thesis and giving me insightful comments, a big thank you to Arnaud Bertsch.

A thank you for their help to all my past and present colleagues (in random order): Sophie, Sylvie, Ludovica, David, Willyan, Pierre, Pietro, Robert, Yufei, Mojtaba, Fabien, Thomas, Nicolas, Marc, Sébastien, Harsha, Anja, Alessandro, André, Lynda, Raphaël, Ana, Rodrigo, Guillaume, Niccolò, Harald, Bilge, Jules, Elodie, Camille, Shun-Ho, Carmen, Fanny, Julien, Olivier, Amine, Steve, Sylvain, Vladimir, Friedrich, Sandra, Ryo, Silvia, Erika, Edith, Artur, Mario, the people of the CMI staff and the other I may have forgotten.

Per aver provato a diradare la nebbia delle domeniche mattine, un grazie ora consapevole a Mattia.

Per l'amicizia che ha saputo regalarmi e le pause caffè, un grazie colorato ad Enrico.

Per avermi preso per mano e avermi mostrato luoghi che sul mappamondo della vita non

## Acknowledgements

---

sapevo nemmeno collocare, un grazie dal profondo del cuore a Luca,

Infine, non un grazie, visto che mai potrebbe esprimere la riconoscenza che ho per lei, bensì un pensiero, per mia mamma, che da sempre sa ascoltarmi, infondermi sicurezza e rendere il mio quotidiano più spensierato:

“ Perché nessuno possa dimenticare di quanto sarebbe bello se, per ogni mare che ci aspetta, ci fosse un fiume, per noi. E qualcuno - un padre, un amore, qualcuno - capace di prenderci per mano e di trovare quel fiume - immaginarlo, inventarlo - e sulla sua corrente posarci, con la leggerezza di una sola parola, addio. Questo, davvero, sarebbe meraviglioso. Sarebbe *dolce*, la vita, qualunque vita. E le cose non farebbero male, ma si avvicinerebbero portate dalla corrente, si potrebbe prima sfiorarle e poi toccarle e solo alla fine farsi toccare. Farsi *ferire*, anche. *Morirne*. Non importa. Ma tutto sarebbe, finalmente, *umano*. Basterebbe la fantasia di qualcuno - un padre, un amore, qualcuno. Lui saprebbe inventarla una strada, qui, in mezzo a questo silenzio, in questa terra che non vuole parlare. Strada clemente, e bella. Una strada da qui al mare. ”

*Alessandro Baricco*

Tu, quella strada da lì al mare, hai saputo inventarla e per questo ti ammiro e ti sono grata.

# Contents

<b>Abstract</b>	<b>v</b>
<b>Version abrégée</b>	<b>vii</b>
<b>Riassunto</b>	<b>ix</b>
<b>Acknowledgements</b>	<b>xi</b>
<b>Nomenclature</b>	<b>xix</b>
<b>1 Introduction</b>	<b>1</b>
1.1 Scope of this thesis . . . . .	4
1.2 Literature review . . . . .	5
1.2.1 Arsenic detection methods . . . . .	5
1.2.1.1 Laboratory assays . . . . .	5
1.2.1.2 Analyses in the field . . . . .	6
1.2.1.3 Other assays for arsenic in the environment . . . . .	9
1.2.1.4 New analytical technologies with possible applications for ar- senic analysis . . . . .	10
1.2.1.5 Discussion . . . . .	11
1.2.2 Whole-cell living biosensors and their integration in microfluidic platforms	13
1.2.3 Flow control in microfluidic chips . . . . .	16
1.2.3.1 Pressure-driven flow . . . . .	16
1.2.3.2 Electroosmotic flow . . . . .	17
1.2.3.3 Other methods to drive the flow . . . . .	18
1.2.3.4 Valves incorporation in microchannels . . . . .	18
1.2.4 Cell trapping in microfluidic chips . . . . .	20
1.2.4.1 Chemical trapping . . . . .	21
	<b>xiii</b>

## Contents

---

1.2.4.2	Hydrodynamic trapping . . . . .	21
1.2.4.3	Dielectrophoretic (DEP) trapping . . . . .	22
1.2.4.4	Optical trapping . . . . .	23
1.2.4.5	Acoustic trapping . . . . .	23
1.2.4.6	Magnetic trapping . . . . .	24
1.2.4.7	Gel trapping . . . . .	24
1.2.5	Chemostat on chip . . . . .	25
1.3	Research objectives . . . . .	30
1.4	Thesis structure . . . . .	31
<b>2</b>	<b>Agarose beads system</b>	<b>33</b>
2.1	Introduction . . . . .	33
2.2	Materials and methods . . . . .	33
2.2.1	Reporter cells working principle . . . . .	33
2.2.2	Reporter cells preparation . . . . .	35
2.2.3	Encapsulation of reporter cells in agarose beads . . . . .	35
2.2.4	Microfluidic cartridge design and microfabrication . . . . .	36
2.2.4.1	Design . . . . .	36
2.2.4.2	Microfabrication . . . . .	38
2.2.5	Beads storage . . . . .	40
2.2.6	Arsenic induction assay . . . . .	40
2.2.7	Quantification of EGFP fluorescence . . . . .	41
2.2.8	Viability of cells in agarose beads . . . . .	41
2.2.9	Flow cytometry measurements . . . . .	41
2.2.10	Kinetics . . . . .	42
2.3	Results . . . . .	42
2.3.1	Microfluidic cartridge . . . . .	42
2.3.2	Sensitivity of the bioreporter assay to arsenite . . . . .	42
2.3.3	Effect of storage conditions . . . . .	48
2.3.3.1	Storage outside the microfluidic cartridge . . . . .	48
2.3.3.2	Storage in the microfluidic cartridge . . . . .	51
2.3.4	Response kinetics . . . . .	54
2.3.5	Pre-incubation . . . . .	54
2.4	Discussion . . . . .	57

2.5	Conclusions and outlook . . . . .	59
2.5.1	Summary of results . . . . .	59
2.5.2	Perspectives . . . . .	60
<b>3</b>	<b>Free cells system</b>	<b>61</b>
3.1	Introduction . . . . .	61
3.2	Materials and methods . . . . .	61
3.2.1	Microfluidic cartridge design and microfabrication . . . . .	61
3.2.2	Reporter cells preparation . . . . .	65
3.2.3	Arsenic induction assay . . . . .	65
3.2.4	Quantification of EGFP fluorescence . . . . .	65
3.2.5	Kinetics . . . . .	66
3.3	Results . . . . .	66
3.3.1	Microfluidic cartridge . . . . .	66
3.3.2	Sensitivity of bioreporter assay to arsenite . . . . .	68
3.3.3	Response kinetics . . . . .	70
3.4	Discussion . . . . .	71
3.5	Conclusions and outlook . . . . .	72
3.5.1	Summary of results . . . . .	72
3.5.2	Perspectives . . . . .	72
<b>4</b>	<b>Chemostat on chip</b>	<b>75</b>
4.1	Introduction . . . . .	75
4.2	Differences between a traditional chemostat and our chemostat on chip . . . . .	76
4.3	Chemostat theoretical basis . . . . .	76
4.4	Materials and methods . . . . .	81
4.4.1	Microfluidic cartridge design and microfabrication . . . . .	81
4.4.2	PDMS valves control . . . . .	85
4.4.3	Microfluidic cartridge principle of operation . . . . .	86
4.4.4	Bioreporter strain . . . . .	88
4.4.5	Reporter cells, nutrients and arsenite solutions preparation . . . . .	88
4.4.6	Measuring the physiological state of reporter cells in the chemostat chamber and quantification of EGFP fluorescence in the measurement zone . . . . .	89
4.5	Results . . . . .	89

## Contents

---

4.5.1	Microchemostat operation . . . . .	89
4.5.2	Chemostat parameters for continuous reporter cell growth . . . . .	90
4.5.3	Nutrient medium optimization . . . . .	96
4.5.4	Cellular physiology in the microchemostat . . . . .	100
4.6	Discussion . . . . .	102
4.7	Conclusions and outlook . . . . .	103
4.7.1	Summary of results . . . . .	103
4.7.2	Perspectives . . . . .	103
<b>5</b>	<b>Arsenite transport effect on the bioreporter signal production</b>	<b>105</b>
5.1	Introduction . . . . .	105
5.2	Materials and methods . . . . .	105
5.2.1	Microfluidic chip design and micofabrication . . . . .	105
5.2.2	Bioreporter strain . . . . .	107
5.2.3	Reporter cells preparation . . . . .	107
5.2.4	Microchip bioreporter induction . . . . .	107
5.2.5	Quantification of EGFP fluorescence . . . . .	108
5.2.6	Modeling . . . . .	108
5.3	Results . . . . .	112
5.3.1	Microfluidic chip . . . . .	112
5.3.2	Bioreporter signal development as function of arsenite flux . . . . .	112
5.3.3	Model . . . . .	117
5.4	Discussion . . . . .	122
5.5	Conclusions and outlook . . . . .	122
5.5.1	Summary of results . . . . .	122
5.5.2	Perspectives . . . . .	123
<b>6</b>	<b>Conclusion and outlook</b>	<b>125</b>
6.1	Summary of results . . . . .	125
6.1.1	Miniaturized microfluidic system . . . . .	125
6.1.2	On chip actively maintenance of bioreporter cells . . . . .	126
6.1.3	Arsenite transport effects and conditions for an optimal signal-to-noise ratio . . . . .	126
6.2	Perspectives . . . . .	127

6.2.1	Technical improvements . . . . .	127
6.2.2	From the laboratory to the in-field situation . . . . .	127
6.2.3	Other applications . . . . .	128
	<b>Bibliography</b>	<b>129</b>
	<b>A Matlab code of the arsenite transport effect model</b>	<b>143</b>
	<b>B Curriculum Vitae</b>	<b>151</b>





# Nomenclature

## Acronyms

AC	Alternating current
AFS	Atomic fluorescence spectroscopy
ASV	Anodic stripping voltammetry
CMOS	Complementary-metal-oxide-semiconductor
DEP	Dielectrophoresis
DNA	Deoxyribonucleic acid
DO	Dissolved oxygen
EDTA	Ethylenediaminetetraacetic acid
EGFP	Enhanced green fluorescent protein
EOF	Electroosmotic flow
GCE	Glassy carbon electrode
GFP	Green fluorescent protein
HES-SO	University of Applied Sciences and Arts of Western Switzerland
HGAAS	Hydride generation atomic absorption spectroscopy
ICP-AES	Inductively coupled plasma-atomic emission spectrometry
ICP-MS	Inductively coupled plasma-mass spectrometry

## Nomenclature

---

LB	Luria-Bertani (medium)
LED	Light-emitting diode
LIBS	Laser induced breakdown spectroscopy
MDL	Method detection limit
MOPS	3-(N-morpholino)propanesulfonic acid
n-DEP	Negative dielectrophoresis
NFI	Normalized fluorescence intensity
OD	Optical density
OMS	Organisation mondiale de la Santé
OMS	Organizzazione mondiale della Sanità
PAA	Polyacrylic acid
p-DEP	Positive dielectrophoresis
PDF	Pressure-driven flow
PEG	Polyethylenglycol
PMMA	Polymethylmethacrylate
PTFE	Polytetrafluoroethylene
rpm	Round per minute
RSD	Relative standard deviation
SAMS	Sensor assay microbe system
SERS	Surface-enhanced Raman spectroscopy
UNIL	University of Lausanne
WHO	World Health Organization
XRF	X-ray fluorescence

**Variables**

$\alpha_{beads}$	Slope of the function describing the natural logarithm of the normalized fluorescence intensity of bioreporter cells encapsulated in agarose beads in function of time	[Arbitrary units/min]
$\alpha_{cells}$	Slope of the function describing the natural logarithm of the fluorescence intensity of bioreporter cells in function of time	[Arbitrary units/min]
$[ArsB]$	Concentration of efflux pumps	$[\frac{\text{molecules}}{\text{cell}}]$
$[ArsB]_{\max}$	Maximum concentration of efflux pumps	$[\frac{\text{molecules}}{\text{cell}}]$
$[ArsR_d]$	Concentration of ArsR-dimers	$[\frac{\text{molecules}}{\text{cell}}]$
$[AsArsR_d]$	Concentration of ArsR-dimers that have bound <i>As</i> molecules	$[\frac{\text{molecules}}{\text{cell}}]$
$As_{efflux, slice n}$	Arsenite efflux from a slice of cells	$[\frac{\text{molecules}}{s}]$
$[As_{in}]$	Arsenite concentration in the cell	$[\frac{\text{molecules}}{\text{cell}}]$
$As_{influx, slice n}$	Arsenite influx in a slice of cells	$[\frac{\text{molecules}}{s}]$
$[As_{out}]$	Arsenite concentration outside the cell	$[\frac{\text{molecules}}{\text{slice}}]$
$As_{uptake, slice n}$	Arsenite uptake by a slice of cells	$[\frac{\text{molecules}}{s}]$
$B$	Biomass of bacteria in the microchamber	[g]
$[B]$	Biomass of bacteria $B$ divided by the chamber volume $C_V$	$[\frac{g}{\mu L}]$
$[B]_0$	Initial biomass of bacteria $B$ divided by the chamber volume $C_V$	$[\frac{g}{\mu L}]$
$c_{beads}$	Constant of the function describing the natural logarithm of the normalized fluorescence intensity of the bioreporter cells encapsulated in agarose beads in function of time	[Arbitrary units]
$c_{cells}$	Constant of the function describing the natural logarithm of the fluorescence intensity of bioreporter cells in function of time	[Arbitrary units]
$C_V$	Micro chemostat chamber volume	$[\mu L]$
$D$	Dilution rate	$[h^{-1}]$

## Nomenclature

---

$[DNA]$	Concentration <i>DNA</i> molecules	$[\frac{\text{molecules}}{\text{cell}}]$
$[DNAArsR_d]$	Concentration of ArsR-dimers bound to the operator- <i>DNA</i>	$[\frac{\text{molecules}}{\text{cell}}]$
$D_{optimum}$	Optimum dilution rate under which the biomass productivity is optimized	$[\text{h}^{-1}]$
$f$	Frequency	$[\text{s}]$
$F_{cells}$	Fluorescence intensity of bioreporter cells	[Arbitrary units]
$FN_{beads}$	Normalized fluorescence intensity of bioreporter cells encapsulated in agarose beads	[Arbitrary units]
$K_{d,1,2}$	Equilibrium constants	$[\frac{\text{molecules}}{\text{cell}}]$
$K_m$	Substrate concentration at which the reaction rate is half of $V_{max}$	$[\frac{\text{g}}{\mu\text{L}}]$
$K_{m,g}$	Substrate concentration at which the growth rate is half of $\mu_{max}$	$[\frac{\text{g}}{\mu\text{L}}]$
$K_{m,in}$	Arsenite concentration outside the cell at which the reaction rate is half of $V_{As,in,max}$	$[\frac{\text{molecules}}{\text{slice}}]$
$K_{m,out}$	Arsenite concentration in the cell at which the reaction rate is half of $V_{As,out,max}$	$[\frac{\text{molecules}}{\text{cell}}]$
$\mu$	Cell growth rate	$[\text{h}^{-1}]$
$\mu_{max}$	Maximum cell growth rate	$[\text{h}^{-1}]$
$P$	Pressure	[bar]
$Q$	Flow rate	$[\frac{\mu\text{L}}{\text{h}}]$
$[S]$	Concentration of growth limiting substrate	$[\frac{\text{g}}{\mu\text{L}}]$
$[S]_0$	Initial concentration of growth limiting substrate	$[\frac{\text{g}}{\mu\text{L}}]$
$t$	Time	$[\text{s}]$
$V$	Reaction rate	$[\frac{\text{molecules}}{\text{s}}]$
$V_{As,in}$	Arsenite influx rate in the cell	$[\frac{\text{molecules}}{\text{s}\cdot\text{cell}}]$

## Nomenclature

---

$V_{As,in,max}$	Maximum arsenite influx rate in the cell	$[\frac{\text{molecules}}{\text{s-cell}}]$
$V_{As,out}$	Arsenite efflux rate from the cell after taking into account the efflux pumps ratio	$[\frac{\text{molecules}}{\text{s-cell}}]$
$V_{As,out,max}$	Maximum efflux rate from the cell	$[\frac{\text{molecules}}{\text{s-cell}}]$
$V_{As,out,MM}$	Arsenite efflux rate from the cell before taking into account the efflux pumps ratio	$[\frac{\text{molecules}}{\text{s-cell}}]$
$V_{max}$	Maximum reaction rate	$[\frac{\text{molecules}}{\text{s}}]$
$Y$	Change in mass of bacteria per unit time divided by the change in mass of nutrients per unit time	-
$y$	Yield parameter proportional to $Y$	-



# 1 Introduction

Arsenic, also known as the King of Poisons, has been known to humankind for thousands of years: it was used to harden bronze in the Middle East around 3000 BC, prized as a dye by Egyptians, Greeks and Romans, utilized as an ulcer treatment by Hippocrates, and as a poison since Roman times to the mid-nineteenth century because of its lack of color, odor and taste (especially to murder political rivals) [Drever, 2002; Gilbert, 2012]. The use of arsenic as a poison began decreasing in the 18th century, when English chemist James Marsh developed a chemical test that identifies arsenic in the body [Gilbert, 2012]. However, we will not describe the use (and abuse) of arsenic any further, as here we are interested in the detection of arsenic in natural water and especially in groundwater used as drinking water. This arsenic is almost never found at acutely poisonous concentrations<sup>1</sup>, but in the past 20 or 30 years has surely accounted for many more deaths than all the arsenical poisoning in history [Drever, 2002].

The range of arsenic concentrations found in natural waters is large, going from less than 0.5 µg/L to more than 5000 µg/L [Smedley and Kinniburgh, 2002]. Typical concentrations in freshwater are less than 10 µg/L and frequently less than 1 µg/L [Smedley and Kinniburgh, 2002]. However, especially in groundwater, much higher concentrations are found. This is a recurring problem in both developing and industrialized countries (Figure 1.1) and drinking water supplies for large populations can contain arsenic concentrations which are much higher than the permissible levels, which since 2001 have been set by the World Health Organization (WHO) to 10 µg/L in most European countries and in the United States and to 50 µg/L

---

<sup>1</sup>Acute poisoning occurs when few grams of arsenic are ingested over a short space of time and leads in life-threatening illness. Chronic poisoning results from month or years of exposure to low levels of arsenic and causes no immediate suffering.

## Chapter 1. Introduction

elsewhere [Amini *et al.*, 2008; Smedley and Kinniburgh, 2002; Diesel *et al.*, 2009; Nordstrom, 2002]. The worse case of arsenic contamination probably takes place in Bangladesh, where about 50 million people (40% of the total population) are at risk of arsenic poisoning-related diseases because of affected wells [Ravenscroft *et al.*, 2009; Hossain, 2006; Alam *et al.*, 2002; Nickson *et al.*, 1998]. Estimates of the rural population exposed to unsafe arsenic levels by drinking untreated groundwater in India, China, Myanmar, Pakistan, Vietnam, Nepal, and Cambodia have grown to over 100 million [Ravenscroft *et al.*, 2009].

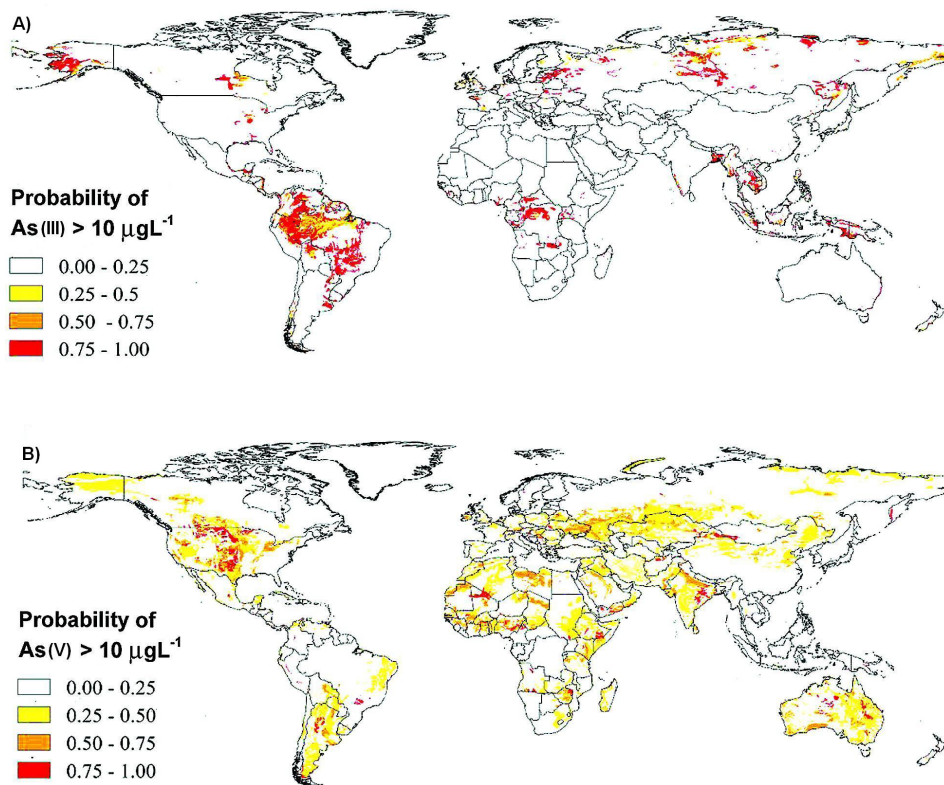


Figure 1.1: Modelled global probability of geogenic arsenic contamination in groundwater for (A) arsenite and (B) arsenate. Figure adapted from [Amini *et al.*, 2008].

The effects of arsenic exposure are cumulative: chronic exposure to low levels of arsenic in water is known to lead to serious disorders, such as vascular diseases (blackfoot disease and hypertension) and irritations of the skin and mucous membranes as well as dermatitis, keratosis, and melanosis. Furthermore, inorganic arsenic is a human carcinogen and its ingestion increases the risk of developing cancer of the skin, lungs, urinary bladder, and kidney [Abernathy *et al.*, 1999]. However, it has to be noted that there are other drinking water



---

pollutants, chemical or bacteriological, which are more relevant in terms of public health. In particular, diarrheal diseases contracted through bacteriological (fecal) contamination of drinking water is one of the leading causes of death among children globally [Gadgil, 1998; WHO, 2009; Valsangiacomo, 2010].

Sources of arsenic contamination in groundwater can be of natural or anthropogenic origin. Arsenic is a common element of minerals in the earth's crust and weathering of such minerals can be accelerated by microbial activity, specifically in anoxygenic groundwaters with abundant available respirable organic matter, which leads to high concentrations of dissolved inorganic arsenic species [Fendorf *et al.*, 2012; Jain and Ali, 2000]. However, contamination can also be the result of industrial activities [Han *et al.*, 2003], which include the application of organoarsenical pesticides, the combustion of fossil fuels, the use of organoarsenical feed additives, mining activities, the disposal of industrial wastes, and the application of arsenical desiccants and preservatives.

Arsenic occurs in nature in varied compounds and in different oxidation numbers. Organic arsenic, which is an association of arsenic, carbon and hydrogen, is most of the time less hazardous than inorganic arsenic, which is an association of arsenic, oxygen, chlorine and sulfur [Smith *et al.*, 1992]. Most frequently, the dominant forms occurring in natural waters, and thus in drinking waters, are trivalent arsenite [As(III) in  $\text{AsO}_2^-$ ] or pentavalent arsenate [As(V) in  $\text{AsO}_4^{3-}$ ] [Hung *et al.*, 2004].

Current laboratory techniques, such as atomic absorption and atomic fluorescence spectrometry, inductively coupled plasma techniques, and high-pressure liquid chromatography, can accurately measure arsenic in an environmental sample to parts per billion (ppb) concentrations but are expensive to operate and maintain, bulky, and they require fully equipped and staffed laboratories [Melamed, 2005]. Moreover, regions that have the most extensive arsenic contamination are also the areas with the least access to these particular techniques, making the need for in-field arsenic detection even more critical. For this reason, over the last decade sensors for the in-field detection of arsenic have been developed and tested, such as colorimetric tests, electrochemical sensors, and anodic stripping voltammetric probes [Laschi *et al.*, 2008]. However, large-scale field testing of the most common colorimetric tests showed that they are not sufficiently reliable in the concentration range below 50  $\mu\text{g/L}$ , giving rise to a large number of false-positive and false-negative results [Rahman *et al.*, 2002]. On the basis of this poor performance, a new generation of colorimetric tests has been developed and tested

in the field [Steinmaus *et al.*, 2006], showing that they can reliably detect arsenic concentrations close to 10 µg/L. However, their use remains controversial because of their bulkiness, their use of toxic chemicals (i.e. mercury bromide and zinc), and the release of arsine gas during the test [Melamed, 2005].

For these reasons, various alternative protocols and methods have been proposed. One of the alternatives to the abiotic sensors for arsenic detection are the bacteria-based bioassays [van der Meer *et al.*, 2004], which exploit the extremely sensitive defense system against arsenite and arsenate present in most bacteria and couple this defense reaction to the production of an easily measurable output signal [Diesel *et al.*, 2009; Stocker *et al.*, 2003; Scott *et al.*, 1997; Tauriainen *et al.*, 1997].

One of the most attractive characteristics of these bacteria-based reporters is their suitability to be incorporated into microfabricated platforms, leading to the miniaturization as a single device, a very promising route to reach the goal of cheap in-field analysis [Vadgama, 2004; Hierlemann *et al.*, 2003]. Furthermore, microfabrication techniques can also ameliorate the characteristic of the sensor with respect to conventionally fabricated devices [Vadgama, 2004], improving for example the mass transport and the mixing rates and thus reducing the analysis times [Kumar, 2010; Yalcin and Otlis, 2010]. This thesis contributes to this effort to explore the advantages of microfabrication and microfluidics as applied to bacterial reporters for arsenic detection in aqueous samples.

### 1.1 Scope of this thesis

This thesis involves the development of a microfluidic cartridge in which bacterial reporter cells producing a fluorescent signal in presence of arsenic can be actively maintained as long as possible and exposed to aqueous arsenic samples. The target application is a "proof of principle" whole-cell living biosensor for the in-field arsenic detection constituted of a microfluidic cartridge, which can be sled in a hand-held opto-electronic device allowing direct detection of the reporter signal produced by the cells. The engineering of the reporter cells and the construction of the opto-electronic device will not be presented, as these two parts were developed by two other research groups. However, the constraints given by these two components on the construction of the microfluidic cartridge will be treated in detail. In particular, the behavior of the cells in the chip in terms of response to arsenic and survival

will be extensively discussed. More precisely, the different approaches explored and the steps required for the construction of the microfluidic cartridge are described. The first solution investigated is the encapsulation of the bioreporter cells in agarose gel beads: a microfluidic trap concentrate the beads exposed to arsenic, making the produced signal easy to detect. The storage of the chip containing the beads in a freezer permits their active maintenance on chip for several weeks. The second one consists in a system based on the direct incorporation of bioreporter cells in the microfluidic chip. The challenges in the fabrication and operation of a suitable trap for single cells are reported. Subsequently, the development of a continuous growth microfluidics systems is illustrated: in this case cells can be directly cultured in the chip for several days and when a measurement is needed part of them can be exposed to the aqueous arsenic sample. This second approach leads to the need to perform multiple measurements on the same chip, requirement satisfied fabricating a flexible trap able to release the trapped cells. Furthermore, an important portion of this thesis was dedicated to the study of the effect of the arsenic flow rate and the number of reporter cells exposed on the fluorescent signal produced. A Matlab model of these measurements, which gives a better understanding on the mechanisms responsible for the reporter signal production, is also introduced.

## 1.2 Literature review

A review of existing methods to detect arsenic in the environment is presented in the first part of this section. Subsequently, a short description of whole-cell living biosensors and their incorporation into microfabricated platforms is given. Then, the different techniques to drive the flow, as well as to trap and concentrate the cells in microfluidic chips are illustrated. Finally, the existing solutions to maintain cells on chip are explored.

### 1.2.1 Arsenic detection methods

#### 1.2.1.1 Laboratory assays

The preferred laboratory techniques for the measurement of arsenic involve pre-treatment of the environmental sample with acidic extraction or acidic oxidation digestion [Melamed, 2005]. In this way all of the arsenic in the sample is transferred into an arsenic acid solution, which is then measured using one of several accepted analytical methods, such as atomic fluorescence

## Chapter 1. Introduction

---

spectroscopy (AFS), graphite furnace atomic absorption (GFAA), hydride generation atomic absorption spectroscopy (HGAAS), inductively coupled plasma-atomic emission spectrometry (ICP-AES), and inductively coupled plasma-mass spectrometry (ICP-MS) [Melamed, 2005]. Although these instruments can accurately measure arsenic in an environmental sample to parts per billion (ppb) concentrations, they are expensive to operate and maintain, bulky, and they require fully equipped and staffed laboratories [Melamed, 2005; Diesel *et al.*, 2009]. Because regions in which the arsenic contamination problem is more critical are also the areas with the least access to these advanced techniques, there is an urgent need for in-field arsenic detection.

### 1.2.1.2 Analyses in the field

In this section technologies at various stages of development will be discussed for arsenic detection in the field.

#### Colorimetric test kits

Current colorimetric field test kits are based on the Gutzeit method, developed over 100 years ago, which involves the reduction of arsenic compounds present in the water into arsenic trihydride (arsine gas). The arsenic trihydride diffuses out of the sample and stains a filter paper impregnated with mercuric bromide. The color intensity on the paper is then compared with known references. This test method is inexpensive and can be performed by minimally trained personnel [Melamed, 2005]. However, it presents some important drawbacks. First of all, it shows accuracy and reproducibility problems: rigorous comparisons of three field kits that were used during the arsenic Bangladesh crisis in 1997 have all shown significant variations when compared with accepted laboratory methods, and they appear to produce a high fraction (up to 50% in some cases) of false negative and false positive readings that could not readily be attributed to any external factor [Erickson, 2003]. Secondly, it generates highly toxic arsine gas well above the threshold limiting value of 0.05 parts per million by volume recommended by the Occupational Safety and Health Administration (OSHA) plus toxic mercury solid wastes [Hussam *et al.*, 1999]. Thirdly, detection is based on visual inspection, which increases the risk of errors, and finally, sulfur, selenium, and tellurium compounds have the potential of interfering with the assay [Melamed, 2005]. Although the poor performance of the test kits during the Bangladesh crisis created a strong incentive to improve the performance

of the colorimetric field kit technology (as they use absorption spectrometers for quantitative readings), their reliability still lags behind laboratory studies [Melamed, 2005]. Also, these assays do not detect any of the organic arsenates that may be found in groundwater, and the problem of the release of poisonous arsine gas that poses a hazard to the operator, as well as the fact that test strips constitute mercury solid wastes, are still not solved [Melamed, 2005].

### **Portable X-ray fluorescence**

X-ray fluorescence is an effective technology to directly measure arsenic in solid samples, such as soil and dried sludge [Melamed, 2005]. Environmental samples are irradiated with X-rays or gamma rays: the sample atoms may absorb the photon, dislodging an electron from their inner shell, and the resulting vacancy is filled by an electron that cascades in from outer electron shells (photoelectric effect). This rearrangement of electrons results in emission of X-rays characteristic of each atom, termed X-ray fluorescence (XRF). Measuring the energy of the XRF photon emitted by the sample it is possible to accurately identify the elements present in a sample. In fact, several studies [Pottes *et al.*, 2002; EPA, 1997] demonstrated the reliability of portable XRF devices in measuring arsenic in solid samples down to concentrations of 100 ppm. More interestingly, another study [Sbareto and Sanchez, 2001] showed that after pre-concentration on a suitable solid substrate it is possible to use XRF to analyze aqueous samples with a detection limit of 50 ppb, indicating that this technology has good potential for measuring groundwater arsenic sample directly in the field. However, sample preparations is required and interference from lead may be a problem [Melamed, 2005].

### **Anodic stripping voltammetry (ASV)**

Anodic stripping voltammetry (ASV) is an analytical technique which is suitable for measuring low-concentrations of free As(III) (from 0.1 to 300 µg/L) in drinking water [Melamed, 2005]. To detect As(V), this compound has to be first chemically reduced to arsenite [Rasul *et al.*, 2002]. Although not designed specifically for field use, commercially available versions of the laboratory equipment for this method may be readily transported and used in the field [Melamed, 2005]. Analysis by ASV involves three major steps. First, a thin film of gold is plated on a glassy carbon electrode (GCE), which is then conditioned. Once the sample is made acidic and rendered conductive by adding hydrochloric acid, the electrode is placed in it and a fraction of the dissolved arsenite is reduced onto the electrode surface. The arsenite which is removed from solution forms a layer on the gold electrode, that is subsequently oxidized. Mea-

## Chapter 1. Introduction

---

asuring the amount of electrical current required to remove (or strip) the arsenic oxidatively (an anodic process) gives a quantitative measure of the amount of material that was removed from the solution. The arsenite concentration in the sample is determined by comparing electrochemical response from the sample to external standards. This method was used to measure the arsenic content of the groundwater from a series of wells in Bangladesh and demonstrated a detection limit of 0.5 ppb, verified with established laboratory techniques [Rasul *et al.*, 2002]. However, it requires well-trained personnel to perform the measurement and to interpret the obtained data [Melamed, 2005]. Since microelectrodes have become affordable and readily available, gold microelectrode arrays have been used to create field-portable ASV with a detection limit of 0.05 ppb for arsenite [Feeney and Kounaves, 2000; Melamed, 2005]. This could be an important improvement, as the previously described ASV methods require the preparation of a new gold electrode for each new set of experiment, while gold microelectrode arrays can be readily mass-produced using photolithographic methods. Still, arsenate had to be reduced chemically before the measurement and copper, mercury and lead may interfere with the measurement.

### **Biological assays: using bacteria for arsenic detection**

Bacteria have evolved mechanisms for detoxifying arsenic compounds [Silver and Ji, 1994]. Typically, arsenic regulates the synthesis and the production of a wide variety of proteins that chemically modify, transport and extrude the arsenic from the cell [Roberto *et al.*, 2002]. The activation of the genes that encode the proteins for arsenic resistance depends on the reversible binding of a regulatory protein to a deoxyribonucleic acid (DNA) control sequence associated with that gene. When the regulator is bound to arsenic it can switch the gene on to synthesize and produce the required proteins for the detoxification system activation [Francisco *et al.*, 1990; Wu and Rosen, 1991, 1993; Shi *et al.*, 1994]. When creating an arsenic biosensor, the arsenic-responsive DNA control sequence is linked to a so-called reporter gene, which produces a protein whose properties can be readily observed (as for example an enzyme that generates a highly colored material or a fluorescent protein).

An interesting characteristic of using living organism as sensors is that only the fraction of pollutants, in our case the arsenic, which is available to them, i.e. the bioavailable fraction, is detected [Joshi, 2006]. The ability to monitor the arsenic bioavailability instead of the total concentration is important, as it gives more accurate information regarding the risk that the contaminated site poses to human health [Joshi, 2006; Liu *et al.*, 2010].

It has been shown that using bacteria [Stocker *et al.*, 2003; Trang *et al.*, 2005; Diesel *et al.*, 2009] it is possible to detect arsenite and arsenate below the current drinking water limit of 10 µg/L. The challenge remains to build a suitable platform to take the biosensors out of the lab and to eliminate the need of well-trained personnel. As we are going to show in this thesis, the combination of biosensors with microfabrication is one of the most promising approaches to achieve these goals.

### Surface-enhanced Raman spectroscopy

Surface enhanced Raman spectroscopy (SERS) is a surface-sensitive technique that results in the enhancement of Raman scattering<sup>2</sup> by molecules adsorbed on rough metal surfaces and allows to specifically identify and quantify a single chemical specie in a large sampling environment by its vibrational spectrum [Kneipp, 2007; Melamed, 2005]. The enhancement factor can be as much as  $10^{14}$ -  $10^{15}$ , allowing the detection of single molecules.

A feasible route for an in-field arsenic detection is the development of a highly active substrate for SERS of arsenic that can be coupled to commercially available portable Raman systems [Cullum *et al.*, 2000; Xua *et al.*, 2010]. Recently, Z. Xua and co-workers [Xua *et al.*, 2010] were able to develop a silver nanofilm that was reproducible and sensitive for the SERS of arsenic. They could discriminate between As(V) and As(III) species and they could investigate the effect of eight common ions in natural waters. In a similar way, M.-J. Han *et al.* [Han *et al.*, 2011] determined the limit of detection for As(V) to be 5 µg/L.

#### 1.2.1.3 Other assays for arsenic in the environment

This section discusses techniques that have been successfully used for the measurement of arsenic in the laboratory but have not been widely applied to field applications.

### Capillary electrophoresis

Using capillary electrophoresis one can extract and separate ions species from an environmental matrix but can not detect or measure the concentration of these species. However, when this technique is combined with instruments such as inductively coupled plasma mass spec-

---

<sup>2</sup>When photons are scattered from an atom or a molecule, most photons are elastically scattered so that the energy of the incident photons equals the energy of the scattered photons. However, a small fraction of the scattered photons (approximately 1 in 10 millions) have energies different than that of the incident photons. This is called the Raman effect.

## Chapter 1. Introduction

---

trometry (ICP-MS), it has potential as an analytical technique [Melamed, 2005]. The principle of operation is the following [Melamed, 2005; EPA, 1994; Huang and Whang, 1998]: a voltage is applied through a fused silica capillary containing an electrolyte that absorbs UV-light, causing the electrolyte and anions to migrate towards the anode and through the capillary's UV detector window. Anions are separated based upon differential rates of migration in the electrical field. As the anion of interest migrates down the capillary, it displaces the buffer, changing the absorption spectrum for that region of the capillary and allowing the anion to be detected and quantified. Using this technique, Huang and Whang [Huang and Whang, 1998], showed detection limits for arsenic down to 40 µg/L.

### Laser induced breakdown spectroscopy (LIBS)

This technique, which can determine the elemental composition of aerosols, liquids, gases, and solids qualitatively and quantitatively in real time, consists in directly focusing a high-powered pulsed laser beam into the targeted sample to form a small laser-induced breakdown, called a laser spark [Fisher *et al.*, 2001; Melamed, 2005]. The resulting high-temperature plasma is sufficient to vaporize, atomize, and electronically excite a small amount of the sample matter. As the plasma cools and the previously excited electrons relax to their original condition, they emit light at characteristic wavelengths. Although improvements to this technique have brought the arsenic detection limit down to 400 ppm [Fisher *et al.*, 2001], this technology requires more research to be competitive.

#### 1.2.1.4 New analytical technologies with possible applications for arsenic analysis

In this section we consider analytical techniques that have been successfully applied to other environmental species and that could be applied to arsenic detection in the field.

#### Microcantilever sensors

These sensors use micrometer scale cantilevers coated with a "detector film" that interacts with the desired species as sensing element. When the desired species adsorbs onto this film, it causes one of several changes: surface stress, a temperature change, or increased mass, which translate in the microcantilever deforming (bending). Usually, this deformation is measured by laser reflection.

We mention this technique as it has successfully been used for the *in situ* detection of low



concentrations (below ppm) of chromate [Ji *et al.*, 2000] and cesium [Campion and Kambhampati, 1998], inorganic oxyanions that have a similar structure and chemical behavior to their arsenic counterparts (e.g., chromate, phosphate and perchlorate), and thus could be applied to arsenic detection in the field.

### 1.2.1.5 Discussion

The central goal of developing a cheap and portable field assay that does not require trained personnel to be operated and that reliably and reproducibly quantify arsenic has not been achieved yet. Table 1.1 resumes the different arsenic detection methods with their characteristics. Colorimetric assays are still not sufficiently reliable and the release of toxic arsine gas remains a problem. XRF hand held devices have the advantage to measure a wide spectrum of metals in addition to arsenic but, especially in the case of liquid samples, they require sample preparation. Furthermore, interference from lead is a concern. ASV appears to be very promising except for the limitations on whether arsenate can be directly measured and for possible interference from other environmental metals. Surface-enhanced Raman-based sensors are promising but more research effort is required in an in-field arsenic detection view. Microcantilever-based sensors also offer strong potential for use in arsenic detection. However, a cantilever-based sensor for arsenic has not been developed yet. From our point of view, thanks to their selectivity and sensitivity, biosensors combined with microfabrication techniques are one of the most promising approaches for an inexpensive and robust in-field arsenic detection.

## Chapter 1. Introduction

Method	Media	Method detection limit (MDL)	Comments
<i>Current technologies</i>			
Colorimetric assays	Liquid	1-30 ppb [Kin-niburgha and Kosmusb, 2002]	Quantitative readings can only be obtained with the use of an absorption spectrometer.
Use of portable XRF devices to measure arsenic in groundwater	Liquid and solid	50 ppb (liquid)	Capable of measuring a wide spectrum of metals in a sample.
ASV	Liquid	0.05-0.5 ppb	High sensitivity.
<i>Promising technologies</i>			
Bioassay	Liquid	4 ppb	Promising selectivity and sensitivity. Challenges for in-field measurements.
Surface-enhanced Raman-based sensors	Liquid	5 ppb	Promising selectivity and sensitivity.
Capillary electrophoresis	Liquid	40 ppb	Some possibilities for a compact sensor unit.
LIBS	Solid	400 ppm	Poor sensitivity.
<i>Analytical technologies not yet applied to arsenic</i>			
Microcantilever-based sensors	Liquid	NA	Has not been applied to arsenic but outstanding selectivity and sensitivity for chromate and other anions are promising.

Table 1.1: Methods for in-field arsenic detection.

### 1.2.2 Whole-cell living biosensors and their integration in microfluidic platforms

A general definition for the term "biosensor" is "the coupling of a biological material with a microelectronic system or device to enable rapid, accurate, low-level detection of various substances in body fluids, water and air" [Belkin, 2003]. There are two main advantages in using biological material as sensitive elements [Belkin, 2003]. First, biological molecules are extremely highly specific [Belkin, 2003]. In fact, successful biosensors are based on the specificity endowed by the unique biorecognition of two molecules. Secondly, they can sense only the bioavailable fraction of the target chemical, thus allowing its differentiation from the non-available fraction, information which might be highly valuable for risk assessment. In a "whole-cell living biosensor" a live, intact cell is used as the biological entity [Belkin, 2003]. In this way, even if much of the specificity described above might be lost, we are able to detect very complex series of reactions that can exist only in an intact, functioning cell. Parameters such as bioavailability, toxicity and genotoxicity can only be assessed using whole cells [Belkin, 2003].

The idea to use living organisms as indicators for the presence of toxic compounds probably stems from the Romans, who used canaries to detect too high carbon monoxide concentrations in mines [Tecon and van der Meer, 2008]. But we had to wait until 1990 to see the first cell-based biosensing system: a genetically modified bioluminescent bacterial sensor could sense naphthalene and, upon sensing, produce bioluminescence in a concentration-dependent manner [King *et al.*, 1990]. The biologic part of the existing cell-based biosensors often consists of genetically engineered bacteria, whose large population size, rapid growth rate, low cost and easy maintenance make them a valuable option for pollution monitoring. In the presence of a chemical, physical or biological signal, these microorganisms express a specific reporter gene which translates into the synthesis of a reporter protein (luciferase,  $\beta$ -galactosidase or autofluorescent proteins, as for example green fluorescent protein (GFP)) [Tecon and van der Meer, 2006]. This amount or activity of reporter protein is then measured by secondary sensors (mostly by spectrometry, fluorometry or electrochemistry) [Tecon and van der Meer, 2006]. The common methodology for cell-based biosensors analysis consists in exposing the living bioreporter cells to the target compound for a certain amount of time and subsequently measure the overall reporter response from the cells population, which in the case of the GFP will be a fluorescent signal [Tecon and van der Meer, 2006]. The obtained reporter response can then be interpreted using the previously established calibration curves of the reporter

response as a function of the target chemical concentration (Figure 1.2).

For several reasons microengineered platforms are highly suitable for bioreporter cell incorporation [Andersson and van den Berg, 2003]. In fact, analytical standard operations can be easily integrated, microfluidic systems are compatible with the size of the cells (1-100  $\mu\text{m}$ ) and capable of manipulating single cells as well as large numbers of cells simultaneously, using geometries with small dimensions, large electrical field strengths can be obtained with small voltages, and heat and mass transfer are very fast. Furthermore, an important characteristic for a whole-cell living biosensor intended to be used in the field, as in the case of the monitoring of environmental pollution, is their portability and autonomy. Microengineered platforms, as they constitute a solid support and allow long-term maintenance, are a promising way to reach this goal. Ideally, a microengineered platform incorporating a whole cell living biosensor should constitute a solid support for bioreporter cell containment and long-term maintenance, provide the fluidics for sample and reagent transport as well as for control and process electronics, perform signal detection and transduction, use signal analysis algorithms, perform temperature control and have communication capacities [van der Meer and Belkin, 2010].

One of the first examples of a whole-cell bacterial biosensor implementing some of these functions was presented by Simpson *et al.* in 1998 [Simpson *et al.*, 1998; Nivens *et al.*, 2003]. In their outline the bioreporter cells were immobilized on a silicon-based complementary-metal-oxide-semiconductor (CMOS) integrated circuit, which was able to detect the bioluminescence produced by the cells. Since then, even if a whole-cell living biosensor satisfying all the characteristics required for an in-field application has not yet been described, several papers reported different and improved solutions. Bacterial bioreporter cells have been directly integrated into a photodiode optical circuit on which the bioluminescence of cells could be detected; a porous, light tight enclosure allows chemical diffusion into the bioreporter unit and efficiently blocks out daylight [Nivens *et al.*, 2003]. In 2009, Ben-Yoav and co-workers [Ben-Yoav *et al.*, 2009] were able to build a microfluidic whole-cell biosensor for water toxicity analysis in which bacterial cells were genetically "tailored" to generate a sequence of biochemical reactions that eventually generated an electrical signal in the presence of genotoxicants: the bacteria were integrated onto a chip containing microwells and electrodes for the cells response measurement on chip. Recently, Prindle *et al.* [Prindle *et al.*, 2012] were able to build a microfluidic device containing an array of thousands of oscillating *E. coli* colony "biopixels"

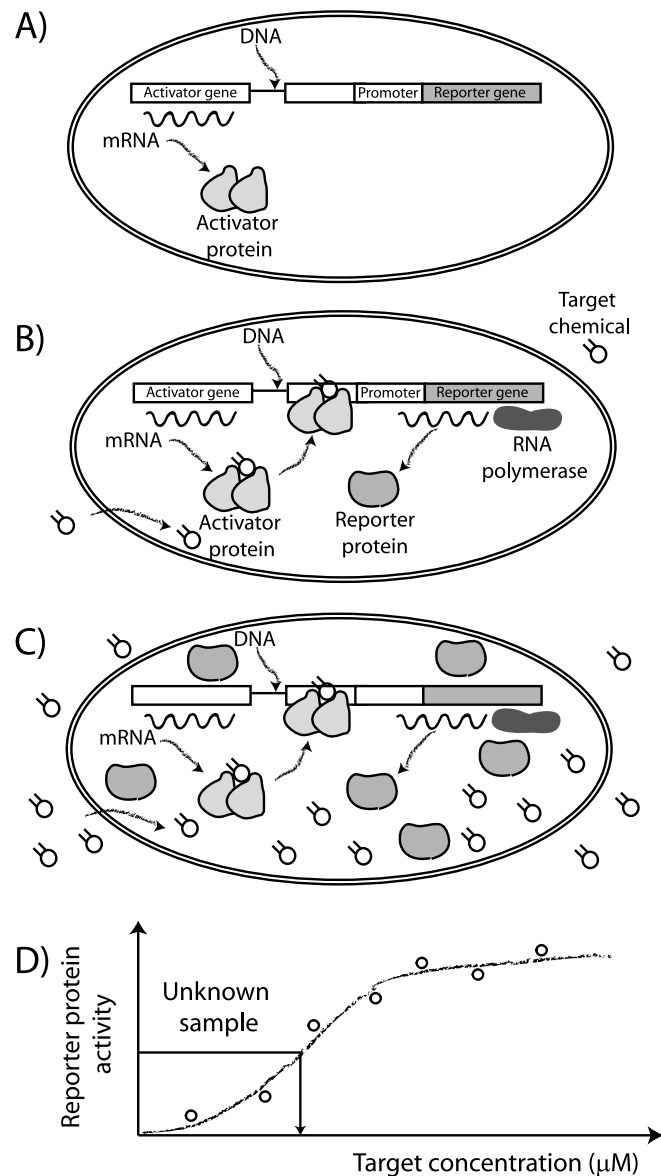


Figure 1.2: Outline of a whole-cell living bacterial bioreporter. The bacterial bioreporter cell contains a short signalling network, which consists of a fusion between an inducible promoter of interest and a promoterless reporter gene, which can be for example the *gfp* gene. The promoter is activated (or derepressed) by a transcriptional regulator, shown here as an activator protein, usually after binding of a specific chemical effector compound. The activation (or derepression) of the promoter leads to the transcription of the reporter gene and eventually to synthesis of the reporter protein. In absence of the effector the transcription of the reporter gene is repressed (A). When the concentration of the effector is relatively low, only few reporter proteins are synthesized in the cell (B), while at higher concentration there are more reporter protein produced (C). The number or the activity of the reporter protein can be calibrated as a function of the chemical effector concentration, so that its concentration in unknown sample can be tested.

which were able to synchronize between them thanks to a gas-phase redox signaling and could be used to sense arsenic via modulation of the oscillatory period of the GFP fluorescence signal produced. Measuring the period of oscillation allowed the authors to avoid some of the issues of optical intensity readings (the cells growth state did not influence the measurement) and they are now focusing on the development of a handheld sensor by integrating a LED (light-emitting diode) exciting the array and a photodetector collecting the emitted light.

An alternative solution to the incorporation of bioreporter cells in microengineered platform is to freeze-dry cells. Shin *et al.* [Shin *et al.*, 2005] showed that freeze-dried recombinant bacteria able to detect phenolic compounds by a color change can be rehydrated and used instantly, without any growth step. Recently, Siegfried and co-workers [Siegfried *et al.*, 2012] developed lyophilized bacterial bioreporters emitting bioluminescence as a response to arsenite and arsenate. Tests on the field were in satisfying agreement with the results of spectroscopic analyses of the same samples conducted in the lab. However, depending on the type of cells, freeze-drying may result in considerable amounts of dead cells [Bjerketorp *et al.*, 2006].

### 1.2.3 Flow control in microfluidic chips

In the majority of microfluidic devices the flow is driven by pressure (PDF) or by electroosmosis (EOF) [Pennathur, 2008] and valves incorporated in the microchannels constitute an important element for its control. In the case of a microfluidic platform in which are incorporated biosensor cells, the driving and the control of the flow are two fundamental operations for the exposure of the cells to the sample to be tested.

#### 1.2.3.1 Pressure-driven flow

Pressure-driven flow is the most well-characterized flow control system in microfluidics, mainly because the flow profile follows the well-known Poiseuille flow theory [Stone and Kim, 2001]. This type of flow is characterized by a smooth parabolic profile induced by the no-slip condition at the wall [Pennathur, 2008]. The most common way to drive microfluidic flow with pressure is by using syringe pumps attached to capillary tubing and fluidic interconnects onto a chip. The advantage of using this packaging solution is that it is well-designed and straightforward to implement. However, syringe pumps are expensive and hardly amenable to miniaturization. For this reason there are several recent studies creating pressure-driven flow

on the chip itself, as mechanical displacement pumps, such as peristaltic and rotary [Unger *et al.*, 2000; Lee *et al.*, 2004] pumps, and dynamic pumps, such as ultrasonic and centrifugal pumps [Madou *et al.*, 2006; Wixforth, 2004]. The shortcomings of this type of flow are that its profile leads to hydrodynamic dispersion effects, which can be undesirable in many separation applications, and that it does not scale very well to channel diameters of  $<10\ \mu\text{m}$  [Pennathur, 2008].

### 1.2.3.2 Electroosmotic flow

Electroosmosis is produced by the interaction of the solution layers near the solid/solution interface and an axially applied electric field: if the walls of a microchannel have an electric charge, an electric double layer of counter ions will form at the walls and applying an axial electric field the ions in the double layer move towards the electrode of opposite polarity [Kirby, 2010]. This creates motion of the fluid near the walls and thanks to viscous forces it transfers into convective motion of the bulk fluid. The velocity profile of this type of flow is uniform across the entire width of the channel except for within the double layer, minimizing the hydrodynamic dispersive effects present in pressure driven flow. It also offers a significant advantage for driving liquids in smaller channels when compared to PDF flows: for a given electric field, the EOF flow rate is proportional to the thickness times the width, whereas, a given pressure drop induces a flow rate proportional to the thickness cubed times the width. Furthermore, the integration of microelectrodes in microfluidic channels permits local generation and control of the electric fields and the small cross-sectional area of microchannels allows high electric fields ( $>100\ \text{V/cm}$ ) to be maintained with low currents [Pennathur, 2008]. However, EOF often requires very high voltages, which can cause local electrochemical reactions resulting in local nonuniformities in the flow and which make it a difficult technology to miniaturize without off-chip power supplies. Another significant shortcoming is that it is difficult to control due to variability in surface properties and it is significantly influenced by fluid properties. In addition, the flow rate is proportional to the axial potential field gradient, and therefore higher flow rates can not be achieved without large applied gradients. Finally, ohmic heating from large applied voltages can cause local changes in pH and flow characteristics within the flow, as well as electrolytic bubbles within the channel [Pennathur, 2008].

### 1.2.3.3 Other methods to drive the flow

Although pressure and electroosmosis are the most used methods to drive the flow in microfluidic devices, there exist other methods to control a flow. In particular, capillary flow and Marangoni flow are two methods that are extremely amenable to a fully integrated on-chip device [Pennathur, 2008].

Capillarity, or surface-tension driven flow is well suited to microdevices because a large force can be generated in a small channel. Since it requires a discontinuity such as an air/liquid interface or immiscible liquids it is more suitable for filling devices or one-time applications. However, different research groups have shown that electrowetting methods can drive droplets with electric fields due to differences in contact angle changes [Cho, 2003; Cooney *et al.*, 2006]. Electrowetting chips can mimic the basic operations of biochemistry: droplets, which can be used as individual wells of less than 100 nL volume, can be extracted from reservoirs, displaced on an electrode matrix, mixed with other droplets for chemical reactions to occur, and moved to a measurement zone on the electrode matrix where sensors can be integrated [Cho, 2003; Cooney *et al.*, 2006]. Furthermore, high potentials can be applied without electrochemical reactions [Pennathur, 2008]. The shortcomings are that a lower capacitance requires a stronger applied potential to achieve a given contact angle change, and biomolecules tend to nonspecifically adsorb to the surface [Pennathur, 2008].

Another type of flow that involves free surfaces in microfluidics is known as Marangoni flow, which is well suited especially for mixing, droplet motion and spreading of thin films [Pennathur, 2008]. It is a result of gradients in interfacial tension along a free surface, which set the interface into motion. These gradients can be created with thermal, chemical, electrical or light gradients, but the most popular microfluidic Marangoni flow is thermocapillary flow [Darhuber *et al.*, 2004; Kataoka and Troian, 1999]. The drawback is that it requires an interface or immiscible liquids.

### 1.2.3.4 Valves incorporation in microchannels

Valves incorporated in microchannels constitute an important element since they allow to stop and direct the flow. The current literature presents a variety of designs that involve both mechanical and chemical actuation [Pennathur, 2008]. Regarding mechanical actuation, the most illustrative example is the work done by Unger *et al.* [Unger *et al.*, 2000], who developed a



technique called "multilayer soft lithography", in which multilayer structures are constructed by bonding layers of elastomer, each of which is separately cast from a micromachined mold. They designed and built a crossed-channel architecture (typically with a height of 10  $\mu\text{m}$  and a width on 100  $\mu\text{m}$ ) so that, when a pressure is applied to the upper channel, the membrane between the two layers deflects downward and closes the lower channel (Figure 1.3).

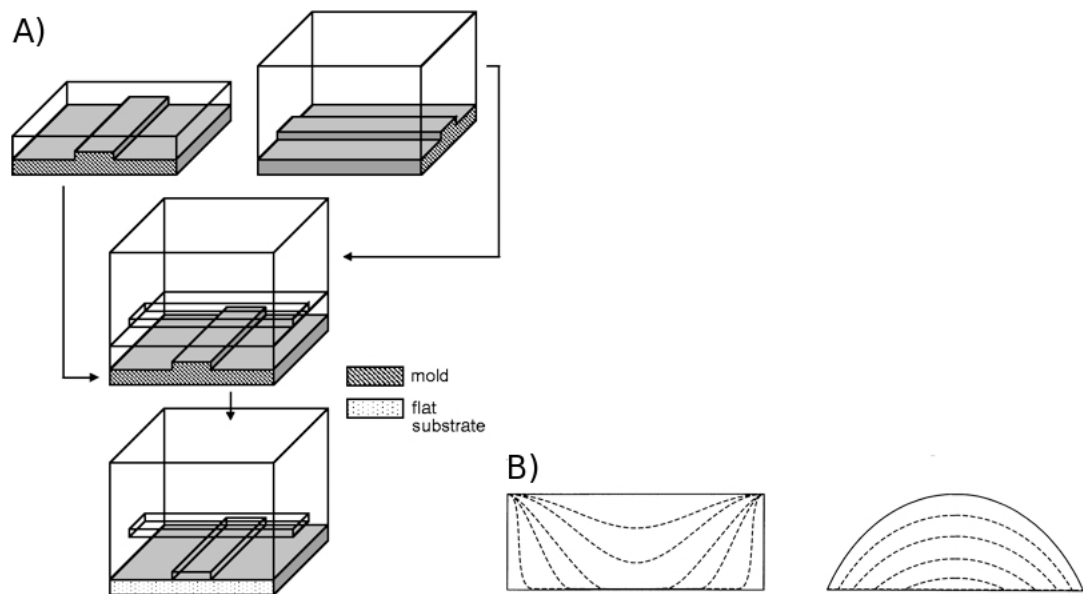


Figure 1.3: A) The two layers are separately cast from a micromachined mold and bonded together. B) When pressure is applied on the upper channel, the membrane between the two layer deflects and closes the channel. In order to have a good sealing, the lower channel needs to be rounded. Figure from Unger *et al.* [Unger *et al.*, 2000].

Chemical actuation is also possible: Beebe *et al.* [Beebe *et al.*, 1999] reported the fabrication of hydrogel components inside microchannels which reversibly expand and contract depending on the pH of the surrounding environment. The response of this type of valves is slow: usually it is more than 5 s, while in the mechanical actuated valves it can be in the range of ms [Beebe *et al.*, 1999; Yu *et al.*, 2003; Unger *et al.*, 2000]. However, the off-chip control is significantly reduced [Satarkar *et al.*, 2009; Beebe *et al.*, 1999; Yu *et al.*, 2003].

### 1.2.4 Cell trapping in microfluidic chips

Manipulation of single cells and particles is a fundamental operation required in any microfluidic cell-based system. In an on chip integrated biosensor system, means of retaining cells at defined locations over time in order to be exposed to the target chemical are required. This section will concentrate on the description of the techniques for microfluidic cell trapping, which partly imply cell concentration capability, an important feature to increase the overall signal produced by each cell to be detected. Cells immobilization methods can be classified as contactless cell trapping or as cell immobilization on a surface (Figure 1.4). The first category comprises optical, dielectrophoretic (DEP), acoustic, and magnetic trapping, while the second comprises chemically driven cell attachment to a surface and hydrodynamic trapping. Cell encapsulation in a polymer is regarded as being situated in between [Johann, 2006].

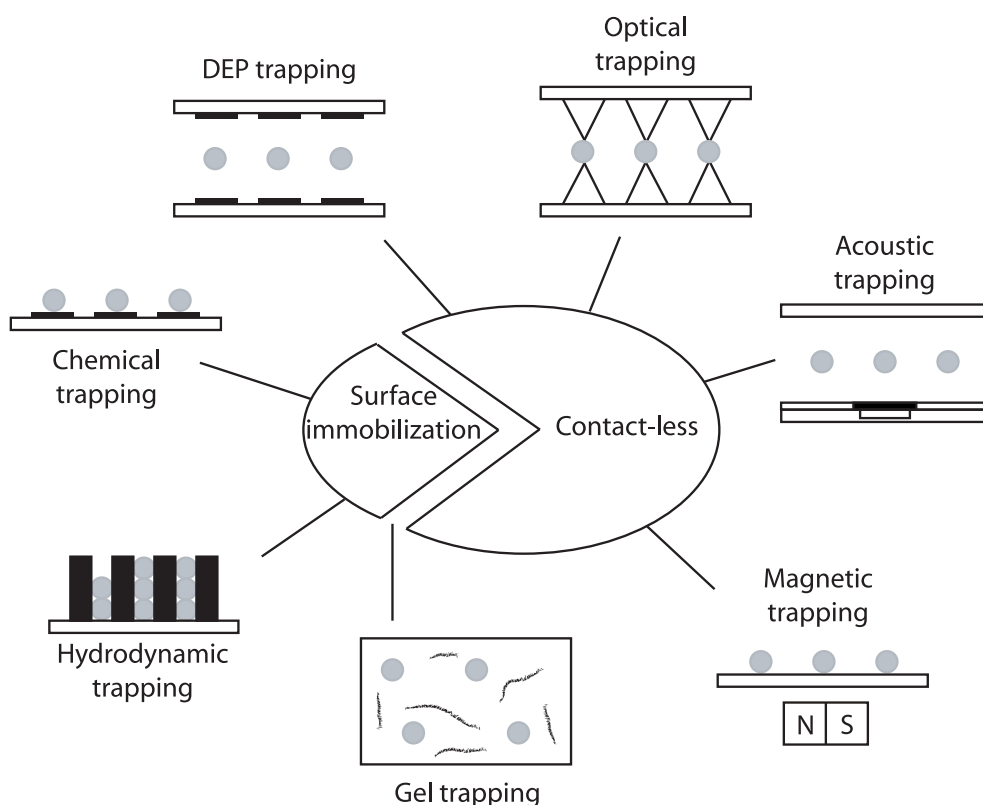


Figure 1.4: Cell trapping methods.

### 1.2.4.1 Chemical trapping

With this technique, surfaces are modified in chemical composition, providing a discrete location for cell adhesion. In recent years, surface modifications has been integrated with microfabrication to achieve high precision cell trapping [Delamarche *et al.*, 2005; Bhatia *et al.*, 1997]. However, this method presents some drawbacks, as it is not applicable for non-adherent cells, cells need time to firmly attach and the deposition is often irreversible [Johann, 2006]. Furthermore, the choice of the surface coatings is also challenging: it must be highly effective for all deposited cell types and it must be able to inhibit cell migration and overgrowth.

### 1.2.4.2 Hydrodynamic trapping

This term includes all methods which use variations of surface topography to separate particles from a flow and immobilize them on certain sites [Johann, 2006]. Mechanical obstacles or barriers are tailored to the dimension of the cells, so that they are captured while the flow can pass through. An illustrative example are the U-shaped traps developed by Wu *et al.* [Wu *et al.*, 2008], which with their the large number (7'500 traps per square centimeter) and a narrow cells distribution ( $10\pm 1$  cell per trap) provide a good platform for anticancer drug assay (Figure 1.5). Another interesting kind of hydrodynamic trapping is the one presented by Mengsu Yang *et al.* [Mengsu *et al.*, 2002]: two microfluidic channels are connected via a dam structure leaving a 5  $\mu\text{m}$  high opening. The dam retains cells along the full channel length by defining a net cross flow over it, allowing monitoring of cellular reactions.

In order to dock cells in engraved or hollow structures, it is also possible to exploit the gravitational force [Khademhosseini *et al.*, 2004]. The principle of operation of such a device is to introduce the cells into the channel, stop the flow to sediment the cells into the microwells and then restart the flow. Although this is a simple, low-expertise route, its efficiency, which is determined by local dispersion of cell solution as well as flow conditions, is relatively low with poor reproducibility: cells are usually deposited non-uniformly over an area with many empty sites [Sun *et al.*, 2008]. Another approach consists in using capillary force [Park *et al.*, 2008]: cells are introduced into the microfluidic channel by surface tension driven capillary flow and then a receding meniscus is generated by evaporation: as the meniscus progresses, one to multiple cells are spontaneously captured onto microwells by lateral capillary force created at the bottom of the meniscus. In this case cell docking can be performed without additional

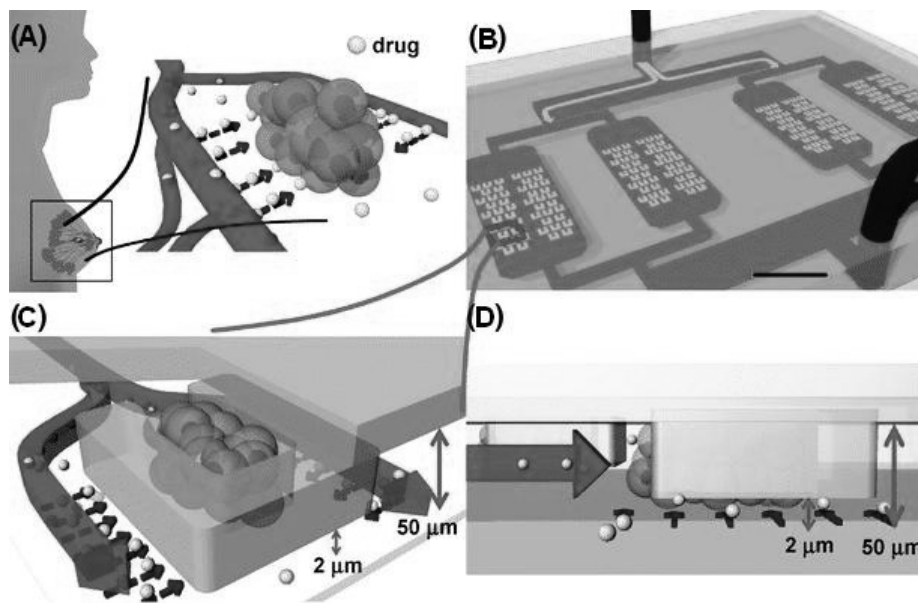


Figure 1.5: Microfluidic spheroid culture array developed by Di Carlo *et al.* A) Schematic of the tumor spheroids exposed to the target drug. B) Diagram of the device containing the U-shaped traps. C) Perspective view of one of the U-shaped traps. (d) Side-view of the trap.

accessories, such as a syringe pump. However, because cells are exposed to air for a certain period of time (<5 min), cell viability might be a concern [Sun *et al.*, 2008]. These methods are fast, compared to chemical trapping, and the devices using it are often simple and inexpensive. However, the contact between the cell and the surface is not avoidable, which may result to irreversible attachment, and single cell deposition is difficult to achieve, leading to sites empty or filled with aggregates [Johann, 2006].

#### 1.2.4.3 Dielectrophoretic (DEP) trapping

As cells are polarizable, the dielectrophoretic force can be used for their manipulation. Dielectrophoresis is a phenomenon that uses a non-uniform AC electric field to exert a force on polarized neutral particles [Pohl, 1978]. Permittivity and conductivity of the cells and the liquid medium varies as a function of the frequency of the applied electric field and depending on the difference of these two values, cells can experience either a positive (attracted toward the higher field, p-DEP) or a negative (pushed away from it, n-DEP) dielectrophoretic force [Pohl, 1978]. A good example of simultaneous p-DEP and n-DEP trapping of viable and non-viable yeast cells was shown by Wang *et al.* [Wang *et al.*, 1993]: due to the difference in permittivity,

the viable cells experienced a p-DEP force collecting them at the electrode surface corners, while the non-viable cells, experiencing a n-DEP force, were collected in the center of the trap. When using planar electrodes, the DEP force acting on a particle rapidly decreases when it moves away from the electrode's plan [Nilsson *et al.*, 2009]. To improve the DEP forces acting on a particle, Shnelle *et al.* [Schnelle *et al.*, 1993] introduced a 3D trap design using two layers each consisting of 4 planar electrodes spaced 220  $\mu\text{m}$  apart. The main drawback of dielectrophoresis is the presence of strong AC fields that causes Joule heating and sets up transmembrane voltage. Furthermore, many conventional cell culture biomaterials, such as collagen and alginate, are too conductive and viscous to be used in this trapping method [Johann, 2006].

### 1.2.4.4 Optical trapping

An optical trap exerts two forces on the cell. The first one is the scattering force that drives the cell away from the light source by radiation pressure, the second one is the gradient force that pulls the cell into the high density region of the trap: the balance of these two forces is a critical parameter to obtain a stable trap [Ashkin *et al.*, 1987; Johann, 2006]. Common light sources are laser and infrared light. To use optical trapping, particles need to be transparent, non-absorbing at the trapping wavelength, and their refractive index has to be different from the one of the surrounding medium [Johann, 2006]. A illustrative example of what can be done using optical tweezers is the work of Arai *et al.* [Arai *et al.*, 1990]: a polystyrene bead was attached to each end of DNA and actin filaments and trapped using a dual optical tweezers. While keeping one optical tweezer fixed, the other moved the second bead tying a knot on the filament. Successively, tightening the knot, the force required to rupture the filament could be measured and the mechanical properties of the different filaments could be compared. A general drawback of this method is that because of the fixed amount of power required by each trap, the number of traps is limited by the available power of the light source [Johann, 2006]. Furthermore, the absorption of laser light by trapped cells may result in a dramatic temperature increase causing cell damage [Ashkin *et al.*, 1987; Rasmussen *et al.*, 2008].

### 1.2.4.5 Acoustic trapping

The acoustic trapping technique usually use an ultrasonic standing wave generated by an integrated transducer to create a pressure node that will attract cells [Johann, 2006; Evander

*et al.*, 2007]. This force, which scales linearly with the cell volume and the acoustic frequency, results from the different densities and sound speeds of cells and fluid [Johann, 2006]. A major application area for ultrasonic trapping is the study of non-adherent cell cultures in perfusion systems [Nilsson *et al.*, 2009]. A frequently applied configuration is the confinement of free-floating objects in thin parallel lines of (anti)nodes in which the objects can move freely within a line [Wiklund *et al.*, 2006]. It is also possible to create two-dimensional patterns [Lilliehorn *et al.*, 2005] or acoustic tweezers for capturing and stably positioning single cells in 3D [Hertz, 1995], but in these cases more sophisticated designs are needed. It has often been questioned on the viability of trapped cells after being exposed to ultrasounds [Nilsson *et al.*, 2009], but there are no indications that ultrasound exposure influence viability and it has even been demonstrated that yeast cells can be cultured in an acoustic trap [Evander *et al.*, 2007].

### 1.2.4.6 Magnetic trapping

Usually, magnetic manipulation involves the attachment of magnetic particles to cells. Commonly, super-paramagnetic beads in 10-100 nm of diameter are used, which, because of their small size, do not affect the cellular function and viability [Changqing *et al.*, 2006]. The magnetic field gradients generated by various methods can be employed to trap the bead and, consequently, the cell attached to it. However, Frazier and co-workers [Han and Frazier, 2004] were able to separate red and white blood cells from whole blood based on their native magnetic properties, without using any magnetic tagging. This technique enables accurate, selective and reversible cell positioning, parking, sorting and concentration [Johann, 2006]. However, cells are permanently exposed to weak electromagnetic forces and to slightly increased temperatures [Johann, 2006].

### 1.2.4.7 Gel trapping

The trapping of cells in a gel is often regarded as being in between the "contact" and the "contact free" immobilization. In fact, it is based on the contact of the cells with the polymer scaffold that serves as mechanical support but at the same time it has many elements in common with the contact-free techniques [Johann, 2006]. The polymers used, called hydrogels, are usually very hydrophilic and can have a water content of more than 99%. Under such conditions, cells are expected to be completely surrounded by water and the contacts with the hydrophilic polymer chains are very few. Different strategies have been employed

for the preparation of micro scale three-dimensional cell-hydrogel scaffolds. The simplest approach is to inject into a microchannel a solution containing cells and matrix (for example collagen) and to incubate it for gelation [Tan and Desai, 2003]. It is also possible to structure hydrogels using photolithography [Revzin *et al.*, 2001] or, in case of agar-gels, photo-thermal etching [Kojima *et al.*, 2003]. Combining hydrogel-photopolymerization by selective exposure of polyethyleneglycol (PEG) derivatives to UV radiation with microfluidic component allows the production of diverse hydrogel features which differ in matrix composition and cell content [Koh *et al.*, 2003]. However, the exposure to UV light and the presence of radicals may lead to cell damage and the inclusion into a photopolymerized gel is usually irreversible. An interesting alternative method was proposed by Braschler *et al.* [Braschler *et al.*, 2005]: they used alginate as a gel and they were able to control its growth and shrinkage varying the ratio of  $\text{Ca}^{2+}$  and ethylenediaminetetraacetic acid (EDTA) previously added. Trapped cells were released during the shrinkage process. The cells release is a feature that is hard to achieve with chemical or hydrodynamic trapping [Johann, 2006]. Furthermore, using this method cells can be trapped and then cultured in a three-dimensional environment [Tibbitt and Anseth, 2009] and they are not exposed to a continuous electromagnetic field or light source, preventing overheating or mechanical stress.

### 1.2.5 Chemostat on chip

An essential point for the development of a portable whole-cell living biosensor which can be used in the field is the long term preservation of cells in an active form. For this purpose, microengineered platforms offer interesting solutions.

When cells grow in static cultures, their final density is limited by their depletion of nutrients from the surrounding environment [Weibel *et al.*, 2007]. In chemostatic growth, a small number of cells is constantly removed from the culture and fresh nutrients are added continuously: under these conditions, cells cultures can achieve steady-state growth [Novick and Szilard, 1950]. Several groups have designed "microbioreactors" based on microfluidics, thus creating chemostats on chip for growing bacterial and yeast cells. Balagaddé *et al.* [Balagaddé *et al.*, 2005] were able to develop a microfluidic PDMS chemostat for the long-term culture (until 200 h) of bacterial cells. Each microchamber was composed of a fluidic loop of 16 nL in volume with an integrated peristaltic pump and a series of micromechanical valves to add medium, remove waste, and recover cells. Circa  $10^4$  *E. coli* were cultured in each microchamber. The

## Chapter 1. Introduction

liquid in each chamber was constantly recirculated at a rate of 250  $\mu\text{m/s}$ . In order to prevent biofilm formation, the chambers were periodically washed: a segment is isolated from the rest of the reactor with micromechanical valves and a lysis buffer was flushed through the isolated segment for 50 s to expel the cells contained in it, including any wall-adhering cells (Figure 1.6).

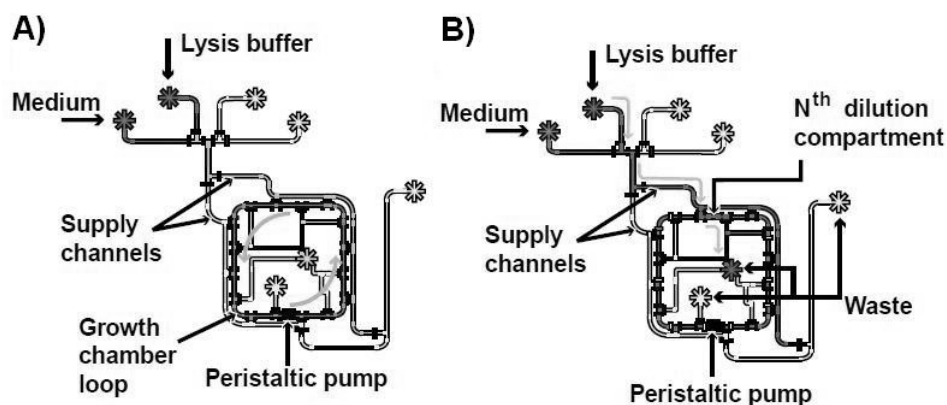


Figure 1.6: A) Schematic diagram of a microchemostat in continuous circulation mode. B) Isolation of a segment from the rest of the growth chamber during cleaning. Figure adapted from Balagaddé *et al.* [Balagaddé *et al.*, 2005].

Groisman et and co-workers [Groisman *et al.*, 2005] were able to maintain chemostatic conditions for bacterial and yeast colonies growing in an array of shallow microscopic PDMS chambers. The chemostat is mainly composed of an array of parallel channels with continuous flowthrough of fresh medium (maintained with a syringe pump) and parallel rows of chambers between the channels. Capillaries, which are impenetrable to *E. coli* cells and to other bacterial and yeast (yeast cells are ca. 1  $\mu\text{m}$  in diameter and the capillaries are 600 nm in height), allow the diffusion of chemicals from channels to chambers. The characteristic time of diffusive exchange between the chambers and the channels for small molecules is estimated at least 50 times faster than the bacterial cell division cycle. The problem concerning the chamber filling was solved taking advantage of the height flexibility of PDMS: when the gauge pressure inside the device increases, the microchannels inflate, increasing the capillary depth and allowing the passage of cells (Figure 1.7).

Zhang and co-workers [Zhang *et al.*, 2006] proposed another interesting solution: they developed a polymer-based microbioreactor system integrated with optical density (OD), pH,



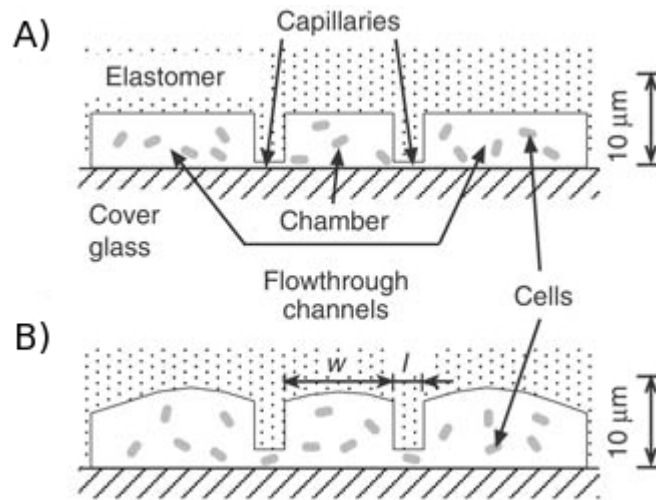


Figure 1.7: A) Cross-section showing two channels, a chamber and two capillaries connecting the channels with the chamber. B) The capillaries are impermeable to the cells, but they become permeable when a high gauge pressure is applied. Figure adapted from Groisman *et al.* [Groisman *et al.*, 2005].

and dissolved oxygen (DO) real-time measurements for continuous cultivation of microbial cells. *E. coli* cells were continuously cultured in a 150 mL, membrane-aerated, mixed (using a ringed magnetic stir bar) microbioreactor fed by a pressure-driven flow of fresh medium (0.5 to 2  $\mu\text{L}/\text{min}$ ) through a microchannel. By implementing a PEG-grafted polyacrylic acid (PAA) PDMS and polymethylmethacrylate (PMMA) surfaces into the microbioreactor, adhesion and wall growth of *E. coli* in the microbioreactor was effectively reduced. Chemotaxial back growth of bacterial cells into the medium feed channel was prevented by local heating. With time profiles of optical density, pH, and dissolved oxygen measurements (the latter two based on fluorescence lifetime), they could demonstrate the dynamic balance between cell growth rates and medium feed rates at steady state conditions: after about 80 hours, dissolved oxygen, pH, and optical density reached stable levels and steady state conditions in the microchemostat were established for 100 hours.

It is also interesting to mention the device developed by Cookson *et al.* [Cookson *et al.*, 2005], which is based on the implementation of the Tesla diode loop [Tesla, 1920]. The side-arm of the diode constitutes a shallow trapping region that constrains a population of cells to the same focal plane (Figure 1.8) and the cells that grow beyond the trapping region boundaries are continuously purged by flow, so that the device can function as a standard chemostat.

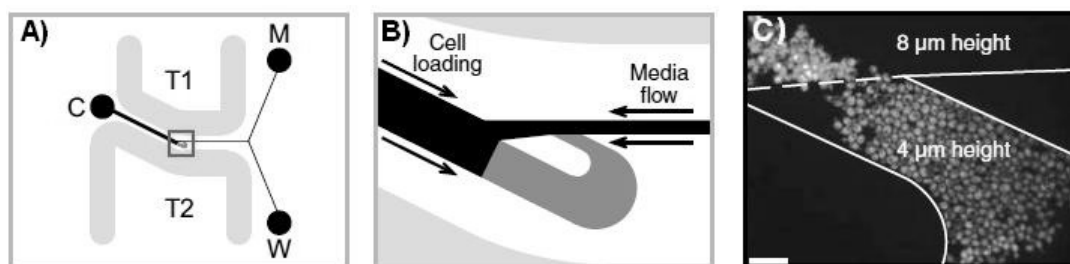


Figure 1.8: A) Cells are loaded through reservoirs (labeled C) and trapped in the imaging region. Once enough cells are trapped, the flow is reversed. Excess media is routed through port W. Heated water is passed through two channels (labeled T1 and T2) on either side of the imaging chamber to control the temperature on the chip. B) Close-up diagram of the imaging region. Once the flow has reversed, the trapping region (grey) is isolated from the flow and only receives nutrients through a combination of diffusion and advection. C) Fluorescence image of *Saccharomyces cerevisiae* expressing GFP. To force the cells to grow in a monolayer and to create a uniform focal plane, the height of the imaging chamber is 4  $\mu\text{m}$ . Outside the chamber, the channels are twice as tall, which allows cells to be easily washed away by the flow. Scale bar, 20  $\mu\text{m}$ . Figure adapted from Cookson *et al.* [Cookson *et al.*, 2005].

Three other examples have also been recently published. Luo *et al.* [Luo *et al.*, 2010] developed a nanolitre scale chemostat in which they were able to cultivate cells for 120 hours. However, cell removal was performed diffusively, resulting in biofilm formation on the chamber walls. Edlich *et al.* [Edlich *et al.*, 2010] developed a larger scale system with a volume of 8  $\mu\text{L}$  with measurements of dissolved oxygen and optical density. However, mixing was performed diffusively, resulting in biofilm growth rather than suspension growth. Finally, Lee *et al.* [Lee *et al.*, 2011] were able to build a plastic-PDMS device with integrated peristaltic valves and pumps capable of supporting automated microscale continuous culture experiments for 3 weeks in which temperature, cell density, dissolved oxygen, and pH were continuously monitored (Figure 1.9).

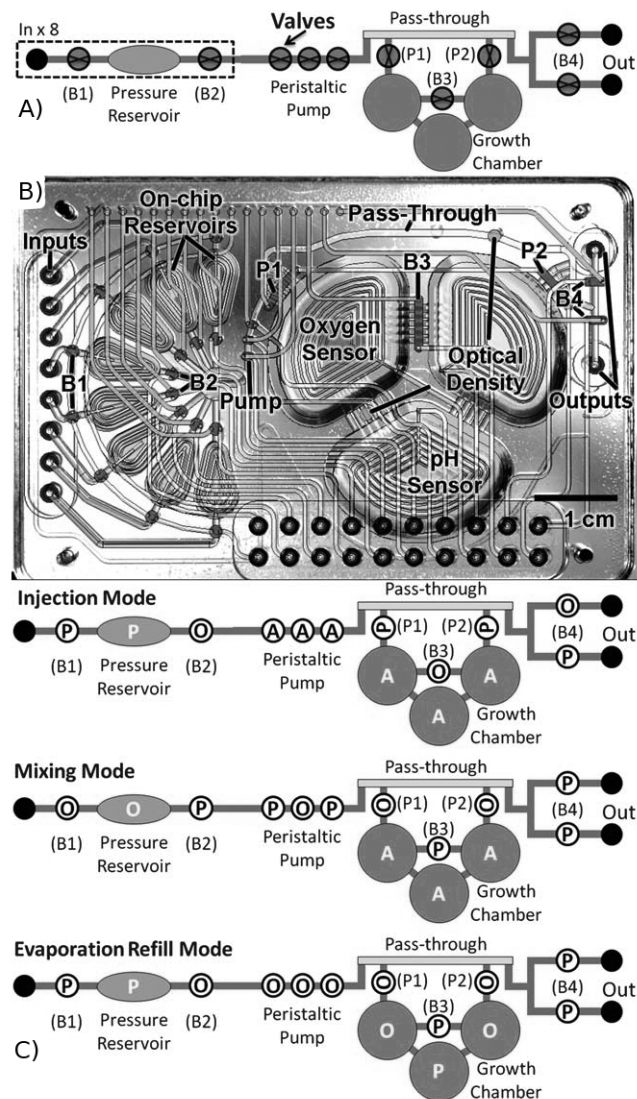


Figure 1.9: Working principle of the chemostat on chip developed by Lee *et al.* [Lee *et al.*, 2011]. A) Schematic of the microfluidic device. B) Photograph of the continuous culture device. C) For continuous culture there are three operation modes. P means closed/pressurized, O open/vented, and A actively switched on/off. Injection mode replaces the fluid in the pass-through channel with new media. The mixing mode mixes the newly injected pass-through contents with the rest of the growth chamber and the evaporation refill mode uses the on-chip water reservoir to inflate the growth chamber back to full volume.

## Chapter 1. Introduction

Type	Working volume	Control	Analysis	Cells on chip time
Circular micro-channel [Balagaddé <i>et al.</i> , 2005]	16 nL	Temperature, OD, Flow	Imaging	200 hours
Perfusion chemostat [Groisman <i>et al.</i> , 2005]	50 nL	Temperature	Imaging	14 hours
Stirred membrane aeration [Zhang <i>et al.</i> , 2006]	150 $\mu$ L	Temperature	DO, pH, OD, sample	100 hours
Tesla diode loop [Cookson <i>et al.</i> , 2005]	N. R.	Temperature, OD	Imaging, OD	20 hours
Diffusive removal [Luo <i>et al.</i> , 2010]	1 nL	Temperature, OD, flow	Imaging	10 hours
Flow through [Edlich <i>et al.</i> , 2010]	8 $\mu$ L	Temperature and flow	OD, DO, sample	120 hours
Integrated mixing [Lee <i>et al.</i> , 2011]	1 mL	Temperature, DO, OD, flow	DO, pH, OD, sample	3 weeks

Table 1.2: Summary of existing microfluidic continuous culture reactors.

### 1.3 Research objectives

Whereas several studies showed the proof of principle of the arsenic bioreporter assay [Diesel *et al.*, 2009; Trang *et al.*, 2005; Baumann and van der Meer, 2007], they did not attempt to develop a combined arsenic biosensor instrument in which the cells would be exposed to the sample and their reporter output measured within a potentially small device. Also, the active maintenance of the cells on chip remains challenging. The primary goal of the present work was thus to design a miniaturized arsenic biosensor cartridge, which would be suitable to be inserted in a microfluidics system with integrated optical detector and in which cells could be actively maintained as long as possible. In more detail, the objectives for the investigations done as a part of this thesis can be summarized as follows:

- Design and construction of a miniaturized microfluidics system (the Sensor Assay Microbe System cartridge, SAMS) in which the bioreporter cells engineered by the biologists team from the University of Lausanne (UNIL) can be exposed to aqueous arsenic sample and which allows direct detection of the reporter signal produced.
- Design and construction of miniaturized microfluidics system, in which the bioreporter cells can be actively maintained for at least one week, which allows multiple exposures to the aqueous arsenic samples and upon which the reporter signal can be measured

directly on the cartridge by the opto-electronic device (ReaderLab) developed by the engineers team from the University of Applied Sciences and Arts of Western Switzerland (HES-SO). The fulfillment of this objective will lead to a "proof-of-principle" SAMS device for stand-alone measurements of arsenic in potable water sources.

- Study under which conditions, in terms of flow rate and number of cells exposed, the bioreporter cells express the maximum signal-to-noise ratio.

## 1.4 Thesis structure

This dissertation includes 6 chapters. In the present chapter, the motivation and the scope of this thesis were first introduced. An exhaustive review of literature was presented to understand the state-of-the-art of the existing arsenic detection methods and of the existing microfabrication techniques which can be exploited for the development of an in-field arsenic biosensor. After a brief mention of the position of this thesis with respect to the existing knowledge, the research objectives were stated. Chapter 2 is dedicated to the development of the agarose beads system. It describes how agarose beads containing bioreporter cells can be stored in the microfluidic chip and, when needed, exposed to the arsenic sample to be tested. Part of this chapter was published in two peer-reviewed journals [Buffi *et al.*, 2011a,b]. Chapter 3 introduces the system in which the cells are not encapsulated in beads, called "free cells system". Chapter 4 describes the development of the chemostat on chip for the active maintenance of the "free cells system". Chapter 5 is a more theoretical chapter in which the influence of the arsenic sample flow rate and the number of cells exposed on the produced signal are investigated. A Matlab model that helps to understand the observed cells behavior is also presented. The final chapter concludes the dissertation, summarizing the previous chapters and putting this work in perspective.



## 2 Agarose beads system

### 2.1 Introduction

This chapter is intended to present an alternative to high-end instruments for arsenic analysis which consists in a microfluidic platform containing reporter cells encapsulated in agarose beads that can be exposed to liquid arsenic samples. It starts explaining the materials and methods used for the development and the testing of the system. Then, the results obtained in terms of functioning of the chip, sensitivity of bioreporter cells to arsenite, storage conditions, and kinetic response are presented. The last section is dedicated to the discussion of strengths and limitations of this system.

### 2.2 Materials and methods

#### 2.2.1 Reporter cells working principle

For the present work we used the bioreporter strain *Escherichia coli* DH5 $\alpha$  (pPROBE-arsR-ABS), which was previously developed for the detection of arsenic [Stocker *et al.*, 2003]. It carries a plasmid DNA with a transcriptional fusion between the promoter P<sub>ars</sub> of *E. coli* and the gene encoding the enhanced green fluorescent protein (EGFP). The strain also encodes ArsR, a regulatory protein which controls the level of EGFP expression in response to arsenite. The working principle is the following: in the absence of arsenite, most ArsR repressor molecules bind to their operator sites within the P<sub>ars</sub> promoter and allow only low basal expression of their-self and the *egfp* gene (Figure 2.1 A). When arsenite molecules enter the cell, they bind

## Chapter 2. Agarose beads system

with the ArsR molecules, which as a consequence undergo a conformational change and dissociate from their operator. The result is a higher expression of the *arsR* and *egfp* genes (Figure 2.1 B). The EGFP levels attained in the cells over time are proportional to the external concentration in a range of approximately 10 µg/L - 1 mg As/L [Stocker *et al.*, 2003; Wells *et al.*, 2005].

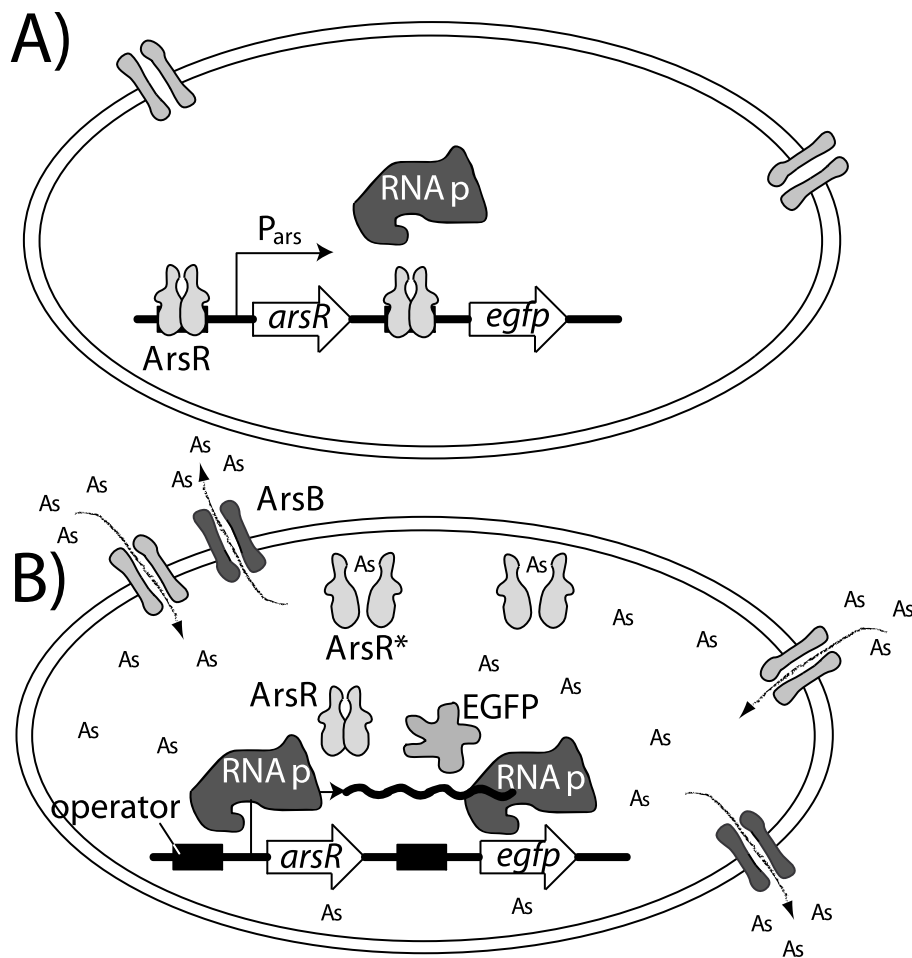


Figure 2.1: Schematic outline of the principle of the arsenic bacterial bioreporter. A) In absence of arsenite, transcription of *arsR* and the *egfp* reporter gene is repressed. B) When arsenite enters the cell, it interacts with the ArsR repressor leading to a conformational change (ArsR\*) and dissociation of the ArsR protein from its operator. In this way the *arsR* gene and the reporter gene are de-repressed, EGFP is produced and fluorescence can be detected.



### 2.2.2 Reporter cells preparation

Starting from a single colony, *E. coli* DH5 $\alpha$  strain 1598 (pPROBE-arsR-ABS) is grown in Luria-Bertani (LB) medium in the presence of 50  $\mu$ g/mL kanamycin at 30°C for 18 h and with 180 rounds per minute (rpm) of rotary shaking of the culture flask. The bacterial culture is then 1000-fold diluted into fresh LB medium plus kanamycin and incubated for a further 24 h at 25°C and with 150 rpm agitation. At a culture turbidity at 600 nm of between 3 and 4 (representative for early stationary phase cells), cells from 30 mL of culture are harvested by centrifugation at 3000 rpm for 10 min and room temperature. The cell pellet is resuspended into 300  $\mu$ L of MOPS medium at pH 7.0 (MOPS medium contains 10% [v/v] of MOPS buffer, 2 mM MgCl<sub>2</sub>, 0.1 mM CaCl<sub>2</sub>, 2 g glucose per L). MOPS buffer itself is prepared by dissolving, per liter: 5 g NaCl, 10 g NH<sub>4</sub>Cl, 98.4 g 3-([N- morpholino]propanesulfonic acid, sodium salt), 0.59 g Na<sub>2</sub>HPO<sub>4</sub>·2H<sub>2</sub>O and 0.45 g KH<sub>2</sub>PO<sub>4</sub>. The final concentration of cells in the suspension equals about 4·10<sup>11</sup>/mL.

### 2.2.3 Encapsulation of reporter cells in agarose beads

Material for bacterial cell encapsulation is preheated to 42°C and a freshly prepared sterile 2.5% (w/v) agarose solution in deionized water (Agarose D1 low EEO, Conda) is cooled down to 42°C 20 min before starting. The encapsulation procedure is carried out at 37°C and the following components are added in sequence with continuous mixing at high speed vortexing (Vortex-Genie 2, Scientific Industries, Inc.). Aliquots of 1 mL of agarose solution, 30  $\mu$ L of pluronic acid (Pluronic F-68 solution 10%, Sigma) and 200  $\mu$ L of cell suspension were mixed in a 10 mL sterile glass tube. The cell-agarose-pluronic acid mixture (0.5 mL) is added drop by drop into 15 mL of silicon oil (Dimethylpolysiloxane, Sigma) in a 25 mL glass tube. After 2 more minutes of continuous vortexing, the tube containing the cell-agarose-silicon mixture is plunged in a water-ice bath for 10 min. Beads are harvested by centrifugation for 10 min at 2000 rpm and room temperature, after which the oil is carefully removed; first by decanting and draining out (tube standing up side down), then by rinsing with 5 mL of phosphate buffered saline (PBS) solution, followed by bead centrifugation, pipetting oil from the surface and decanting wash solution. This rinsing procedure is repeated once more. Beads are size-fractionated between 40 and 70  $\mu$ m, first by collecting the flow-through from 20 a 70  $\mu$ m strainer (Cell strainer 70  $\mu$ m Nylon, BD Falcon). In a next step the recovered bead solution from 70  $\mu$ m is poured over a 40  $\mu$ m strainer (Cell strainer 40  $\mu$ m Nylon, BD Falcon), and beads

retained on the filter surface are recovered by rinsing with 6 mL of MOPS medium.

### 2.2.4 Microfluidic cartridge design and microfabrication

#### 2.2.4.1 Design

The first requirement on the microfluidic cartridge is the ability to trap and concentrate the beads containing the reporter cells, in order that the produced fluorescent signal can be easily detected. Thus, we designed a microfluidic cage of a size of  $500 \times 500 \mu\text{m}^2$  composed by three rows of pillars on each side, interspaced by  $5 \mu\text{m}$  (Figure 2.2 B), so that the liquid can pass through. At such a distance between pillars individual cells would not be retained since *Escherichia coli* is  $2\text{-}5 \mu\text{m}$  long and  $1\text{-}1.5 \mu\text{m}$  in diameter. However, by encapsulating thousands of reporter cells in agarose beads, which are between  $40$  and  $70 \mu\text{m}$  in diameter, they can be trapped in the cage.

Another requirement is that the number of trapped beads remains constant during the measurement and that it is the same between different measurements. In this way the beads undergo the same conditions in terms of nutrients and arsenite distribution, and the measured signal is only dependent on the bioreporter activity and not on the number of beads trapped. When using a microscope for the fluorescence detection, this last point is not so important as the detection area can be defined by the user, however it becomes critical when the microfluidic cartridge is integrated in a hand-held opto-electronic device, which just collects the fluorescence coming from the cage. This necessary feature is satisfied thanks to the fact that we designed a cage instead of a filter wall and thus when the cage is filled with beads all the upcoming ones pass around it.

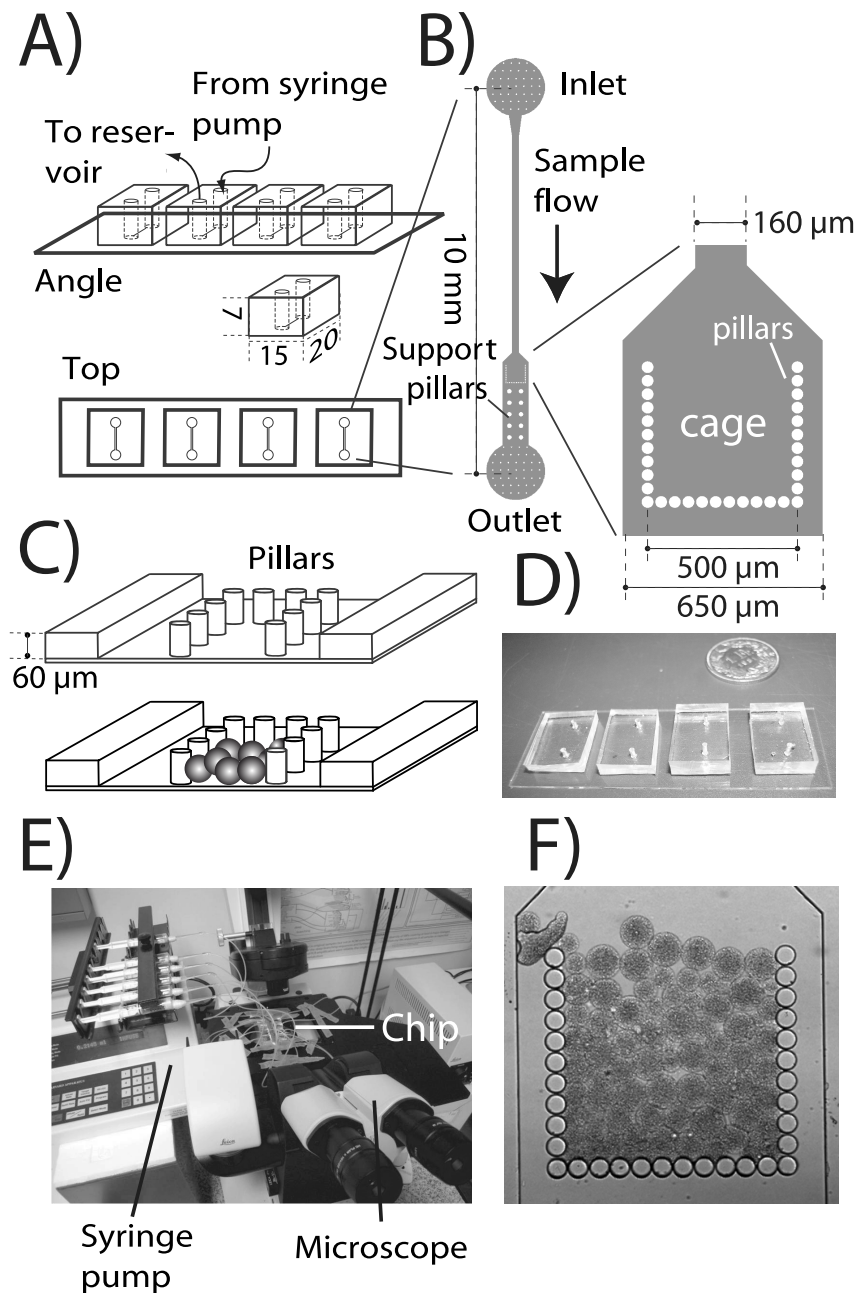


Figure 2.2: Working principle of the microfluidic chip. A) Four PDMS blocks, each containing one or four microfluidic channels, are bonded on a single glass slide. B) The channel is composed of one inlet, one outlet and a cage. Support pillars (in white) avoid collapsing of the channel. C) The cage traps the beads containing the reporter cells, while allowing sample flow through the pillars spaced at 5 μm distance. D) Picture of the four replica PDMS chips on glass (size marker is a 1 Swiss Franc piece). E) The complete setup comprises the microfluidic cartridge mounted on an epifluorescence microscope and connected to a syringe pump. F) Composed epifluorescence and phase contrast image at 200-fold magnification of the beads trapped in the cage and exposed to arsenic. Figure first published in [Buffi *et al.*, 2011a].

### 2.2.4.2 Microfabrication

The microfluidic cartridge is composed of a polydimethylsiloxane (PDMS) block containing the designed channels and cages (Figure 2.2 A-C) bonded on a typical microscopy glass slide (Figure 2.2 D). PDMS is an elastomer ubiquitous in the field of lab-on-a-chip thanks to its excellent optical and chemical properties as well as its ease of use [Whitesides, 2006]. Optical detection of the reporter signal requires the transparency of the chip, property satisfied by both glass and PDMS. The PDMS block is fabricated from a silicon mold, which contains the negative imprint of the cages and channels (Figure 2.3 A).

To fabricate the silicon mold, a 4 inch silicon wafer is structured by dry etching (Bosch process, Alcatel 601E) using a photolithographically structured AZ1512 resist (Clariant) as a mask (Figure 2.3 A). A dicing step yields the 16 individual molds contained in the wafer. Designs are made using Clewin (WieWeb) and transferred to a chrome mask by laser writing. Then, using this mask, they are transferred to the positive photoresist by selective UV exposure.

To fabricate the PDMS block, 10 g of Sylgard 184 silicone elastomer base (Dow Corning) are mixed with 1 g of Sylgard 184 silicone elastomer curing agent (ratio 10:1). Then, PDMS is degassed under vacuum for 20 minutes to remove air bubbles, poured on the silicon mold and baked for 2 h at 80°C to solidity and takes the shape of the mold. Afterwards, the PDMS is peeled off (Figure 2.3 B) and the holes connecting the in- and outlet of the channel to the external tubings are punched. In order to seal the channels, the PDMS block is irreversibly bonded on a 1 mm thick glass slide by treating the surfaces with oxygen plasma (0.6 mbar, 100 W, 1 min, Diener Electronic - Femto) and placing the imprinted PDMS surface onto the glass. One silicon mold served for several dozen PDMS blocks. In order to measure various samples simultaneously, we bond four PDMS blocks on the same glass slide (Figure 2.2 D).

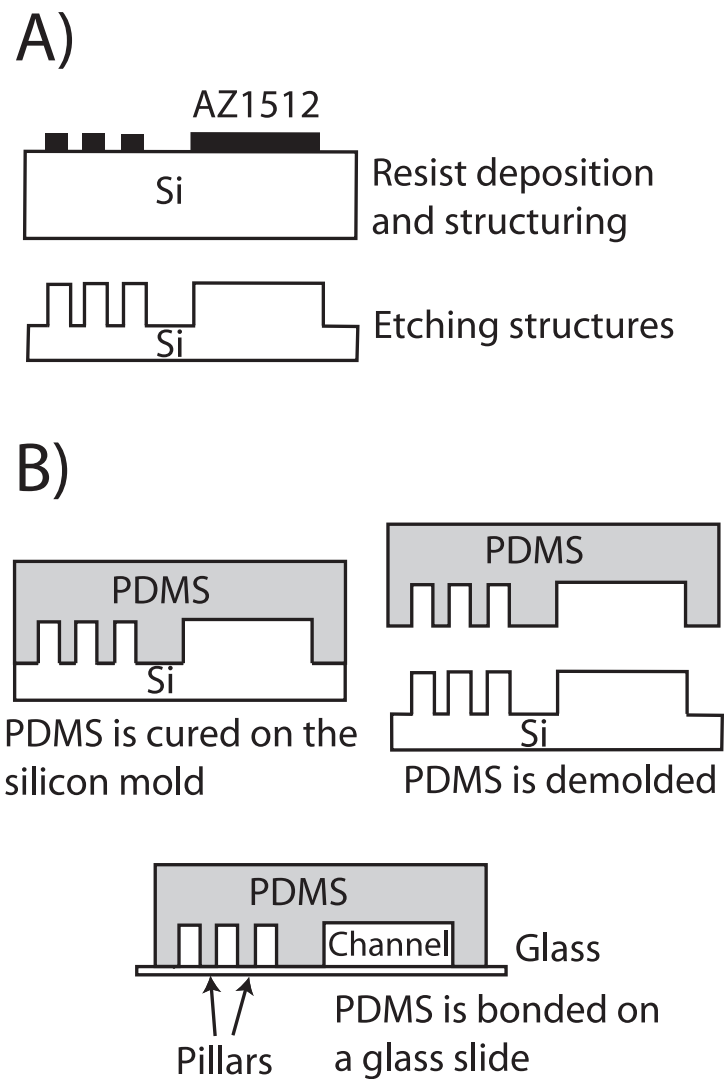


Figure 2.3: Microfluidic chip fabrication. A) Production of the silicon mold. B) Negative imprint of the mold are transferred to the PDMS layer. By demolding the PDMS layer and bonding it to a glass slide, the channels and cages are formed. Figure first published in [Buffi *et al.*, 2011a].

### 2.2.5 Beads storage

We tested two different procedures for the storage of the beads containing the reporter cells. The first consists in storing the beads solution outside the microfluidics cartridge at 4°C in the MOPS solution or at -80°C in MOPS with 15% glycerol. In this case, the beads are introduced into the cartridge when carrying out the arsenic induction assay. In the second procedure, beads are stored directly in the microfluidic cartridge. Hereto, 10 µL of beads solution in MOPS, in the case of storage at 4°C, or in MOPS plus 15% (v/v) glycerol, in the case of storage at -20°C, is filled per channel. In order to prevent evaporation, the inlets and outlets of the microfluidic cartridge are covered with Scotch tape. To test the storage effectiveness, arsenic induction of the reporter cells is periodically tested: a cartridge is removed from storage, equilibrated to room temperature and connected to the syringe pumps containing the sample solution as described in section 2.2.6. Before starting timing of the induction process, beads are flushed at high flow rate (0.5 mL/h) for 30 seconds. We noticed that during the storage time the beads do not necessarily remain within the cage, but distribute across the channel and the cage. However, they quickly perfuse back into the cage as soon as the flow is reconnected.

### 2.2.6 Arsenic induction assay

Beads are induced in the microfluidics cartridge with arsenite solutions of between 4 and 100 µg As/L and compared to MOPS medium alone as negative control. Arsenite solutions are prepared diluting in MOPS a 50 mM stock solution of sodium arsenite (NaAsO<sub>2</sub>, Merck). In the case of beads stored in the microfluidic cartridge, the tape is removed and the inlet is connected to a 5 mL plastic syringe connected to a 1.06 mm in diameter PTFE (polytetrafluoroethylene) tubing (Fisher Scientific) previously filled with the arsenic solution. In case of beads stored outside the cartridge, 50 µL of beads suspension is aspired at the tubing extremity after filling the syringe with the arsenic solution. The tubing is then connected to the inlet of the microfluidic channel in the PDMS block. In both cases, the syringe containing the arsenic solution is mounted on a syringe pump (Harvard, Pump22 Multiple Syringe Pump) and a flow rate of 50 µL/h is imposed. To collect the outgoing flow, a shorter 1.06 mm in diameter PTFE tubing glued to an eppendorf is connected to the outlet of the flow lane. Fluorescence from the cells in the beads is followed by digital microscope imaging over a time period of 200 min at 20°C.

### 2.2.7 Quantification of EGFP fluorescence

EGFP fluorescence from the bioreporter cells encapsulated in the agarose beads is imaged using a Leica DFC320 cooled black-and-white charge-coupled device camera (Leica Microsystems CMS GmbH, Wetzlar, Germany) mounted on a Leica DMI6000B inverted epifluorescence microscope. Digital images are recorded as 16-bit TIFF every 30 min with an exposition time of 260 ms using the Leica AF6000 program, at 200-fold magnification and using the GFP BP470/40 filter set (Leica). The exported images are thresholded at the background signal using ImageJ (National Institutes of Health) and then the average of the signal intensity per unit cage area is calculated. Because the fluorescence in the negative control (MOPS only) also increases slightly with time, we subtract from all averages the average fluorescence value per unit area of cage in the non-induced sample at the corresponding time point. Furthermore, in order to compare measurements across different cartridges and on different days, the average (non-induced control corrected) fluorescence for the first point of a time series is subtracted from all subsequent values. This final value is referred as "normalized fluorescence intensity" (NFI) in this report.

### 2.2.8 Viability of cells in agarose beads

To assess bacterial cell viability in agarose beads, a Live/Dead BacLight Bacterial Viability kit (Invitrogen) is used. A volume of 0.5  $\mu\text{L}$  of both SYTO 9 (green fluorescent, indicative for live cells) and propidium iodide solution (PI, red fluorescent, indicative for dead cells) is mixed with an aliquot of 250  $\mu\text{L}$  of beads suspension and incubated for 15 min in the dark. Afterwards, the cells encapsulated in agarose beads are imaged by confocal laser scanning microscopy (Leica TCSSL) with suitable optical filter sets. The proportion of live and dead cells is calculated from overlays of micrographs taken at SYTO9 or PI fluorescence wavelengths using ImageJ.

### 2.2.9 Flow cytometry measurements

Flow cytometry on a FACScalibur (Becton Dickinson, Erembodegem, Belgium) is used to independently measure the collective fluorescence of all cells in a bead induced or not with arsenite at different concentrations. Beads aliquots of 120  $\mu\text{L}$  that have been stored at  $-80^{\circ}\text{C}$  are thawed and resuspended in MOPS medium, and then exposed in a final volume of 1 mL

to concentrations of between 4 and 100  $\mu\text{g As(III)/L}$  (diluted from the 50 mM stock in MOPS medium). The mixture is incubated in 10 mL glass tubes for up to 3 hours at 30°C with 180 rpm rotary shaking. Samples were retrieved after 2 and 3 h for flow cytometry analysis. EGFP expression is analyzed per individual bead and is expressed as the mean green fluorescence intensity (FL1-H, log-scale) as function of arsenite concentration ( $\mu\text{g/L}$ ).

### 2.2.10 Kinetics

In order to determine the rate of increase of the EGFP fluorescence in the biosensor assays as a function of arsenite concentration, we fit the data using the function  $\ln(FN_{beads}) = \alpha_{beads} \cdot t + c_{beads}$ , where  $\alpha_{beads}$  is the slope,  $c_{beads}$  is a constant, and  $FN_{beads}$  the normalized fluorescence intensity as function of time  $t$ .

## 2.3 Results

### 2.3.1 Microfluidic cartridge

The microfluidic cage effectively traps and concentrates a constant amount of beads containing the reporter cells (Figure 2.2 F) and it takes less than 1 minutes to fill it. The in- and outflow channels, designed with a height of 60  $\mu\text{m}$ , cause no restriction to the beads even though they have a diameter range of 40-70  $\mu\text{m}$ . Bonding four PDMS blocks with between one and four lanes each on one glass slide, it was possible to measure various samples simultaneously (Figure 2.2 A, D).

### 2.3.2 Sensitivity of the bioreporter assay to arsenite

Figure 2.4 A shows the increase of the mean EGFP fluorescence per unit of cage surface resulting from the induction of the cells within freshly made beads as a function of assay incubation time and at two sodium arsenite concentrations, 10 and 50  $\mu\text{g As/L}$ , compared to a control without arsenite. An induction period of 60 minutes was sufficient to significantly distinguish the EGFP fluorescence signals in both 10 and 50  $\mu\text{g As/L}$  from the negative control (Table 2.2). Different batches of cell-beads stored for less than one day at 4°C varied slightly in the absolute signal output at the same induction time and arsenic concentration, which was due to differences in the amount of encapsulated cells (not shown). The mean fluorescence per unit



of cage surface measured after 200 minutes increases linearly proportionally to the arsenite concentration between 0 and 50  $\mu\text{g As/L}$  ( $r^2=0.9576$ ) and for higher concentrations it saturates (Figure 2.6). This behavior may be due to the saturation of the detector (standard exposure setting of the microscope camera) rather than the saturation of the inducible response of the cells. Flow cytometry analysis of beads showed a relatively wide range of bead sizes and individual beads mean fluorescence values (Figure 2.5 E). By inspecting reporter cells within individual beads using laser scanning microscopy, we observed a regular distribution of cells (Figure 2.5 A-D) and similar induction levels (not shown). For instance, we did not observe regions within the beads where cells would not respond (i.e., in the innermost part). Therefore, we can conclude that the process of immobilization and the diameter or material of the beads do not inhibit the reporter cells in their response.

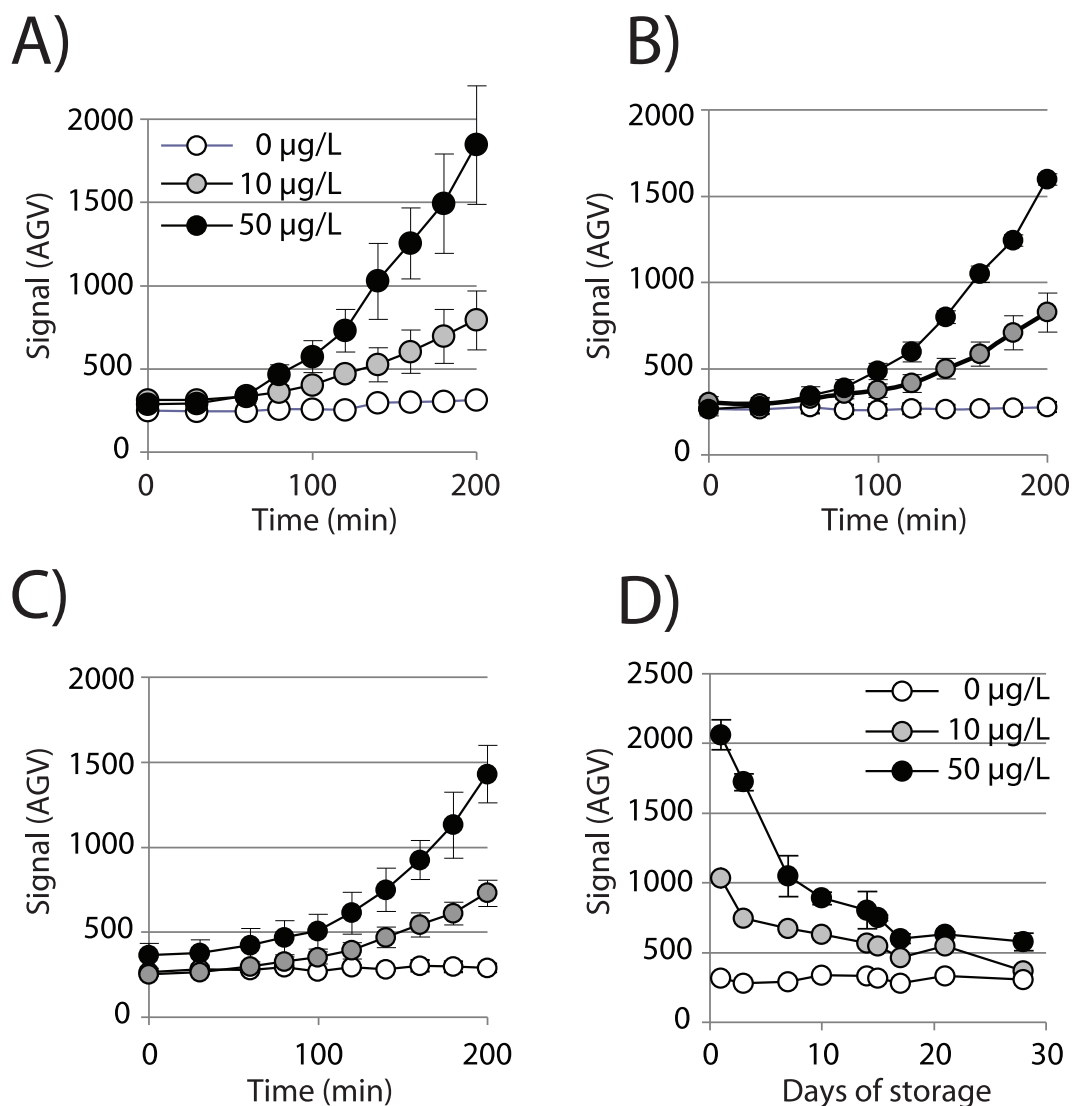


Figure 2.4: Raw fluorescence intensities as function of time and arsenite concentration for differently stored beads. A) Beads stored outside the chip for 1 day at 4°C. B) and C) Beads stored on chip at -20°C for 3 and 7 days, respectively. D) Raw fluorescence intensities after 200 minutes of assay incubation in the microcage as function of storage days at -20°C and arsenite concentrations. All data are averages from triplicate assays simultaneously carried out in a four-lane PDMS chip. Error bars denote calculated deviations from the average. Error bars not shown are smaller than the symbol size. Figure first published in [Buffi *et al.*, 2011a].

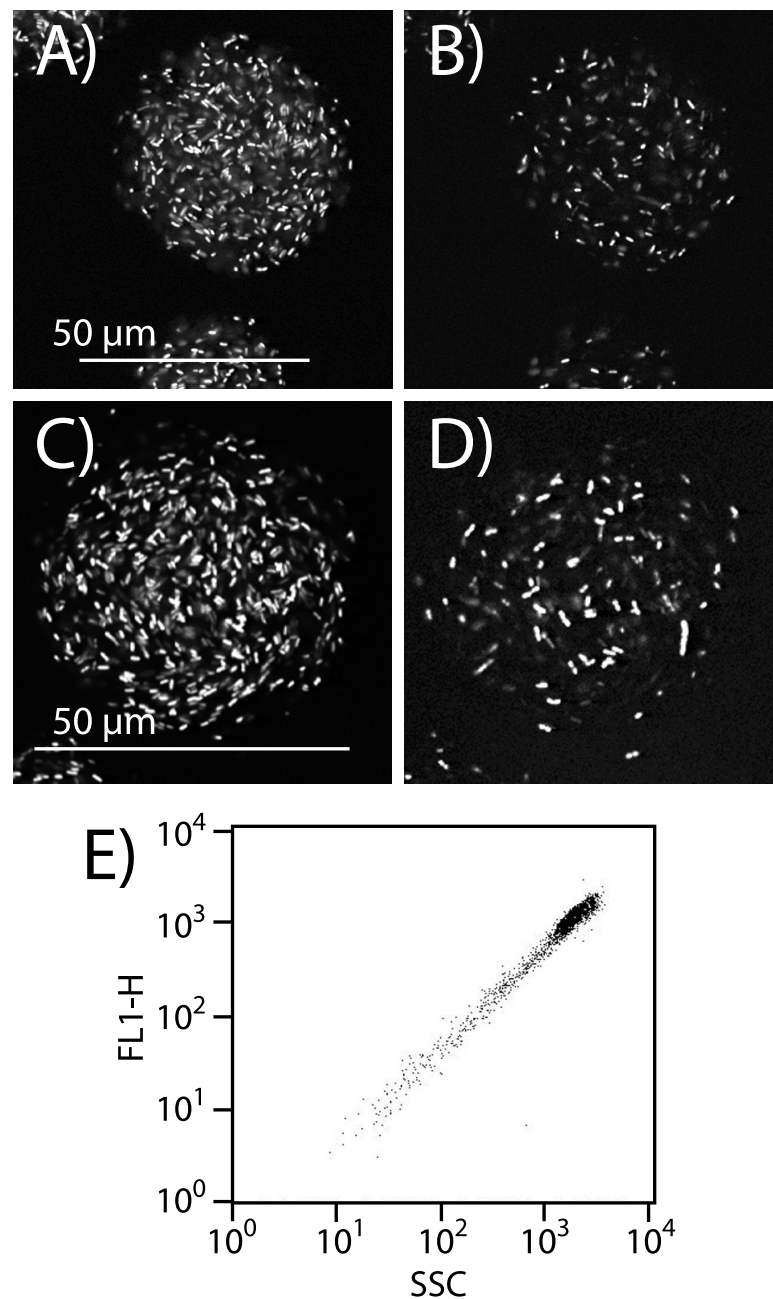


Figure 2.5: Viability and fluorescence variability of cells in beads. A) Reporter cells in beads stored at 4°C for 4 days stained with SYTO9 (indicative for being alive). B) Idem, stained with PI (indicative for being dead). C) Reporter cells in beads stored at -80°C and stained with SYTO9. D) Idem stained with PI. E) Flow cytometry scatterplot showing fluorescence of beads (FL1) versus side-scatter, an indicator of bead size and granularity (SSC). All cells in beads were induced in the microcage with 10 μg As/L for 120 min. Images A-D, confocal laser scanning microscopy. Figure first published in [Buffi *et al.*, 2011a].

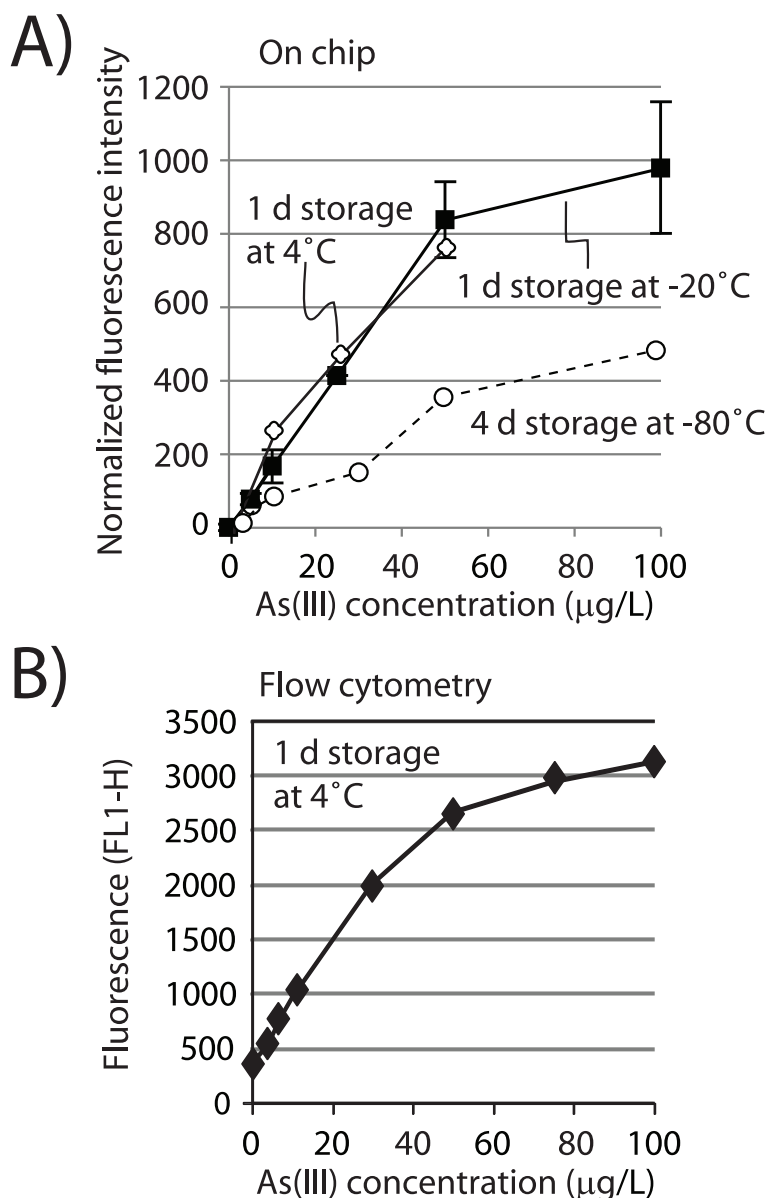


Figure 2.6: Signal calibration as a function of arsenic concentration based on the 200 min end point measurement. A) Calibration curves obtained for beads in microcages after storage outside the chip for 1 day at 4°C (open diamonds, single flow lane analysis), after storage on chip for 1 day at -20°C (closed squares, triplicate lane analysis), or after storage outside the chip for 4 days at -80°C (open circles, single flow lane analysis). B) Calibration curve obtained with beads stored outside the chip for 1 day at 4°C using triplicate suspension assays and flow cytometry analysis of bead fluorescence. Error bars indicate calculated deviation from the average. In case error bars are not visible they are smaller than the symbol size (except for the open diamonds and circles, which are single lane assays). Figure first published in [Buffi *et al.*, 2011a].

Assay <sup>d</sup> time (min)	MDL $\mu\text{g As/L}$ <sup>a</sup>					RSD % <sup>b</sup>					Sensitivity % <sup>c</sup>				
	78 <sup>e</sup>	108	138	168	198	78	108	138	168	198	78	108	138	168	198
<b>Cage, 4°C (1 d, out)</b>	0.5	1.1	1.2	1.3	1.8	7.3	10.7	11.1	11.7	13.4	ND	121.7	139.0	165.2	176.6
<b>Cage, -80°C (4 d, out)</b>	12.7	6.6	1.6	0.6	1.2	70.2	36.7	25.8	17.7	16.4	ND	116.0	116.0	128.6	147.0
<b>Cage, -20°C (4 d, in)</b>	258	6.4	ND	1.7	1.6	184	17.7	ND	6.2	4.4	104.3	116.3	ND	147.9	162.1
<b>FC, -80°C (4 d, out)</b>	ND <sup>f</sup>	ND	ND	8.4	ND	ND	ND	ND	8.4	ND	ND	ND	ND	208.5	ND

Table 2.1: Figures of merit for the bead configuration after different storage conditions and measurement instrumentation. a) MDL, method detection limit. Calculated as the arsenite concentration corresponding to a sample with normalized fluorescence of that in the blank plus three times the standard deviation in the blank. b) RSD, relative standard deviation. Calculated as the average percent deviation in NFI across all samples compared to the calculated NFI according to the linear regression trend function. c) Sensitivity. Calculated as the percent increase of NFI at 10  $\mu\text{g As/L}$  compared to the value in the blank at that time point. d) Cage, beads in microfluidics cage imaged with epifluorescence microscopy. FC, cell-bead signal measured by flow cytometry. 4°C, -80°C, -20°C, storage temperature of beads; "out": storage outside chip; "in": storage inside chip. e) Time of analysis after beginning of exposure of cell beads with arsenite (minutes). f) ND, not determined. Table first published in [Buffi *et al.*, 2011a].

### 2.3.3 Effect of storage conditions

We tested two different procedures for the storage of the beads containing the bioreporter cells. The first method consists in storing the beads outside the microfluidics cartridge (4°C and -80°C), while in the second technique the beads were stored within the flow lanes of the cartridge (4°C and -20°C). We found that the PDMS-glass cartridge could not withstand freezing and thawing at -80°C.

#### 2.3.3.1 Storage outside the microfluidic cartridge

Cells in beads stored at 4°C quite rapidly lost inducibility: although the cells still reacted after 12 days of storage, the calculated NFI after 200 min in response to 10 µg As/L decreased by a factor 15, with the most rapid decline between day 2 and 5 (Figure 2.7 C). After 9 days, the measurement variability prevents the reliable differentiation of a concentration of 10 µg As/L from the negative control.

In contrast, beads stored at -80°C retained inducibility much better. An important initial decrease in inducibility occurred directly as a result of freezing, but afterwards the EGFP fluorescence developed at approximately the same kinetics for storage periods of up to 14 days (Figure 2.8). In order to determine whether this lower response is due to a decrease of the number of viable bacteria within beads after -80°C freezing and thawing, we imaged beads stored at 4°C, -20°C and -80°C and stained them with the Live/Dead BacLight bacterial viability assay. However, this test showed that more or less independently from the storage temperature, cells in beads contained about 20% of cells staining PI positive (indicative for being dead) (Figure 2.5 A-D).

The increase of EGFP fluorescence signal from -80°C stored beads after 200 min induction time even at single-lane measurements was linearly proportional to the arsenic concentration ( $r^2=0.9674$ ) but with a maximum of five-fold induction (Figure 2.6 A). The calculated standard deviation in NFI values for beads batches prepared at different times but stored in the same conditions for the same time period, and assayed with 10 µg As/L for 200 min at room temperature in the microcages, was 20% (data not shown).

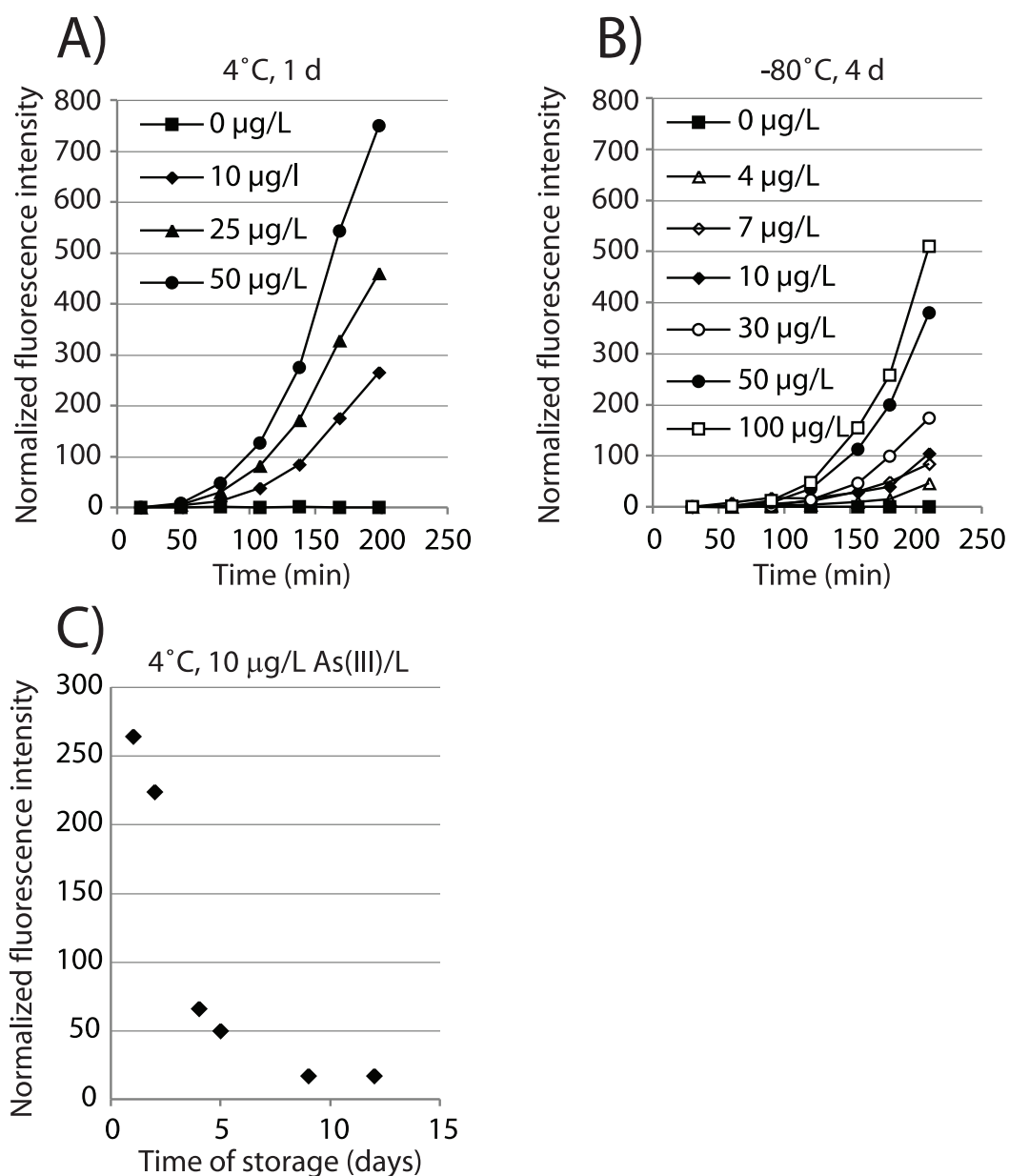


Figure 2.7: Biosensor performance data for 4°C and -80°C stored cells in beads outside the microfluidics chip. A) Normalized EGFP response from cells in beads stored at 4°C for 1 day and exposed to different arsenite concentrations as a function of incubation time (single lane experiment). B) Idem, but with beads stored at -80°C for 4 days. C) Decrease of signal after 200 min with 10 µg As/L in case of 4°C stored cells in beads. Figure first published in [Buffi *et al.*, 2011a].

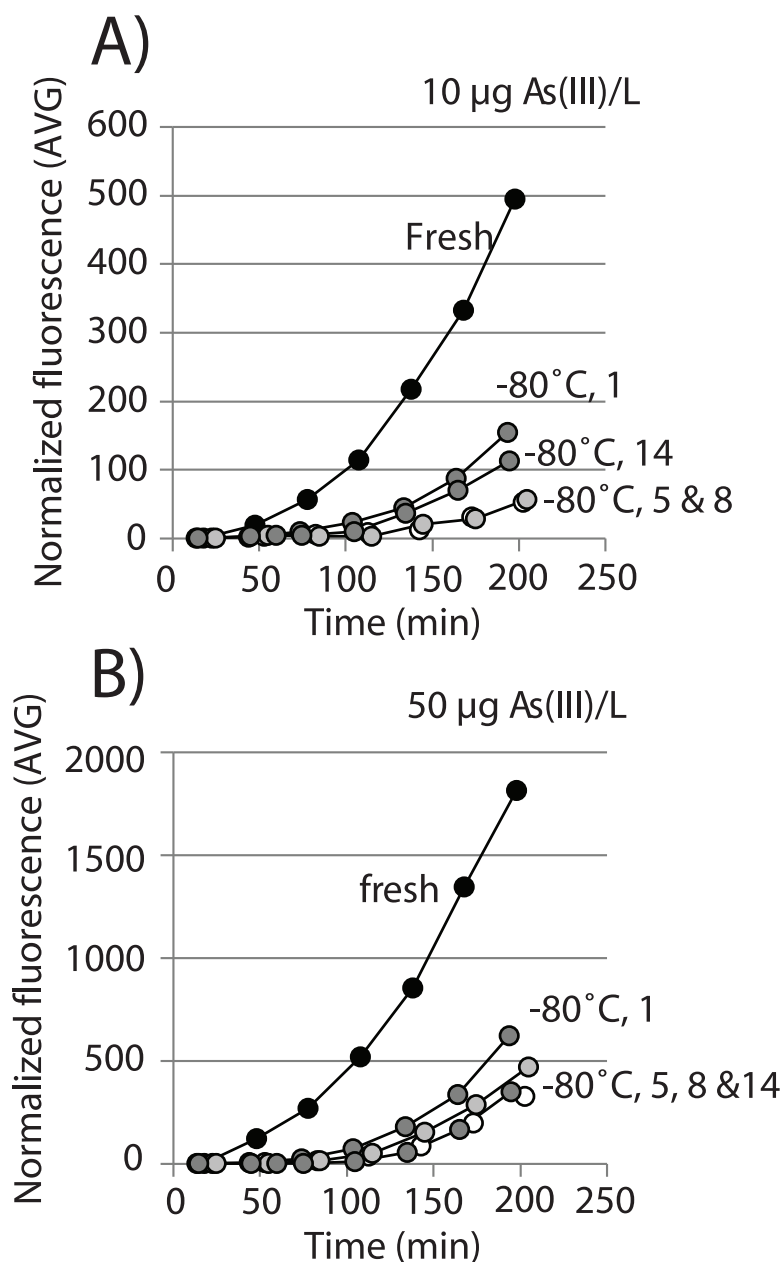


Figure 2.8: Effect of storage of beads at  $-80^{\circ}\text{C}$  on signal development in response to arsenic. A) Normalized fluorescence intensity of beads in microcages exposed to  $10\ \mu\text{g As/L}$  as a function of incubation time, for batches stored for different time periods (fresh, 1, 5, 8 or 14 days, as indicated). B) Idem, for beads exposed to  $50\ \mu\text{g As/L}$ . Data points derive from microcage experiments using a single flow-line (estimated error  $\sim 15\%$ ). Figure first published in [Buffi *et al.*, 2011a].



### 2.3.3.2 Storage in the microfluidic cartridge

We then examined inducibility of bioreporter cells encapsulated in beads prepared in the same batch and stored within the microfluidic chip at either 4°C or -20°C for periods of up to one month. Storage at 4°C resulted in a rapid decrease of inducibility down to undetectable levels (not shown). In contrast, beads stored at -20°C performed much better: although a decrease in signal development over storage time (Figure 2.4 B-D), the contained reporter cells retained inducibility at least until day 28. Kinetic data suggest that this decrease was mainly due to a time delay in the onset of induction (Figure 2.9) and the time needed to significantly discriminate a signal of 10 or 50 µg As/L from the blank increases with prolonged storage time (Table 2.2). As before, calibration curves for beads stored in the microcartridge at -20°C were almost linear in the range of 0-50 µg As/L ( $r^2=0.9997$ ) and saturate after this concentration (Figure 2.6). The calculated method detection limit (MDL) based on signal intensity after 200 min equalled 1.6 µg As/L (Table 2.1).

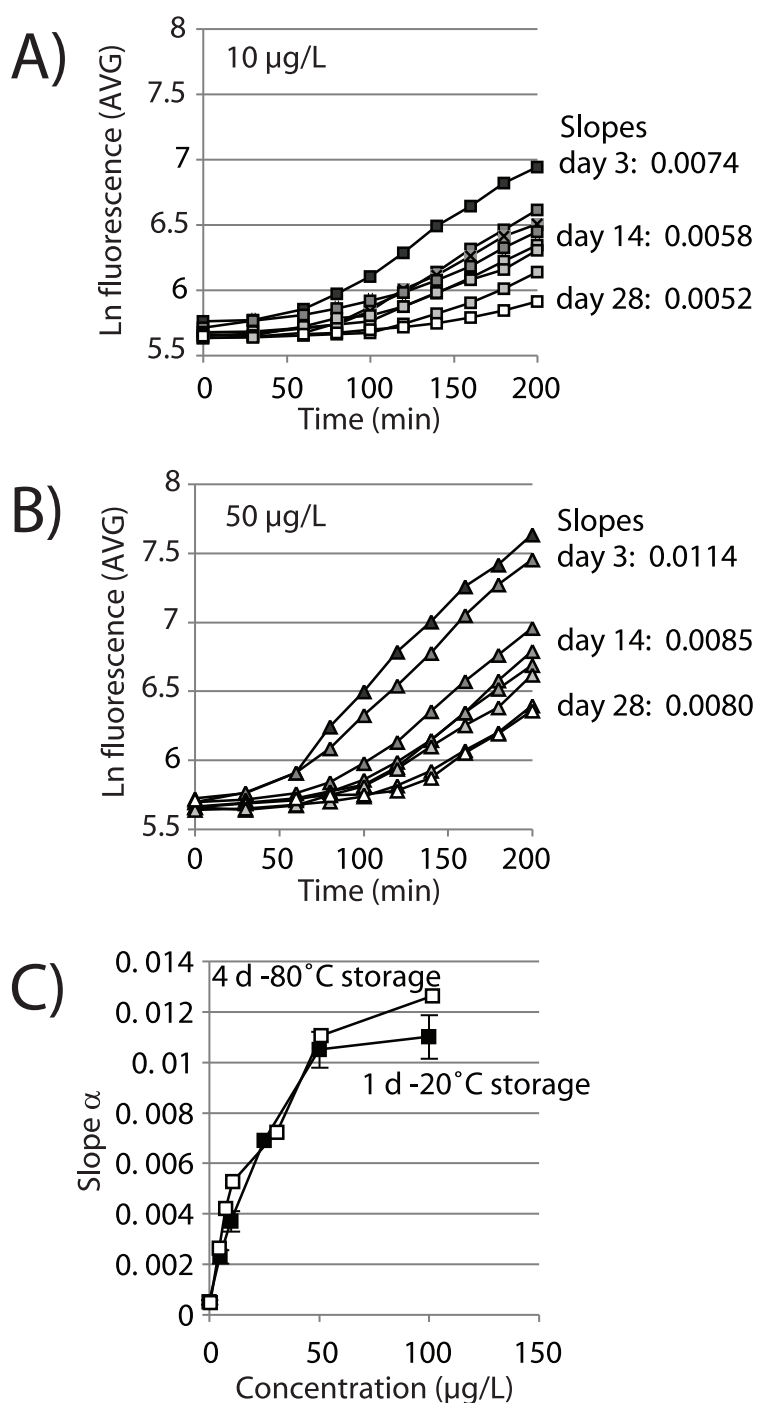


Figure 2.9: Kinetics of signal development in assays with stored beads. A) Semi-ln transformed signal intensities of beads exposed to 10 µg As/L over prolonged storage times on chip at -20°C. Relevant slope values for the "linear" increasing parts of the curves are shown. B) As for (A) but at 50 µg As/L. C) Calibration curve of calculated slopes as a function of arsenite concentration, for cell-beads stored at -20°C on chip (triplicate assays, closed squares) or for cell-beads stored at -80°C outside the chip (single lane assays, open squares). Figure first published in [Buffi *et al.*, 2011a].

Storage (days)	Minimum time to discriminate from background <sup>a</sup>		Pair-wise comparison of rate of signal development calculated over time interval <sup>b</sup>								
	10 µg As/L	50 µg As/L	60-120 min			60-200 min			140-200 min		
			0 vs 10 <sup>c</sup>	10 vs. 50	0 vs. 50	0 vs 10	10 vs. 50	0 vs. 50	0 vs 10	10 vs. 50	0 vs. 50
1	60	60	P<0.05	P<0.05	P<0.05	P<0.05	P<0.05	P<0.05	P<0.05	P<0.05	P<0.05
3	100	80	P<0.05	P<0.05	P<0.05	P<0.05	P<0.05	P<0.05	P<0.05	P<0.05	P<0.05
7	100	60									
10	120	120									
14	120	120	P<0.05	P>0.05	P<0.05	P<0.05	P<0.05	P<0.05	P<0.05	P<0.05	P<0.05
17	60	60									
21	160	120									
28	200	140	P>0.05	P>0.05	P>0.05	P<0.05	P<0.05	P<0.05	P<0.05	P<0.05	P<0.05

Table 2.2: Discrimination parameters for beads stored at -20°C. a) Triplicate simultaneously analysis of flow lanes. b) Rate parameter  $\alpha$ , obtained from linear regression on Ln-transformed signal intensities within the indicated time interval of the induction assay. Pair-wise comparison in two-sided T-test with unequal variance on triplicate data sets. c) 0 vs 10, slopes from the blank compared to 10 µg As/L; 10 vs 50, 10 µg As/L versus 50 µg As/L; 0 vs 50, blank versus 50 µg As/L. Table first published in [Buffi *et al.*, 2011a].

### 2.3.4 Response kinetics

The signal development over time seemed relatively constant for frozen beads batches (on chip at  $-20^{\circ}\text{C}$  or outside chip at  $-80^{\circ}\text{C}$ ) and thus we decided to investigate the kinetic response data as a function of storage time and arsenic concentration. We determined the slope of the signal increase in a semi-log plot and we found that in the range of  $0\text{-}50\ \mu\text{g/L}$  it correlates linearly proportionally to the arsenic concentration (Figure 2.9 C). We found similar slopes for independently stored beads batches at  $-80^{\circ}\text{C}$  outside chip and at  $-20^{\circ}\text{C}$  on chip. However, signal slopes coming from beads stored at  $-20^{\circ}\text{C}$  on chip decreased by  $\sim 30\%$  during one month with the most dramatic decrease in the first 7 days (Figure 2.9 A and B).

Then we calculated the time needed to differentiate a certain arsenite concentration from the blank using the kinetic response. In most cases in the time window 60-120 min of induction 10 and  $50\ \mu\text{g As/L}$  could be differentiated from the blank or from each other by a significantly different slope, except at 28 days storage (Table 2.2). Due to the delayed response, at longer storage times the kinetic windows needs to be shifted (e.g., 140-200 min) in order to obtain a better discrimination (Table 2.2). Standard deviations on the slopes for the 60-200 time window for triplicate values were slightly better than for end-point at 200 min values (10%).

### 2.3.5 Pre-incubation

Considering the  $-20^{\circ}\text{C}$  storage on chip, we observed two effects that, over prolonged storage periods, lead to a decrease in the reporter signal development over time of induction. The main one is the increase of the time delay before the reporter signal development starts, and the second one is the decrease of the rate of signal increase (Figure 2.4 D and 2.9 A-B). Moreover, imaging of beads stained for live or dead cells did not indicate a significant increase in the number of dead cells during storage and this suggests that cells remained alive but somehow lost their potential to become induced with arsenic. We thus decided to investigate whether certain nutrients would become limiting over time in the storage solution. In our standard procedure cells in beads were stored in MOPS: a mineral salts buffered medium with 15% glycerol and with glucose to energize the cells, which however lacks thiamine and further organic micronutrients to prevent reporter cell division within beads. Therefore, we tested whether pre-incubating cells in beads after thawing of a  $-20^{\circ}\text{C}$  frozen PDMS chip with organic micronutrients would be sufficient to reactivate them. We flushed the cages for 30 minutes

with 10  $\mu$ L of rich LB medium before exposing cells in beads to an aqueous arsenic sample. Indeed, we found that this procedure effectively recovers the reactivation potential of the cells: with the batch of beads used for this experiment, after 2 weeks of storage at  $-20^{\circ}\text{C}$ , we were barely able to distinguish 0, 10 and 50  $\mu\text{g}$  arsenite per L, while adding the pre-incubation step with LB we could discriminate the three concentrations even after one month (Figure 2.10). More precisely, LB pre-incubating resulted in a much shorter time delay in the onset of detectable EGFP signal development. However, the decrease of the rate of signal increase can not be avoided and thus the problem of the decrease of the the reporter signal development over time of induction can not be completely solved.

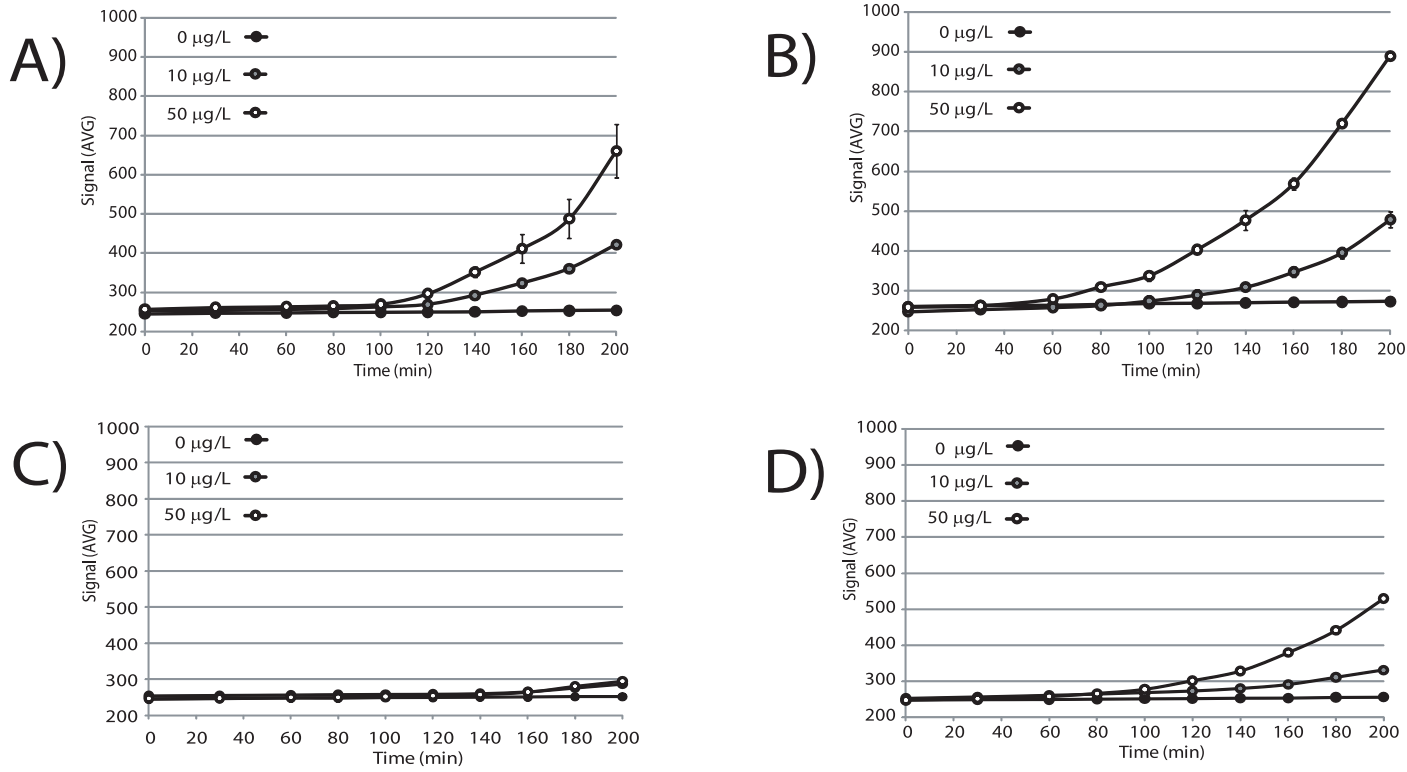


Figure 2.10: Effect of pre-incubation with LB medium on the reporter development of cells in beads in response to arsenic. A) Beads stored for 7 days at  $-20^{\circ}\text{C}$ , measurement without LB pre-incubation step. B) Idem, with pre-incubation step. C) Beads stored for 14 days at  $-20^{\circ}\text{C}$ , measurement without pre-incubation step. (D) Beads stored for 28 days at  $-20^{\circ}\text{C}$ , measurement with LB pre-incubation step. All data are averages from triplicate assays simultaneously carried out in a four-lane PDMS chip. Error bars denote calculated deviations from the average. Error bars not shown are smaller than the symbol size.

### 2.4 Discussion

In our system, we chose to embed reporter cells in agarose beads according to a procedure previously mentioned [Zengler *et al.*, 2002]. Agarose beads satisfy all the conditions needed for bioreporter cells encapsulation and microcage measurements: 1) they do not crash when they are handled on chip; 2) agarose is a very porous polymer allowing easy diffusion of arsenite and nutrients needed for the cells; 3) agarose is transparent and it does not pose any problem for optical observation. Furthermore, the amount of cells per bead is easily tunable by changing the concentration of cells in the original suspension.

There exists different methods for bacterial cell encapsulation, such as alginate [Fesenko *et al.*, 2005], sol-gel matrices [Premkumar *et al.*, 2002] and agar [Lee *et al.*, 2005]. Automated methods for cell encapsulation exist as well, which make use of DNA-arraying instruments that deposit and immobilize nanodrops of cells suspensions [Tani *et al.*, 2004; Bolton *et al.*, 2002]. However, our procedure has the advantage of being cheap, of not needing complicated equipment and of producing very small beads suitable for use in microfluidics devices.

Starting from one silicon mold, the PDMS device can be easily constructed, and hundreds of identical chips can be fabricated inexpensively. Moreover, thanks to PDMS flexibility, the chip can be easily connected to external tubings. The disadvantage of PDMS for bioreporter assays is that organic target compounds may directly interact with the material and be "lost" for the analysis. However, arsenite and heavy metals would rather adsorb to glass than to plastics and we did not find any indications for loss of arsenite through adsorption to PDMS.

In order to trap cells using a microfluidic chip, different structures have been proposed: U-shaped traps [Wu *et al.*, 2008], dam structures which retain cells along the channel by defining a net cross flow over the dam [Mengsu *et al.*, 2002], and microwells on the bottom of a channel that can capture cells by sedimentation [Khademhosseini *et al.*, 2004] or by capillary force [Park *et al.*, 2008]. The advantage of our pillar-made microcage is that it only requires one etching step and is thus very simple to fabricate. It fills with a constant number of beads, which makes them undergo the same conditions in terms of nutrients and arsenite distribution during each experiment, and it allowed us to concentrate beads in a small space where the fluorescence obtained was easily quantified.

With our device, we were able to discriminate arsenite concentrations in the range of 0-100

## Chapter 2. Agarose beads system

---

$\mu\text{g As/L}$  with a calculated method detection limit (MDL) of 1-1.6  $\mu\text{g As/L}$ . Previously, assays with this particular bioreporter strain resulted in MDLs between 5 and 8  $\mu\text{g As/L}$  after 2 h incubation when the signal was measured with steady state fluorimetry or epifluorescence microscopy on single cells [Wells *et al.*, 2005]. This shows that the microfluidics cage method provides an improvement and allows more confident measurements of arsenite samples below 10  $\mu\text{g As/L}$ . However, we think that its main advantage lays in a simplified liquid handling and prefilling system for bioreporter tests.

In terms of measurement errors, fluorescent signals produced by arsenite-exposed beads from a single batch that had been stored at  $-80^{\circ}\text{C}$  showed an average deviation of 15%. Batch to batch variations in beads preparations resulted in variations of 20% on the NFI obtained with the same arsenite concentration and the same induction time. The overall average relative standard deviation (RSD) over all measurement points of the arsenite response curve is slightly better for the  $-20^{\circ}\text{C}$  stored beads on chip (4-6% after 180 min) than for the  $4^{\circ}\text{C}$  stored beads (a little over 10%, more or less independent of the incubation time), and the  $-80^{\circ}\text{C}$  stored beads (a little over 15% after 168 min, Table 2.1). For the  $-20^{\circ}\text{C}$  stored beads on chip (triplicates) this is in the order of RSDs previously calculated for steady state fluorimetry measurements (on six replicates) [Wells *et al.*, 2005]. This RSD shows that fewer calibrations would be sufficient to accompany each sampling series. Thus, a four-lane microfluidics cartridge with one lane for a calibration standard and the other three lanes for the sample to be analyzed is a feasible system.

This biosensor can be used in two different modes. The first consists in endpoint measurements: 100 - 200 min assay time is sufficient to obtain an MDL of 1.6  $\mu\text{g As/L}$  in the case of beads stored at  $-20^{\circ}\text{C}$  for 1 day and for beads stored at  $-80^{\circ}\text{C}$  (Table 2.1). Of course, longer incubation improves the sensitivity of the signal at 10  $\mu\text{g As/L}$  up to around 170% for all storage conditions (Table 2.1). Another possibility is the continuous monitoring of the fluorescence signal produced by the bioreporter cells within beads over time. In this case the relationship between the fitted slope of ln-transformed signal intensities ( $\alpha$ ), which can be estimated at any incubation time point subsequent to time zero from the preceding points, and arsenite concentration is considered (Figure 2.9). For most measurements the induction interval 60-120 min is sufficient to significantly discriminate the slopes at 10 and 50  $\mu\text{g As/L}$  from each other and from the blank (Table 2.2). Likely, when more measurements can be performed at shorter time intervals than in this case (60 min), the rate parameter can be estimated correctly



after a shorter total incubation period. In this case analysis of samples can be stopped as soon as the rate parameter is reliably estimated, which could save time. The fact that beads can be prefilled and stored at  $-20^{\circ}\text{C}$  up to one month before use in the microfluidics cartridge with satisfactory performance in terms of discriminating concentrations of 0, 10 and  $50\ \mu\text{g As/L}$  is a crucial step forward to make the use of such chip devices possible in a field situation. In fact, a common freezer is sufficient to preserve the devices and, as handling of the beads is not required anymore, it is potentially utilizable by a user who is not familiar with the laboratory techniques. Furthermore, if necessary, long-term maintenance and inducibility of reporter cell-beads can be achieved by freezing in 15% glycerol at  $-80^{\circ}\text{C}$ , from where they can be easily reintroduced into the microcages.

## 2.5 Conclusions and outlook

### 2.5.1 Summary of results

We designed a microfluidics cartridge able to contain bacterial bioreporter cells, to expose them to liquid arsenic-containing samples and to obtain an easy read-out of the signal. In order to trap the reporter cells in the microfluidics cage we embedded them in  $40\text{-}70\ \mu\text{m}$  agarose beads. The microcage was filled with beads in less than 1 minute, allowed exposure of the reporter cells to arsenite, and permitted a signal amplification as a result of hundreds of beads accumulating at one position. With this system, we were able to reliably and reproducibly discriminate arsenite concentrations in the range of  $0\text{-}100\ \mu\text{g}$  in less than 200 min with a detection limit of  $1\text{-}1.6\ \mu\text{g As/L}$ , well below the current drinking water limit of  $10\ \mu\text{g As/L}$ . We tested two potential storage methods: outside (at  $4^{\circ}\text{C}$  or at  $-80^{\circ}\text{C}$ ) or inside the chip (at  $4^{\circ}\text{C}$  or at  $-20^{\circ}\text{C}$ ). Bioreporter cells within beads withstand well the freezing process, showing a loss of only  $\sim 20\%$  viability. EGFP signal development remained highly reproducible for beads stored at  $-80^{\circ}\text{C}$ , whereas it decreased for prolonged storage at  $-20^{\circ}\text{C}$ . We showed that this decrease could be reduced with a LB pre-incubation step. Storage at  $4^{\circ}\text{C}$  for a few days resulted in loss of inducibility at  $10\ \mu\text{g As/L}$ . For practical importance, beads could be prefilled and stored at  $-20^{\circ}\text{C}$  up to one month before use in the microfluidics cartridge with satisfactory performance in terms of discriminating concentrations of 0, 10 and  $50\ \mu\text{g As/L}$ .

### 2.5.2 Perspectives

The extremely simple device that we developed is a crucial step forward to the development of a cheap in-field arsenic measurement device: the fabrication of microfluidics chips from a mold is relatively inexpensive with one silicon mold serving for more than one hundred chips, chips have replicate flow-lines, increasing the accuracy of the measurement, and also from the biological point of view the costs are extremely low because from a single batch of beads produced from 0.2 mL of cell culture one can fill more than 20 chips. The next steps in order to achieve the project goal of a simple complete arsenic biosensor instrument for in-field analysis, are the development of an optical detection system and the construction of an instrument housing the microfluidics cage. In order to overcome the drawback of the decrease in reporter signal development over storage time, one solution could be to work with freeze-dried reporter cells [Siegfried *et al.*, 2012]. The problem is that, depending on the type of cells, freeze-drying may result in considerable amounts of dead cells [Bjerketorp *et al.*, 2006]. Another solution could be a chip containing a microchemostat, which produces a continuous supply of fresh cells used for the reporter assay. This possibility is investigated in chapter 4.

## **3 Free cells system**

### **3.1 Introduction**

One of the possibilities to overcome the drawback of the signal decrease upon storage time presented by the agarose beads system, is the development of a chemostat on chip, which would produce a continuous supply of fresh cells. However, before the development of such a system, there are some preliminary steps that need to be fulfilled. First of all, the development of a chip in which it is possible to trap and expose to arsenic bioreporter cells instead of bioreporter cells encapsulated in agarose beads. This chapter focuses indeed on this approach: it starts describing the materials and methods used for the development of this so-called "free cells system" and subsequently it presents the results obtained in terms of functioning of the chip, as well as in terms of sensitivity of bioreporter cells to arsenite. In particular, the method used for the single cells trapping is illustrated in detail. The last section is dedicated to the discussion of strengths and limitations of this approach.

### **3.2 Materials and methods**

#### **3.2.1 Microfluidic cartridge design and microfabrication**

In order to trap and expose the bioreporter cells to arsenic-containing aqueous samples, we designed a straight channel with a filter wall between the inlet and the outlet, whose outflow dimensions are so small that most of the cells cannot escape but sample flow can still occur (Figure 3.1 B and C). The chip itself is composed of a PDMS block bonded on a transparent

### Chapter 3. Free cells system

---

glass slide with a thickness of 1 mm (Figure 3.1 A and D). The channel has a height of 20  $\mu\text{m}$ , whereas the filter outlet channels were designed with a height of 700 nm, obstructing *E. coli* cell passage, which have a diameter of 1  $\mu\text{m}$  and a length of 2-5  $\mu\text{m}$  (Figure 3.1 C). The number of filter pores is between 6 and 10. The flow is driven by air pressure.

For the PDMS block fabrication a silicon mold, which contains the negative imprints of the channels and the filters, is prepared (Figure 3.2 A). To fabricate the mold, a silicon wafer is structured by two dry etching steps (Bosh process, Alcatel 601E) using a photolithographically structured AZ1512 resist (Clariant) as a mask. The first step consists in the fabrication of the negative of the filter structures, while the second in its transfer downwards to define the negative of the channels. The etching depth, besides on the etching time, also depends on the surface area to be etched and, for a given time, a bigger area will be etched deeper [Center of micronanotechnology (CMI) at Swiss Federal Institute of Technology (EPFL), 2012]. This behavior is observable especially when comparing etching depths of surfaces  $< \sim 50 \times 50 \mu\text{m}^2$ , while for larger areas the depths are not significantly different (at least for our application). For this reason, to be sure that the filter wall depth corresponds to the one of the channels walls, which have a surface of several order of magnitude bigger, we designed different filter walls areas (length between 5 and 100  $\mu\text{m}$ , Figure 3.3).

The PDMS block is prepared from a liquid PDMS mixture containing 60 g of Sylgard 184 silicone elastomer base (Dow Corning) and 1 g of Sylgard 184 silicone elastomer curing agent (ratio 10:1). Then, the PDMS is degassed under vacuum for 20 minutes to remove air bubbles, poured on a full 4 inch wafer containing 20 silicon mold and baked for 2 h at 80°C and takes the shape of the molds. Afterwards, the PDMS is cut to have individual blocks, peeled off (Figure 3.2 B), and the holes connecting the in- and outlet of the channel to the external tubings are punched. In order to seal the channels, the PDMS block is irreversibly bonded on a 1 mm thick glass slide by treating both surfaces with oxygen plasma (0.6 mbar, 100 W, 1 min, Diener Electronic - Femto) and placing the imprinted PDMS surface onto the glass (Figure 3.2 C). To be able to test in triplicate three different arsenic concentrations at the same time, four PDMS blocks containing four lanes each are bonded on the same glass slide for a total of twelve lanes that can be run in parallel (Figure 3.1 D and E).

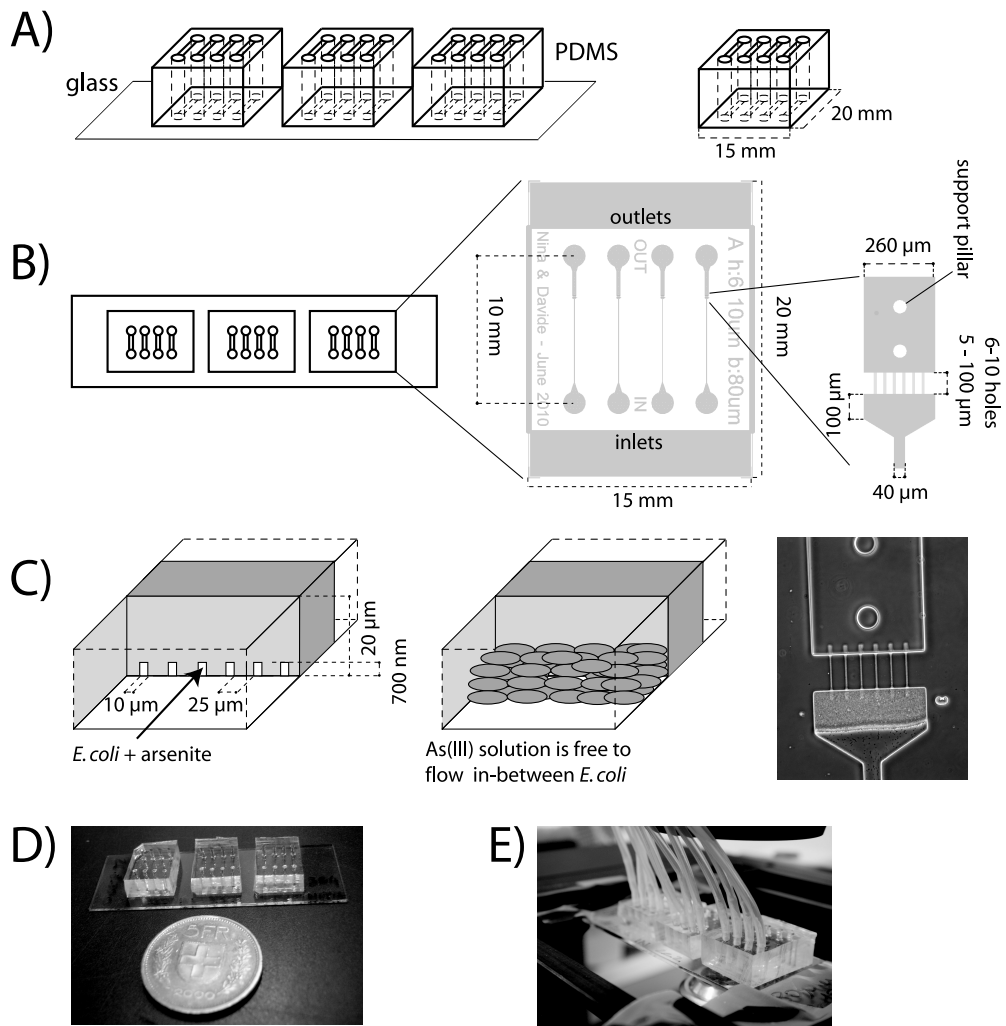
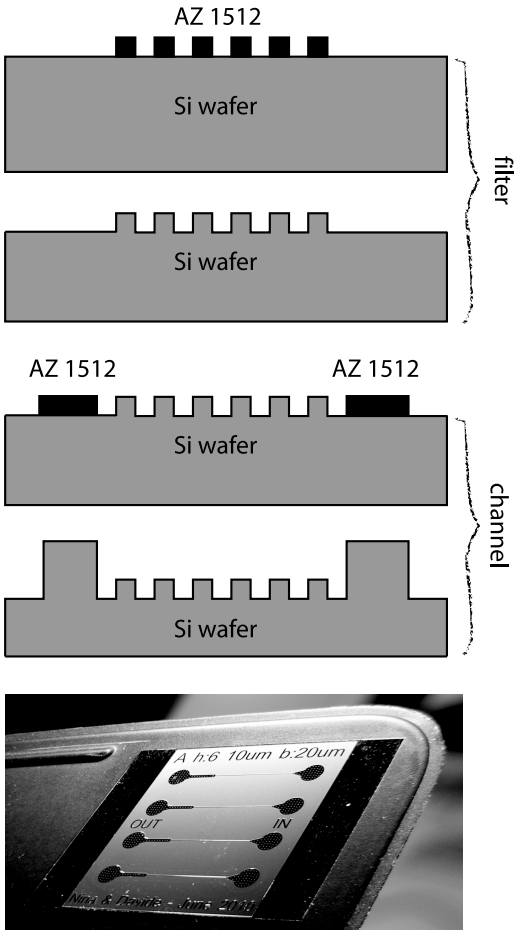
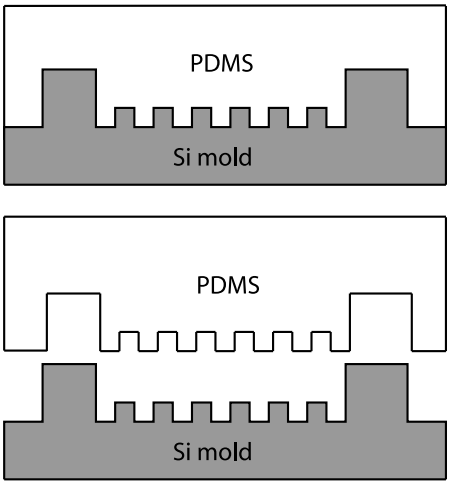


Figure 3.1: Working principle of the microfluidic chip. A) Three PDMS blocks, each containing four microfluidic channels, are bonded on a single glass slide. B) Each channel is composed of one inlet, one outlet and a filter wall. Support pillars (in white) avoid collapsing of the channel. C) The filter pores trap the cells, while allowing sample flow through the holes, which are 700 nm high (image on the right was acquired at 100-fold magnification). D) Picture of the three replica PDMS chips on glass (size marker is a 5 Swiss Franc piece). E) The complete setup comprises the microfluidic cartridge mounted on an epifluorescence microscope and connected to a pressurized air bottle.

A) Silicon mold fabrication



B) PDMS imprint



C) PDMS bonding

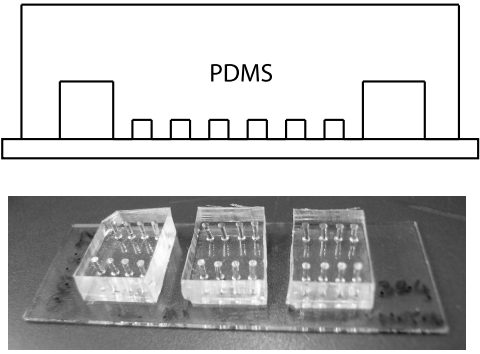


Figure 3.2: Microfluidic chip microfabrication. A) Microfabrication of the silicon mold. B) Negative imprint of the mold are transferred to the PDMS layer. C) By demolding the PDMS layer and bonding it to a glass slide, the channels and filter walls are formed.

### 3.2.2 Reporter cells preparation

We used the same strain as in the case of the the agarose beads system, i.e. the *E. coli* DH5 $\alpha$  strain 1598 (pPROBE-arsR-ABS), whose working principle was explained in section 2.2.1. Starting from a single colony, the strain is grown in LB medium in the presence of 50  $\mu\text{g}/\text{mL}$  kanamycin at 37°C for 18 h and with 180 rpm agitation of the culture flask. The bacterial culture is then 100-fold diluted into fresh LB medium plus kanamycin and incubated for a further 2 h at 37°C and with 180 rpm agitation. At a culture turbidity at 600 nm of between 0.130 and 0.200 (representative for early exponential phase), cells from 8 mL of culture are harvested by centrifugation at 5000 rpm for 6 min and at room temperature. The cell pellet is then resuspended into 8 mL of MOPS medium. The final concentration of cells in the suspension equals about  $1 \cdot 10^8/\text{mL}$ .

### 3.2.3 Arsenic induction assay

Bioreporter cells are induced in the microfluidics cartridge with arsenite solutions of 10, 25 and 50  $\mu\text{g As}/\text{L}$  and compared to MOPS medium alone as negative control. More precisely, 50  $\mu\text{L}$  (for the 50  $\mu\text{g As}/\text{L}$  induction), 25 (for the 25  $\mu\text{g As}/\text{L}$  induction) and 10  $\mu\text{L}$  (for the 10  $\mu\text{g As}/\text{L}$  induction) of cells solution are mixed with 950, 975 and 990  $\mu\text{L}$  of 1 mg As(III)/L solution, respectively. The arsenite solution is prepared diluting in MOPS a 50 mM stock solution of sodium arsenite ( $\text{NaAsO}_2$ , Merck). Then, 7  $\mu\text{L}$  of these new solutions containing arsenite and cells are pipetted in the chip inlets (for the control, 7  $\mu\text{L}$  of cells solution is pipetted directly in the inlets) and the tubing connecting the inlets with the pressurized air bottle are connected (Figure 3.1 E), and a pressure of 0.4 bar is applied.

### 3.2.4 Quantification of EGFP fluorescence

EGFP fluorescence from the bioreporter cells is imaged using a Leica DFC320 cooled black-and-white charge-coupled device camera (Leica Microsystems CMS GmbH, Wetzlar, Germany) mounted on a Leica DMI6000B inverted epifluorescence microscope. Digital images are recorded as 16-bit TIFF every 20 min with an exposure time of 66 ms using the Leica AF6000 program, at 200-fold magnification and using the GFP BP470/40 filter set (Leica). The exported images are thresholded at the background signal using ImageJ (National Institutes of Health) and then the average of the signal intensity per unit filter area is calculated. Fluorescence from

the bioreporter cells is followed by digital microscope imaging over a time period of 180 min at 20°C.

### 3.2.5 Kinetics

In order to determine the rate of increase of the EGFP fluorescence in the biosensor assays as a function of arsenite concentration, we fit the data using the function  $\ln(F_{cells}) = \alpha_{cells} \cdot t + c_{cells}$ , where  $\alpha_{cells}$  is the slope,  $c_{cells}$  is a constant, and  $F_{cells}$  the fluorescence intensity as function of time  $t$ .

## 3.3 Results

### 3.3.1 Microfluidic cartridge

Because the etching rate also depends on the surface to be etched, we observed that if the designed filter wall length it too short (less than 20  $\mu\text{m}$ , Figure 3.3 A), its negative imprint in the silicon mold has a depth that does not match the one of the walls around the channels (Figure 3.3 B). As a consequence, in the PDMS block the filter wall does not touch the glass surface (Figure 3.3 C) and the cells can not be retained. We also observed that because of the downwards transferring, the filter profile is not so well defined as one would expect (Figure 3.3 E). However, this does not cause any problem in the functioning of the filter. In fact, for pressures smaller than 0.5 bar, PDMS pores act as an effective filter trap for the cells whereas the aqueous solution passes through (Figure 3.1 C) and induction could be operated reproducibly. Cells accumulate during all the measurement period in the cavity before the filter wall, which has a volume of  $20 \times 100 \times 250 \mu\text{m}^3$ , and after 180 minutes some  $10^5$  cells are trapped. The number of pores does not affect significantly the chip behavior. We found that thanks to PDMS flexibility this trap is reversible: increasing the pressure applied to the channel ( $>0.5$  bar), the holes expand and the cells are washed away.



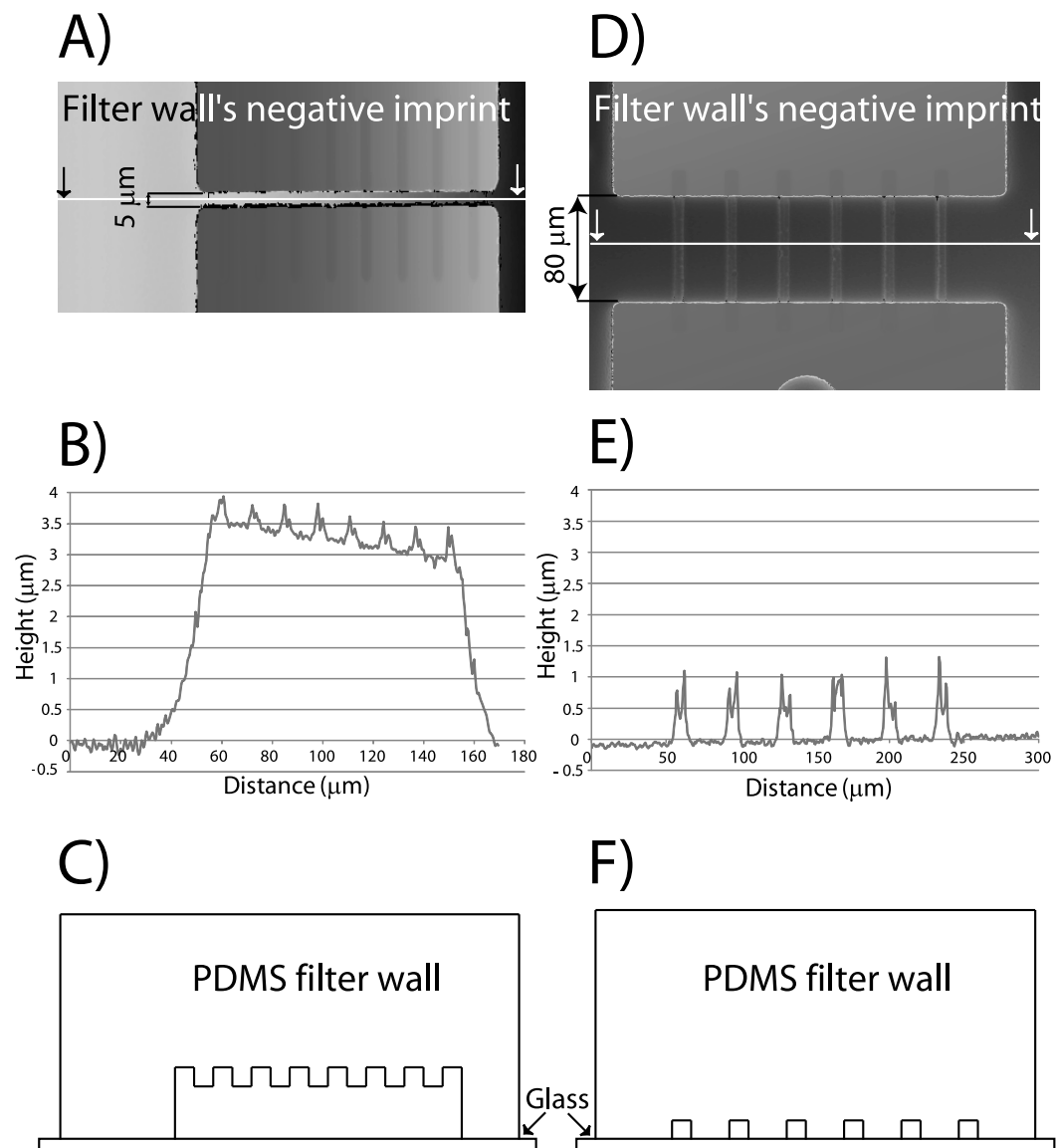


Figure 3.3: When the length of the filter wall is  $<20\ \mu\text{m}$  (A), its depth in the negative imprint is shorter than the depth of the channel walls (B). As a result, the PDMS filter wall does not touch the glass surface (C). In contrast when the length is  $>20\ \mu\text{m}$  (D), its depth in the negative imprint matches the depth of the channels walls (E). In this case the PDMS filter wall touches the glass surface and the cells can be retained (F).

**3.3.2 Sensitivity of bioreporter assay to arsenite**

Figure 3.4 A shows the increase of the mean EGFP fluorescence per unit of trapped cells surface resulting from the induction of fresh cells as a function of assay incubation time and at three sodium arsenite concentrations, 10, 25 and 50  $\mu\text{g As/L}$ , compared to a control without arsenite. To significantly distinguish the EGFP signal at 10  $\mu\text{g As/L}$  from the negative control 80 minutes are required, while for concentrations of 25 and 50  $\mu\text{g As/L}$ , 40 minutes are enough (pair-wise comparison was made using a two-sided T-test with unequal variance on triplicate data sets,  $P < 0.05$ ). The mean fluorescence per unit of trapped cells surface measured after 180 minutes increases linearly proportionally to the arsenite concentration between 0 and 50  $\mu\text{g As/L}$  (Figure 3.4 B) and for higher concentrations it saturates (data not shown). Longer incubation improves the sensitivity of the signal at 10  $\mu\text{g As/L}$  up to around 214%, while the calculated method detection limit (MDL) and the relative standard deviation (RSD) based on signal intensity after 180 minutes equalled 1.3  $\mu\text{g As/L}$  and 9% respectively (Table 3.1).

<b>Assay time (min)</b>	40	60	80	100	120	140	160	180
<b>MDL (<math>\mu\text{g As/L}</math>)<sup>a</sup></b>	11.8	5.1	4.5	3.0	2.5	2.3	1.5	1.3
<b>RSD %<sup>b</sup></b>	5.1	5.7	10.5	9.9	11.1	13.3	12.8	9.1
<b>Sensitivity %<sup>c</sup></b>	90.1	108.1	121.6	147.2	165.4	178.4	194.1	214.0

Table 3.1: Figures of merit for the free cells system. a) MDL, method detection limit. Calculated as the arsenite concentration corresponding to a sample with fluorescence of that in the blank plus three times the standard deviation in the blank. b) RSD, relative standard deviation. Calculated as the average percent deviation in fluorescence intensity across all samples compared to the calculated fluorescence intensity according to the linear regression trend function. c) Sensitivity. Calculated as the percent increase of fluorescence intensity at 10  $\mu\text{g As/L}$  compared to the value in the blank at that time point.

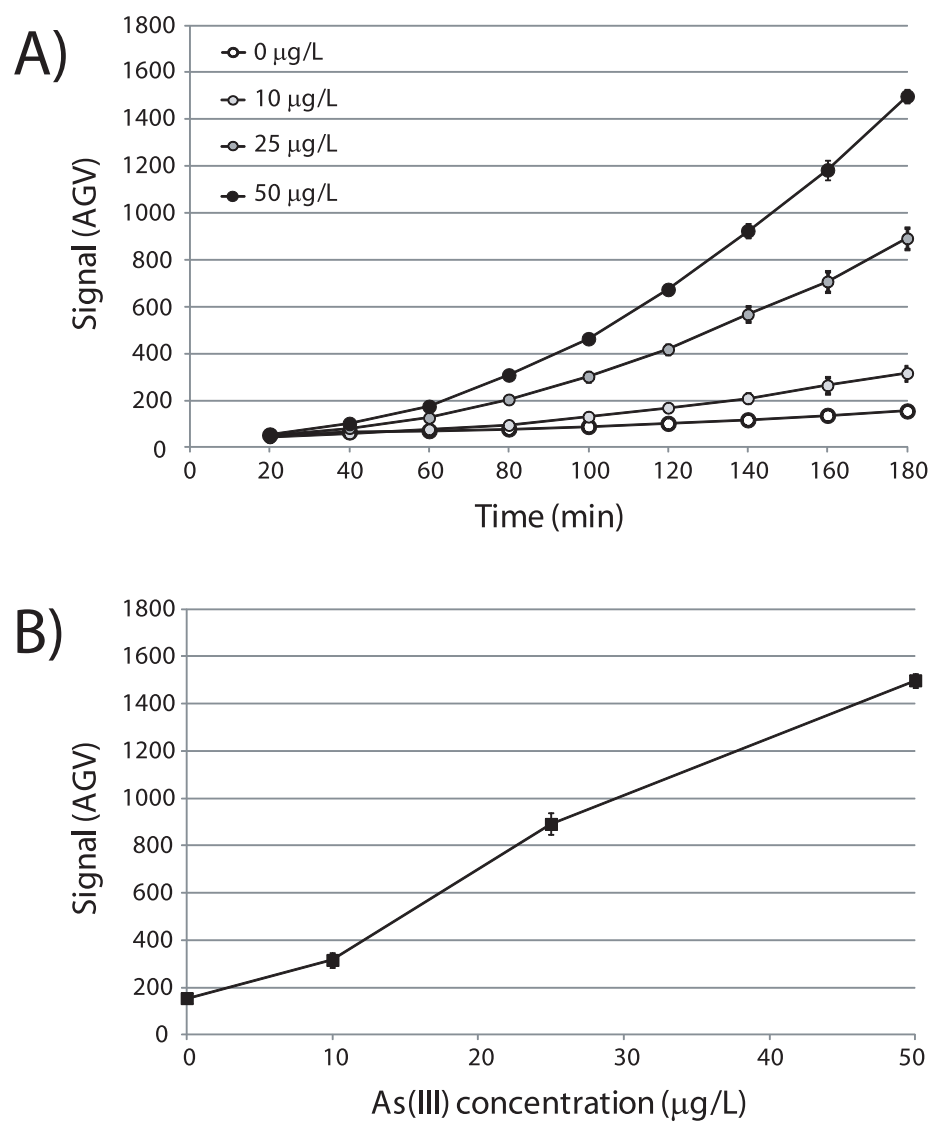


Figure 3.4: A) Raw fluorescence intensities of trapped bioreporter cells as function of time and arsenite concentration. B) Signal calibration as a function of arsenic concentration based on 180 min end point measurement. All data are averages from triplicate assays simultaneously carried out in a three four-lane PDMS chips (twelve lanes in total). Error bars denote calculated deviations from the average. Error bars not shown are smaller than the symbol size.

### 3.3.3 Response kinetics

As in the case of bioreporter cells encapsulated in agarose beads, the slope of the signal increase calculated in a semi-log plot in the range of 0-50  $\mu\text{g/L}$  correlates linearly proportionally to the arsenic concentration (Figure 3.5). Using this kinetic parameter, we determined the time needed to differentiate a certain arsenite concentration from the blank. We found that in a time window of 40-100 min of induction 10, 25 and 50  $\mu\text{g As/L}$  could be differentiated from the blank or from each other by a significantly different slope (pair-wise comparison was made using a two-sided T-test with unequal variance on triplicate data sets,  $P < 0.05$ ).

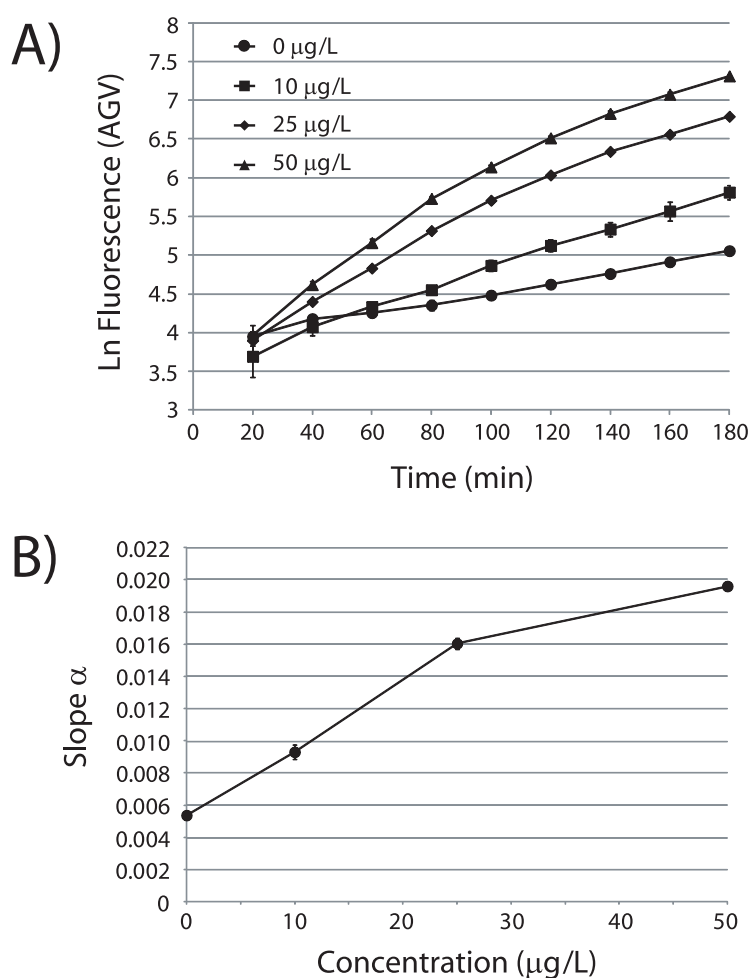


Figure 3.5: Kinetics of signal development in assays. A) Semi-ln transformed signal intensities for different arsenite concentrations. B) Calibration curve of calculated slopes as a function of arsenite concentration. Error bars denote calculated deviations from the average. Error bars not shown are smaller than the symbol size.

### 3.4 Discussion

In order to trap and concentrate single cells, we designed and fabricated a filter wall. Although, as previously shown, different trapping structures as U-shaped traps [Wu *et al.*, 2008], dam structures [Mengsu *et al.*, 2002], and microwells on the bottom of the channels [Khademhosseini *et al.*, 2004; Park *et al.*, 2008] have been described, our method has the advantage to be straightforward to implement in terms of microfabrication and in number of operation needed to control the flow. In fact, the fabrication of the silicon mold only requires two etching steps and once the cells and the arsenite solution are pipetted in the chip inlet, one has just to connect a tubing between it and the pressurized air bottle. Furthermore, starting from one silicon mold, hundreds of identical chips can be easily and inexpensively fabricated.

With this system, we were able to discriminate arsenite concentrations in the range of 0-50  $\mu\text{g As/L}$  with a calculated method detection limit of 1.3  $\mu\text{g As/L}$ , value which is in the same range of the ones obtained with the agarose beads (1-1.6  $\mu\text{g As/L}$ ) and lower than the ones obtained with previous assays (5 and 8  $\mu\text{g As/L}$  after 2 h incubation when the signal was measured with steady state fluorimetry or epifluorescence microscopy on single cells [Wells *et al.*, 2005]). Concerning the measurement errors, the fluorescent signals produced by free cells showed an average deviation of 9%, a value comparable to the ones obtained with cells embedded in agarose beads. As in the previous case, this RSD shows that fewer calibrations would be sufficient to accompany each sampling series. In terms of sensitivity of the signal at 10  $\mu\text{g As/L}$ , free cells perform slightly better than cells in beads, reaching a value of 214%, while for the beads the values were in range of between 150 and 180% (depending on storage method and time).

Also with this free cells system the relationship between the fitted slope of ln-transformed signal intensities and arsenite concentration can be exploited, and an induction interval of 40-100 min is sufficient to significantly discriminate the slopes at 10, 25 and 50  $\mu\text{g As/L}$  from each other and from the blank (in the case of beads stored 1 day at  $-20^\circ\text{C}$  the required interval to discriminate them was 60-120 min). It is interesting to observe that the absolute fluorescence values are higher for free cells than for fresh beads for a factor of about 2.5 (the compared values were corrected for the different exposure times used, *i.e.* 66 ms for the cells and 260 ms for the beads). This could be useful for the integration of an optical detector as less power would be required to perform a measurement.

## Chapter 3. Free cells system

---

This system presents two main limitations. First, cells need to be freshly prepared for each new measurement. Secondly, the number of cells trapped is not constant as they accumulate against the filter during all the experiment. Thus, not all the cells undergo the same conditions in terms of nutrients and arsenite distribution and this could bias the experiment in a non-reproducible way. Furthermore, this aspect is problematic for the implementation of an integrated optical system, as the dimension of the area to be detected varies during the experiment, while the detector area would be constant. To solve this issue, we investigated the possibility to develop a filter cage instead of a filter wall (as in the case of beads), but because the flow resistance is inversely proportional to the cube of the channel height, the flow resistance of the cage (the pores height is 700 nm) is several orders of magnitude higher than the one of the lateral channels (the channels height is 20  $\mu\text{m}$ ) and thus the cells pass around it and are not trapped.

The fact that the filter pores dimension can be tuned by the applied pressure, thus allowing cells wash-out, is an interesting feature in the optic of a chip in which there is a continuous supply of fresh bioreporter cells. In this case the cells that have been exposed to arsenic could be washed away and new fresh cells could be accumulated, making this chip usable for several assays.

## 3.5 Conclusions and outlook

### 3.5.1 Summary of results

We designed a microfluidic cartridge able to contain bioreporter cells, to expose them to liquid arsenic-containing samples and to obtain an easy read-out of the signal. The filter wall permitted cells trapping, exposure to arsenite and signal amplification as a result of thousands of cells accumulating at one position. We were able to reliably and reproducibly discriminate arsenite concentrations in the range of 0-50  $\mu\text{g}$  in less than 180 min with a detection limit of 1.3  $\mu\text{g As/L}$ , which is well below the current drinking water limit of 10  $\mu\text{g As/L}$ .

### 3.5.2 Perspectives

In the optics of the development of a system which would produce a continuous supply of fresh bioreporter cells and in which they can be exposed to arsenic aqueous samples, this

microfluidic chip is a first important step, as it validates the possibility to trap, concentrate and expose single cells to arsenic. Chapter 4 investigates the possibility to go further, implementing a microfluidic valves system to develop a chemostat on chip and to be able to first accumulate the required amount of cells and subsequently expose them to the aqueous arsenic sample, thus solving the problem of the non constant amount of cells trapped.





# 4 Chemostat on chip

## 4.1 Introduction

In Chapter 2, we showed that the agarose beads system presents the drawback of the signal decrease upon storage time, while in Chapter 3 we demonstrated that it is possible to trap and expose single cells to arsenic samples, although from an application point of view the problem of the non constant amount of cells trapped against the filter wall needs to be solved. Therefore, we investigated the possibility to develop a microfluidic valve system working with single cells, mimicking a traditional chemostat which would continuously provide fresh cells and thus overcome the signal decrease limitation, and in which it would be possible to first accumulate the desired amount of cells and subsequently expose them to the arsenic sample, solving the problem of their accumulation during all the measurement.

This chapter starts explaining the differences between a traditional chemostat and our chemostat on chip. A subsequent section describes the fundamental concepts and equations behind a traditional chemostat, which apply also in our case. Then, the materials and methods utilized for the construction and operation of the microfluidic platform are illustrated and the results obtained in terms of function of the chip and in terms of evolution of cells state and cells sensitivity to arsenite are presented. The last section discusses strengths and limitations of the developed chemostat on chip.

### 4.2 Differences between a traditional chemostat and our chemostat on chip

A chemostat is a bioreactor in which fresh medium is continuously added and culture liquid is continuously removed in order to maintain the culture volume constant [Novick and Szilard, 1950]. By changing the rate with which the medium is added the growth rate of the microorganisms in the bioreactor can be easily controlled. One of the most important features of chemostats is that micro-organisms can be grown in a physiological steady state, meaning that growth occurs at a constant rate and all culture parameters (culture volume, cell density, nutrients and products concentrations, dissolved oxygen concentration, etc.) remain constant.

Apart from the obvious difference in size (L versus  $\mu\text{L}$ ), our chemostat on chip differs from a traditional one as the operations of addition of fresh medium and of removal of culture liquid occur simultaneously but not continuously and because it is not provided with a mixing system. Despite these differences, the traditional chemostat concepts of steady state, dilution rate, cell growth rate, substrate consumption and wash-out and the corresponding equations remain valid and they will be introduced in the next section.

### 4.3 Chemostat theoretical basis

We start defining the variables necessary to describe a chemostat. Let:

- $Q$  be the flow rate;
- the flow rate entering the chemostat be equal to the flow rate coming out, *i.e.*  $Q_{in} = Q_{out}$ ;
- $C_V$  be the chamber volume;
- $D$  be the dilution rate;
- $B$  be the biomass of bacteria in the chamber;
- $[B] = \frac{B}{C_V}$ .
- $[S]$  be the concentration of growth limiting substrate;
- $[S]_0$  be the initial concentration of growth limiting substrate;

- $\mu$  be the cell growth rate.

We can describe the chemostat with a coupled set of differential equations [Banks and Davidian, 2009]:

$$\begin{cases} \frac{d[B]}{dt} = \mu([S])[B] - D[B] \\ \frac{d[S]}{dt} = D[S]_0 - D[S] - \frac{1}{y}\mu([S])[B] \end{cases} \quad (4.1)$$

$$\frac{d[S]}{dt} = D[S]_0 - D[S] - \frac{1}{y}\mu([S])[B] \quad (4.2)$$

where  $y$  is the yield parameter proportional to the yield constant  $Y$ , defined as

$Y = \frac{\text{mass of bacteria change per unit time}}{\text{mass of nutrients consumed per unit time}}$ . At steady-state, we have:

$$\begin{cases} \frac{d[B]}{dt} = 0 \\ \frac{d[S]}{dt} = 0 \end{cases} \quad (4.3)$$

$$\frac{d[S]}{dt} = 0 \quad (4.4)$$

which can be rewritten as:

$$\begin{cases} \mu([S])[B] - D[B] = 0 \\ D[S]_0 - D[S] - \frac{1}{y}\mu([S])[B] = 0 \end{cases} \quad (4.5)$$

$$D[S]_0 - D[S] - \frac{1}{y}\mu([S])[B] = 0 \quad (4.6)$$

From Equation 4.5, we obtain:

$$\mu([S]) = D \quad (4.7)$$

We assume that  $\mu([S])$  follows a Michaelis-Menten kinetics<sup>1</sup> [Banks, 1975]:

$$\mu([S]) = \frac{\mu_{max}[S]}{K_{m,g} + [S]} \quad (4.8)$$

where  $\mu_{max}$  is the maximum growth rate and  $K_{m,g}$  is the substrate concentration at which the growth rate is half of  $\mu_{max}$ .

<sup>1</sup>This kinetic model relates the reaction rate  $V$  to  $[S]$ , the concentration of a substrate  $S$ . Its formula is given by  $V = \frac{V_{max}[S]}{K_m + [S]}$ , where  $V_{max}$  represents the maximum rate achieved by the system at saturating substrate concentrations and  $K_m$  is the substrate concentration at which the reaction rate is half of  $V_{max}$ .

## Chapter 4. Chemostat on chip

---

Thus we can rewrite Equation 4.7 as:

$$[S] = \frac{K_{m,g}D}{\mu_{max} - D} \quad (4.9)$$

Using the result of Equation 4.7, Equation 4.6 can be rewritten as:

$$[S]_0 - [S] - \frac{1}{y}[B] = 0 \quad (4.10)$$

This means that:

$$[B] = y([S]_0 - [S]) \quad (4.11)$$

Thus, the steady-state condition is given by:

$$([B], [S]) = \left( y([S]_0 - [S]), \frac{K_{m,g}D}{\mu_{max} - D} \right) \quad (4.12)$$

From Equation 4.12 and Figure 4.1, we see that if  $D$  is too high, cells can not grow fast enough to reach the steady-state and wash-out will occur. We can find the maximum dilution rate by setting  $[B] = 0$  in Equation 4.10:

$$D_{max} = \frac{\mu_{max}[S]_0}{K_{m,g} + [S]_0} \quad (4.13)$$

For real systems,  $K_{m,g} \ll [S]_0$  [Wittrup, 2007] and thus  $D_{max} = \mu_{max}$ .

We investigate now if there is a best operating condition. First, we define the productivity as  $\frac{\text{Biomass}}{(\text{Reactor volume}) \cdot (\text{time})} = [B]D$ . Then, in order to find the optimum  $D$ , we look for a maximum in the expression  $\frac{d([B]D)}{dD}$  solving  $\frac{d([B]D)}{dD} = 0$  (Figure 4.2). The solution is:

$$D_{optimum} = \mu_{max} \left( 1 - \sqrt{\frac{K_{m,g}}{K_{m,g} + [S]_0}} \right) \quad (4.14)$$

With  $K_{m,g} \ll [S]_0$ , the previous expression simplifies in:

$$D_{optimum} \simeq \mu_{max} \simeq D_{max} \quad (4.15)$$

So, the best operating condition is close to the wash-out condition.

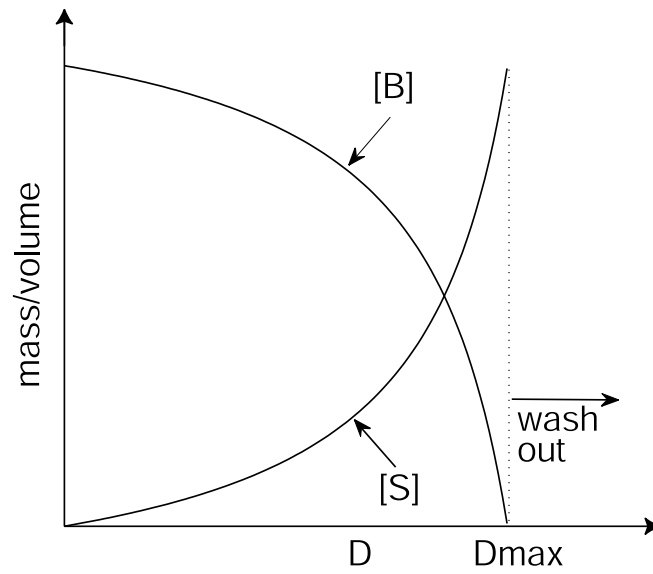


Figure 4.1: Biomass and growth limiting substrate concentrations versus dilution rate. Beyond the maximum dilution rate, wash-out occurs.

Assuming that we are under this optimal condition, we determine now the cells doubling time knowing the (optimum) dilution rate applied to the system. We assume a Malthusian cells growth model [McKelvey, 1995]:

$$\frac{d[B]}{dt} = \mu_{max}[B] \quad (4.16)$$

The solution is:

$$\frac{[B]}{[B]_0} = e^{\mu_{max}t} \quad (4.17)$$

where  $[B]_0$  is the initial biomass. We are looking for the cells doubling time:

$$\frac{2[B]_0}{[B]_0} = e^{\mu_{max}t} \quad (4.18)$$

We solve for  $t$ :

$$t = \frac{\ln 2}{\mu_{max}} \quad (4.19)$$

Under this optimum condition,  $\mu_{max} = D_{optimum}$  and so:

$$t = \frac{\ln 2}{D_{optimum}} \tag{4.20}$$

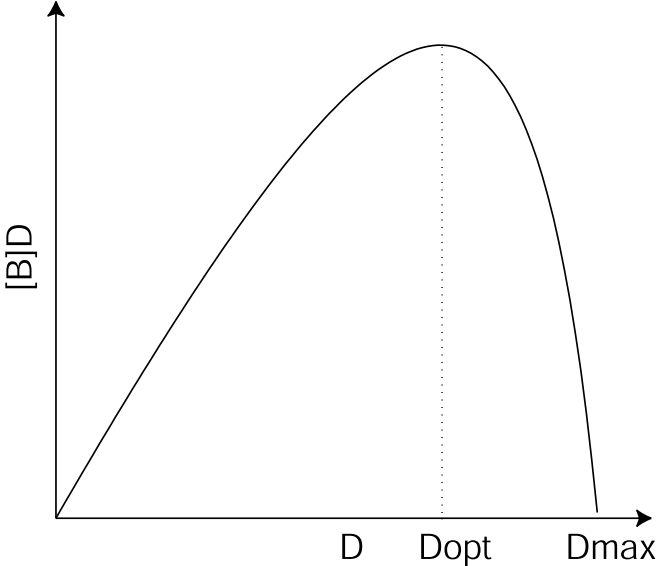


Figure 4.2: Productivity versus dilution rate.

## 4.4 Materials and methods

### 4.4.1 Microfluidic cartridge design and microfabrication

To fabricate the microfluidic cartridge, we use the multilayer soft lithography technique proposed by Unger *et al.* [Unger *et al.*, 2000]. The chip is composed of a two-layered polydimethylsiloxane (PDMS) block bonded on a transparent glass slide with thickness of 1 mm (Figure 4.3 A). The bottom (flow) layer contains the designed chamber, channels, and trap, while the top (control) layer contains a set of pressure-controlled valves, which can open and close the channels in the flow layer (Figure 4.3 C). Valves are operated at an overpressure of 1 bar with respect to the lower flow channels, by which the 30  $\mu\text{m}$  thin PDMS separation between the upper and lower channel deflects and closes the channel below (Figure 4.3 B). The different flows in the bottom layer are also driven by air-pressure. Valve channels are filled with water in order to avoid air bubbles formation in the flow lanes below an their opening and closing was controlled by LabVIEW (National Instruments).

We designed a reactor chamber of 0.8  $\text{mm}^2$  with a height of 17  $\mu\text{m}$  (corresponding to a volume of 13 nL) which mimics a traditional chemostat in a discontinuous way: continuous culture conditions are maintained by inflow of fresh nutrients from a sterile stock solution and simultaneous outflow of the same volume with cells from the reactor at defined time intervals. These intervals are controlled by the frequency of opening of the in- and outflow valves from the reactor cavity (Figure 4.3 D). A waste outlet is dedicated to the reactor outflow with cells (Figure 4.3 C), while a filter between the nutrients inlet and the microchamber prevents backflow of cells into the nutrients solution (Figure 4.3 D). When a measurement is needed, part of them is taken out, trapped and concentrated in a measurement zone, where they are exposed to aqueous samples containing arsenite. The cells trap is composed of a filter wall made of 6 holes 10  $\mu\text{m}$  large and 600 nm high: cells are retained since *E. coli* is 2-5  $\mu\text{m}$  long and 1-1.5  $\mu\text{m}$  in diameter, while the solution passes through (Figure 4.3 E). Thanks to PDMS flexibility, this trap is reversible: increasing the pressure applied to the channel, the holes expand and the cells are washed away. The flow channels have a height of 17  $\mu\text{m}$  and a width of 100  $\mu\text{m}$ .

Both PDMS layers are fabricated separately using a silicon mold, then superimposed and irreversibly bonded. For the PDMS control layer a silicon mold containing the negative imprints of the channels is prepared (Figure 4.4 B). To fabricate the mold, a silicon wafer is structured

by dry etching (Bosch process, Alcatel 601E) using a photolithographically structured AZ1512 resist (Clariant) as a mask. A separate silicon and AZ9260 mold is prepared for the PDMS microfluidics layer, which contains the negative imprints of the chamber, the measurement zone and the channels (Figure 4.4 A). To fabricate the negative of the filters, a silicon wafer is structured by dry etching (Bosch process, Alcatel 601E) using a photolithographically structured AZ1512 resist (Clariant) as a mask. To fabricate the negative of the channels, a layer of AZ9260 resist (Clariant) is deposited (EVG150) on the wafer, structured (MA6) and baked to obtain rounded structures thanks to the resist reflow. This last step is crucial because only rounded channels can be completely closed by the deflection of the membrane in the upper flow control layer [Unger *et al.*, 2000]. The control PDMS layer is prepared from a liquid PDMS mixture containing 60 g of Sylgard 184 silicone elastomer base (Dow Corning) and 12 g of Sylgard 184 silicone elastomer curing agent (ratio 5:1). After degassing, this first mix is poured on the control layer mold (thickness ca. 7 mm). The microfluidics flow layer is prepared from a liquid PDMS mixture containing 10 g of base and 0.5 g of curing agent (ratio 20:1), which is spin coated on the flow layer mold (thickness ca. 30  $\mu\text{m}$ ). Each layer is cured separately at 80°C for 12 min and 20 s. The thick PDMS layer is then peeled off (Figure 4.4 C), superimposed and aligned on the thin layer, and the two are cured at 80°C for 2 h (Figure 4.4 D). Thanks to the different curing agent-base ratios between the two layers, this final curing step bonds the two PDMS layers together. Finally, the resulting PDMS block is peeled off and bonded on a standard glass slide (Figure 4.4 E).



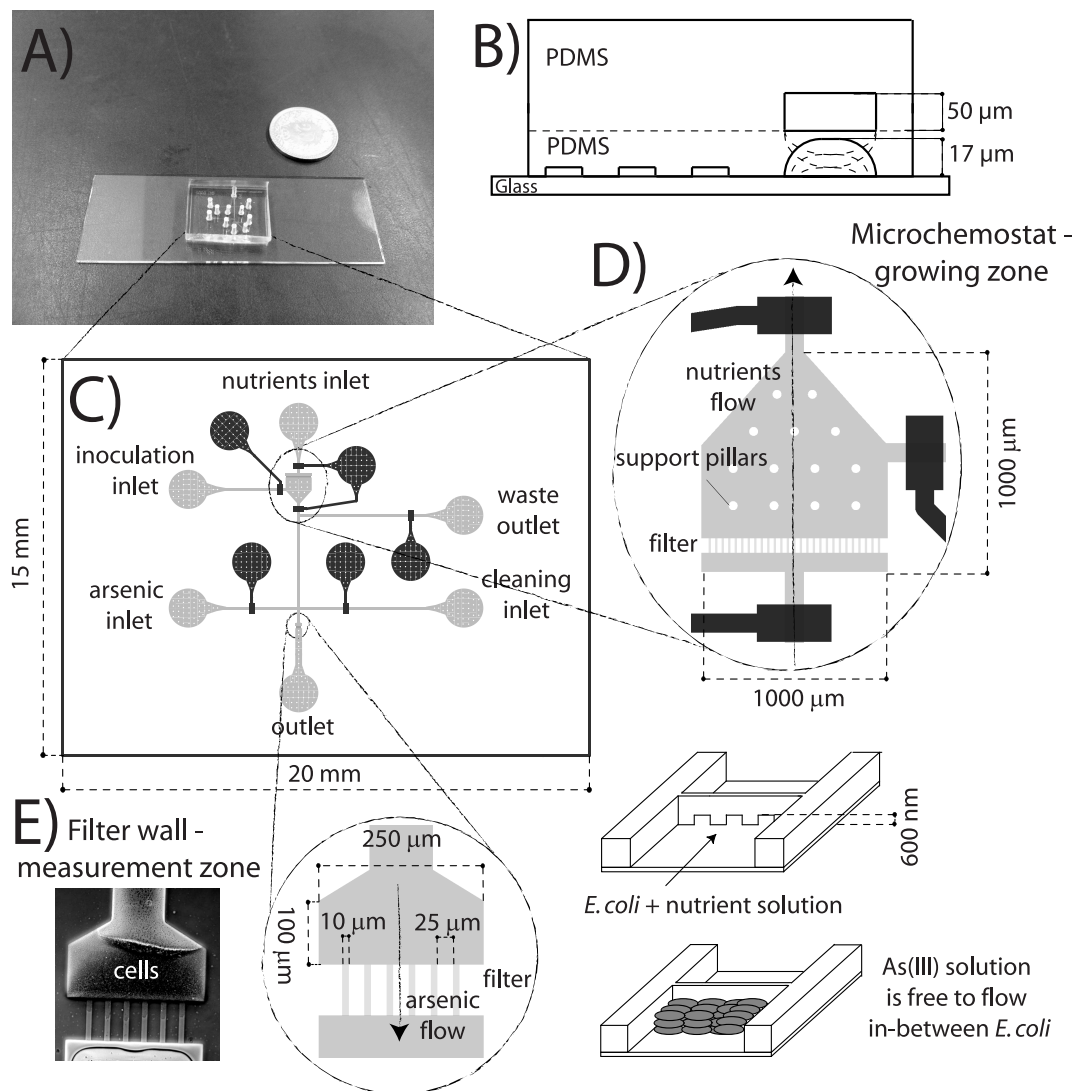


Figure 4.3: Outline of the microfluidic chip. A) The chip is composed of a PDMS block bonded on a glass slide. B) The PDMS block itself is composed of two layers: a thin one ( $30\ \mu\text{m}$ ) containing the flow channels and a thicker one (ca.  $7\ \text{mm}$ ) containing the control channels. When an overpressure of ca.  $1\ \text{bar}$  is applied to the control layer, the thin membrane between the two layers deflects, closing the underlying flow channel. C) The chip contains in- and outflow channels, a microchamber, a filter wall and a set of pressure activated valves. D) The microchamber with its up- and downstream valves mimics a chemostat in a discontinuous way: cells receive fresh nutrients and part of them is removed at a frequency given by the valves opening frequency. The upstream filter prevents the chemotaxial cells growth. Support pillars (in white) prevent the chamber from collapsing. E) The filter wall traps the cells, while allowing flow through the holes. In this way it is possible to accumulate the desired amount of cells and to expose them to the arsenic solution. Image on the left was acquired at 200-fold magnification.

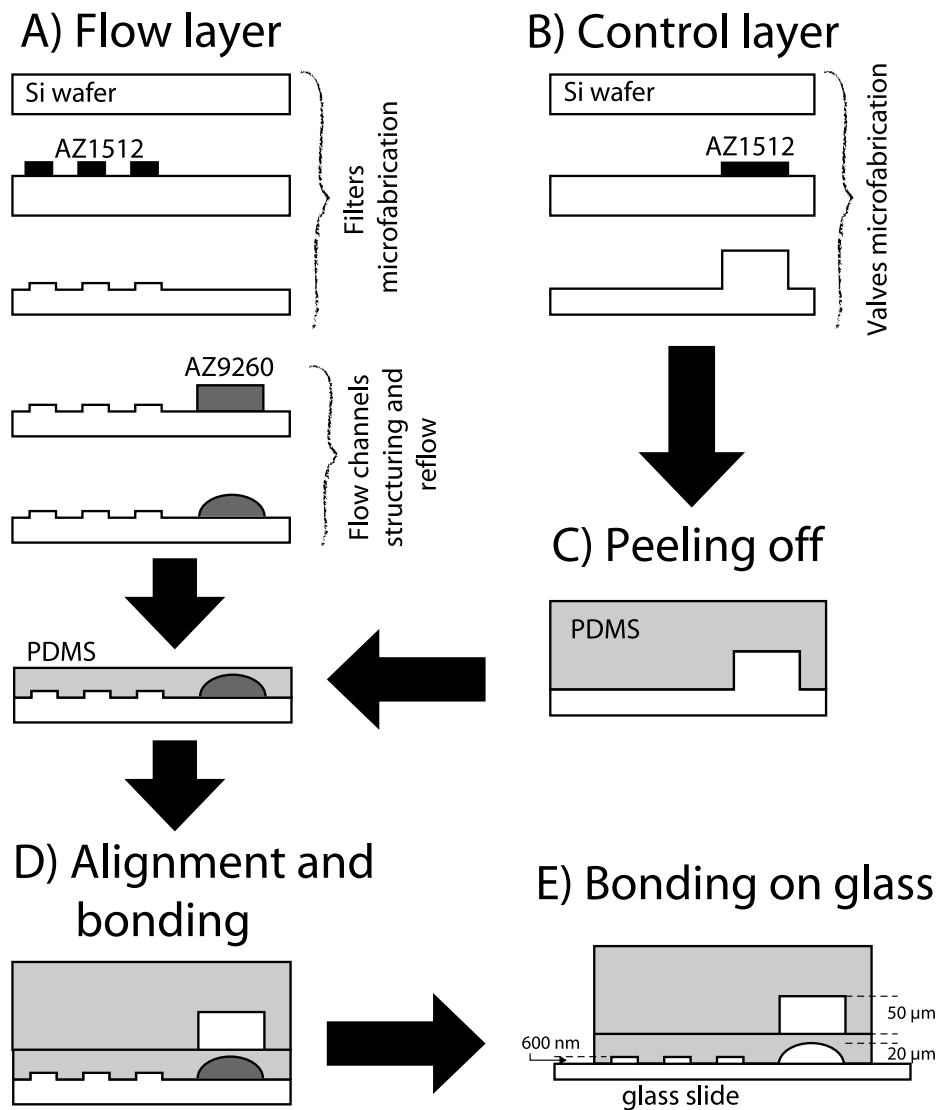


Figure 4.4: Microfluidic chip microfabrication. A) The first step consists of the microfabrication of the flow layer silicon mold. B) The second step consists of the microfabrication of the control layer silicon mold. C-D) In the third step, the flow PDMS layer and the control PDMS layer are fabricated from the silicon molds, aligned and bonded together. E) Finally, the resulting PDMS block is bonded on a glass slide.

#### 4.4.2 PDMS valves control

In order to control the PDMS valves actuation, a pressurized air switching system was built. This system is composed of five solenoid valves (Pneumadyne) and of an electronic circuit coupled to a LabVIEW interface controlling their opening and closing. As each solenoid valve links a pressurized air bottle to the the corresponding PDMS valve channel of the microfluidic chip via a PTFE tubing (Fisher Scientific), when one of them it is activated it enables the pressurized air to deflect the upper PDMS membrane, which in turn closes the lower flow channel. In practice, each solenoid valve is coupled via the electronic circuit shown in Figure 4.5 to an acquisition card controlled by LabVIEW, whose outputs go from 0 to 5 V when activated. Each output is connected to the gate of a MOSFET transistor that becomes conductive when the voltage goes up to 5 V, applying the required voltage (24 V) to the corresponding solenoid valve and activating it.

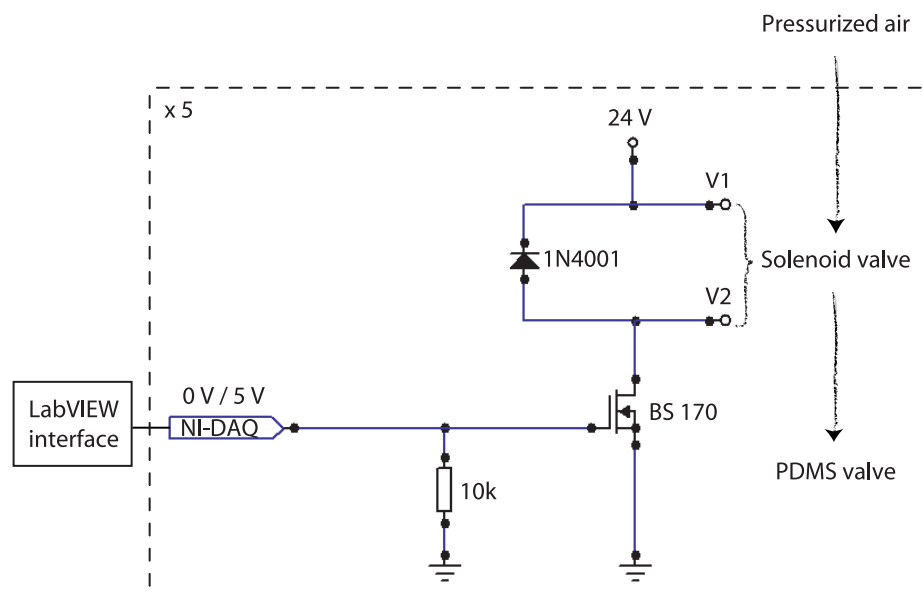


Figure 4.5: Electronic circuit schematic controlling each of the solenoid valves.

### 4.4.3 Microfluidic cartridge principle of operation

The microfluidic cartridge principle of operation is illustrated in Figure 4.6 and it can be summarized as follows. First, reporter cells are inoculated through the designated inlet, which is then permanently closed. Cells are then given fresh nutrients by opening the nutrient inflow valve and the outflow valve simultaneously. The frequency of opening in- and outflow valves while maintaining constant pressure-controlled flow determines the growth rate of the cells. When a measurement is needed, part of the cells coming from the chamber is trapped in the filter of the measurement zone and exposed to the arsenic solution. During the measurement the chemostat chamber needs to stay closed in order to avoid the entry of arsenic, and the in- and outflow frequency is interrupted. Once the measurement is over, the pressure driving the flow is increased and the accumulated cells are washed away. If needed, the channel connecting the chamber with the measurement zone is cleaned by flushing the nutrients solution from the cleaning inlet to the waste outlet. Then, the periodically opening of the chamber valves is restored. For experiments that last more than 3 days, we add a sterile external reservoir (ca. 10 mL in a glass vial) to avoid the depletion of the nutrient inlet reservoir, which can contain ca. 5  $\mu$ L. The chip is operated at room temperature.

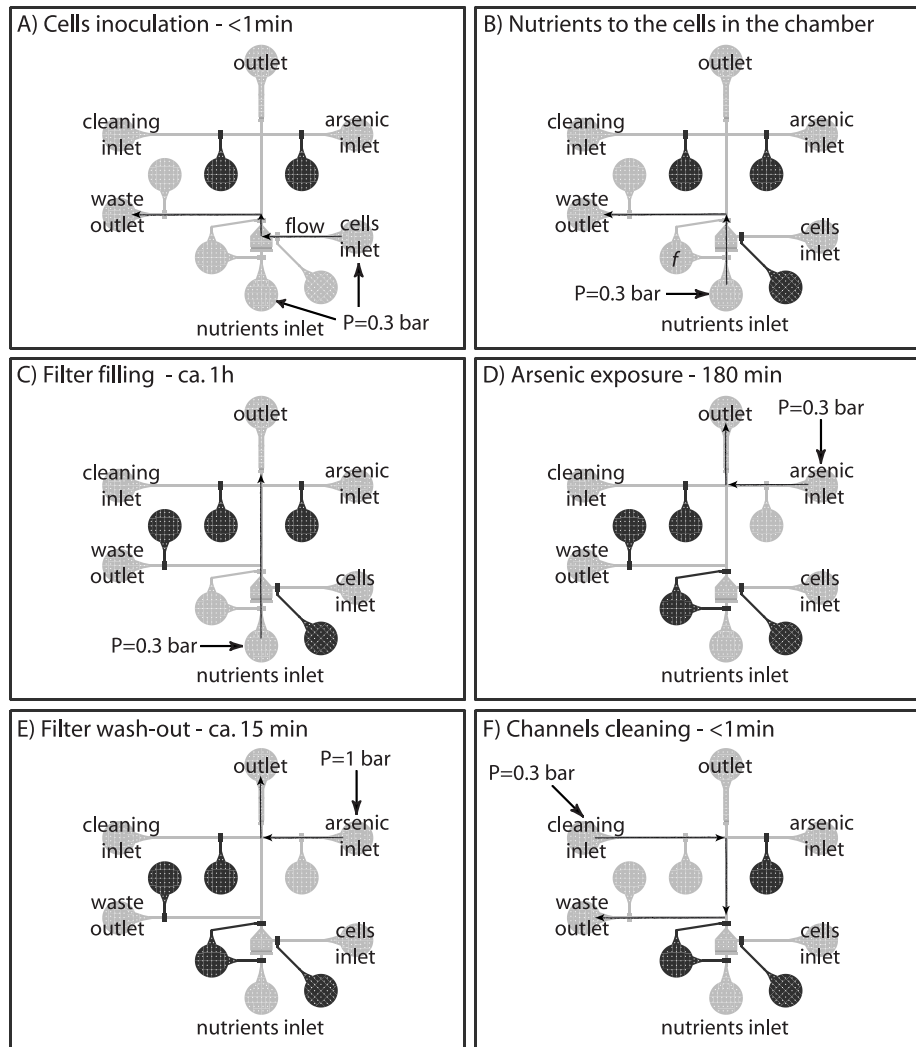


Figure 4.6: Working principle of the microfluidic chip. First, cells are introduced in the microchamber via the inoculation inlet (A). Dark gray indicates closed valves (overpressure of 1 bar with respect to the lower flow channels). Then, the valve controlling this channel is permanently closed, and the valves controlling the inflow of fresh nutrients and the outflow of cells in and from the chamber are simultaneously opened and closed at a given frequency. The cells coming out are collected in the waste outlet (B). When a measurement is needed, the chamber valves are opened, the waste valve is closed, and cells are accumulated against the filter in the measurement zone (C). As soon as the required amount of cells is trapped, the chamber valves are closed and the valve controlling the arsenic inlet and channel is opened (D). Once the measurement is over, the pressure on the arsenic inlet is increased (and, to avoid leakage, on the valves too) so that the filter holes expand and the cells are washed away (E). Then, we set again the pressures to the standard values. If needed, in order to remove the cells stuck to the PDMS and glass of the channel connecting the chamber with the filter wall and thus to avoid its obstruction, we open the cleaning inlet valve and we flush it with the nutrients solution (F). Afterward, we close all valves and we restart the periodically opening of the chamber valves at the chosen frequency (B).

### 4.4.4 Bioreporter strain

In order to test the functioning of our chemostat on chip, we use, as in the case of the beads and the free cells system, the *E. coli* DH5 $\alpha$  strain 1598 (pPR-arsR-ABS), whereas to qualitatively monitor the physiological state of *E. coli* in the chemostat chamber, we created an *E. coli* carrying a plasmid with the *rrnB1* ribosomal promoter fused to an unstable *egfp*. This strain (*E. coli* 4224 [Andersen *et al.*, 1998]) expresses the EGFP protein during exponential growth but not when cells are entering the stationary phase, in which case the fluorescence will decay with an half-life of  $\approx 40$  minutes as a result of the degradation tag (AGV) on the protein.

### 4.4.5 Reporter cells, nutrients and arsenite solutions preparation

Starting from a single colony, *E. coli* DH5 $\alpha$  strain 1598 (pPR-arsR-ABS) or 4224 is grown in Luria-Bertani (LB) medium in the presence of 50  $\mu\text{g}/\text{mL}$  kanamycin at 25°C for 18 h and with 180 rpm agitation of the culture flask. The bacterial culture is then 50-fold diluted into fresh LB medium plus kanamycin and incubated for a further 1.5 h at 37°C and with 180 rpm agitation. At culture turbidity at 600 nm between 0.2 and 0.5 (representative for exponential phase), cells from 20 mL of culture are harvested by centrifugation at 5000 rpm for 6 min at room temperature. The cell pellet is then resuspended in LB medium to obtain a final concentration of cells in the suspension of about  $1 \cdot 10^{10}/\text{mL}$ . 8  $\mu\text{L}$  of this solution is then pipetted into the dedicated inoculation inlet and driven into the chamber.

Nutrient solution is made of 50% MOPS [v/v] (MOPS medium contains 10% [v/v] of MOPS buffer, 2mM MgCl<sub>2</sub>, 0.1 mM CaCl<sub>2</sub>, 2 g glucose per L) and 50% LB plus 50  $\mu\text{g}/\text{mL}$  of kanamycin. Adding this antibiotic is necessary to avoid cells contamination and to maintain the selective pressure for keeping the reporter plasmid. MOPS buffer itself is prepared by dissolving, per liter: 5 g NaCl, 10 g NH<sub>2</sub>Cl, 98.4 g 3-([N-morpholino]propanesulfonic acid, sodium salt), 0.59 g Na<sub>2</sub>HPO<sub>4</sub>·2H<sub>2</sub>O and 0.45 g KH<sub>2</sub>PO<sub>4</sub>.

In the optimized nutrient solution, which prevents the cells sticking, 0.1% of Triton X-100 (t-Oct-C<sub>6</sub>H<sub>4</sub>-(OCH<sub>2</sub>CH<sub>2</sub>)<sub>x</sub>OH, x= 9-10, Sigma-Aldrich) is added to the nutrient solution just described.

Arsenite solutions are prepared by making appropriate dilutions of a 50 mM stock solution of sodium arsenite (NaAsO<sub>2</sub>, Merck) in MOPS medium.

#### 4.4.6 Measuring the physiological state of reporter cells in the chemostat chamber and quantification of EGFP fluorescence in the measurement zone

Reporter cells in the chemostat and in the measurement zone are imaged using a Leica DFC320 cooled black and white charge-coupled device camera (Leica Microsystem CMS GmbH, Wetzlar, Germany) mounted on a Leica DMI6000B inverted epifluorescence microscope. Cells in the chamber are imaged at 100-, 200- and 400-fold magnification, while trapped cells exposed to arsenic in the measurement zone are imaged every 30 min during incubation at 200-fold magnification (Leica AF6000 program). For EGFP fluorescence an exposure time of 66 ms (for the measurement zone and in some cases for the chamber) or 600 ms (for some of the chamber images) is used (BP470/40 filter, Leica). Images are recorded as 16-bit TIFF files and the fluorescence signal intensity per unit surface of the measurement zone or of the chamber occupied by cells was determined using ImageJ (National Institutes of Health).

## 4.5 Results

### 4.5.1 Microchemostat operation

The microfluidic valves effectively close the channels and we could operate them continuously for several days at opening frequencies in the range of  $\text{min}^{-1}$  without observing any malfunction.

Inoculation of the cells into the chemostat was achieved by applying a pressure of 0.3 bar for a few seconds on the inoculation inlet into which the cells were pipetted (Figure 4.6 A). The same pressure is also suitable to drive the nutrients solution to the cells in the reactor and to remove part of them to the designed waste outlet (Figure 4.6 B). It takes ca. 1 h to accumulate against the filter wall the required amount of cells coming from the microchamber (Figure 4.6 C) and by increasing the driving pressure (from 0.3 to 1 bars) the filter holes expand, washing away in ca. 15 minutes the accumulated cells (Figure 4.6 E and Figure 4.7 A and B). To maintain the valves closed, the pressure applied to them has to be 1 bar higher than the pressure applied on the channels below. However, the pressure on the valves has to be kept under 2.5 bar or the two PDMS layers may detach.

The fact that the time-scale of the chamber valves opening used for the measurement zone filling (hours) is different from the one used for the nutrients inflow and cells removal (ms) is

due to the fact that once cells start to accumulate against the filter they partially obstruct it and its resistance dramatically increases.

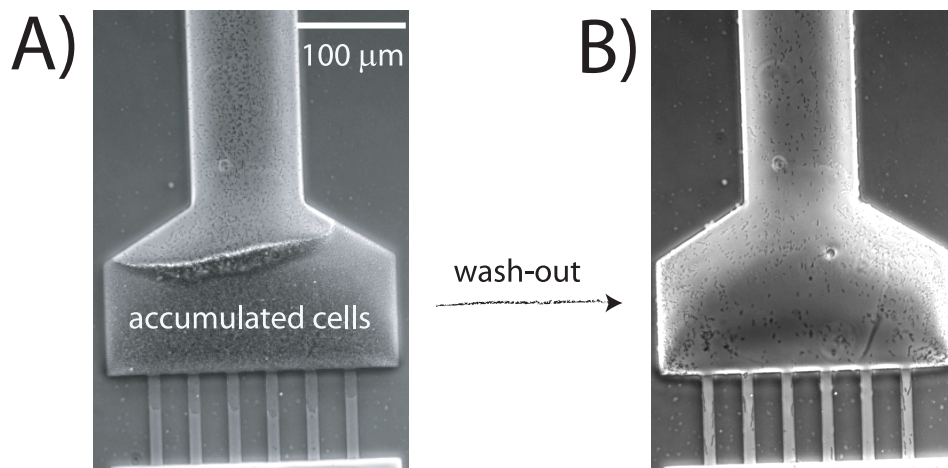


Figure 4.7: A) Contrast-phase picture of the accumulated cells. B) Contrast-phase picture of the filter after the cells wash-out. Almost all the cells were taken away.

### 4.5.2 Chemostat parameters for continuous reporter cell growth

Cells were inoculated into the microchemostat at a concentration of  $1 \cdot 10^{10}$  per mL, which corresponds to  $\approx 1.3 \cdot 10^4$  cells in the 13 nL reactor. The effect of different reactor valves opening times and frequencies on the mean length of cells in the reactor, and on their inducibility by arsenite was tested (Figure 4.8 and Table 4.1). Flow pressure and opening frequencies were converted into an apparent reactor dilution rate ( $\text{h}^{-1}$ ) by using a calculated flow resistance of  $1.44 \cdot 10^{16}$  Pa·s/ $\text{m}^3$  and a chamber volume of 13 nL. At an opening frequency of  $1/4 \text{ min}^{-1}$ , an opening time of 120 ms and a driving pressure of 0.3 bar the corresponding dilution rate is  $0.27 \text{ h}^{-1}$  and around  $2 \cdot 10^3$  cells are on average released during an opening/closing cycle.

At a dilution rate of  $0.27 \text{ h}^{-1}$  cells in the reactor displayed a mean length of  $6.1 \pm 2.1 \mu\text{m}$  and showed a background EGFP fluorescence  $< 20$  units (Figure 3). At dilution rates of  $0.07 \text{ h}^{-1}$  and lower the mean cell length reduced to  $3.3 \pm 0.8 \mu\text{m}$  and the background EGFP fluorescence of the cells increased to 1078 units (Figure 4.8 B, left). The cell length decrease indicated that the cells enter into stationary phase. The higher background EGFP signal of the cells was close to that of cells induced with  $50 \mu\text{g As(III)/L}$  (Figure 4.8 B, right). At a dilution rate of  $0.54 \text{ h}^{-1}$  the number of cells in the chamber decreased visibly, suggesting they are washed



out. Unfortunately, it was not possible to correctly quantify from microscope images the total number of cells in the reactor under the four dilution rates, given the depth of the reactor (17  $\mu\text{m}$ ). At a dilution rate of  $0.27 \text{ h}^{-1}$  the background EGFP signal of the cells after 3 days at continuous operation was still low enough (Figure 4.8 C) to enable arsenite induction assays with  $50 \mu\text{g/L}$  in the measurement zone (Figure 4.10).

Even though a dilution rate of  $0.27 \text{ h}^{-1}$  maintained rapidly growing cells (mean cell length of  $6.1 \mu\text{m}$ ) and low EGFP background fluorescence, after 3 days we observed zones in the reactor with biofilms and patchy increase in the background signal (not shown), and an overall increase in the number of cells in the reactor chamber (Figure 4.9). This suggests that in the absence of turbulent mixing in the microfluidic reactor the reporter cells start sticking to the glass and PDMS surface over time, forming biofilms (Figure 4.11), which causes preferential flow of nutrients and local occurrence of slow-growing or stationary phase cells. Sticking also occurred in the flow lines and prevented proper emptying of the measurement zone.

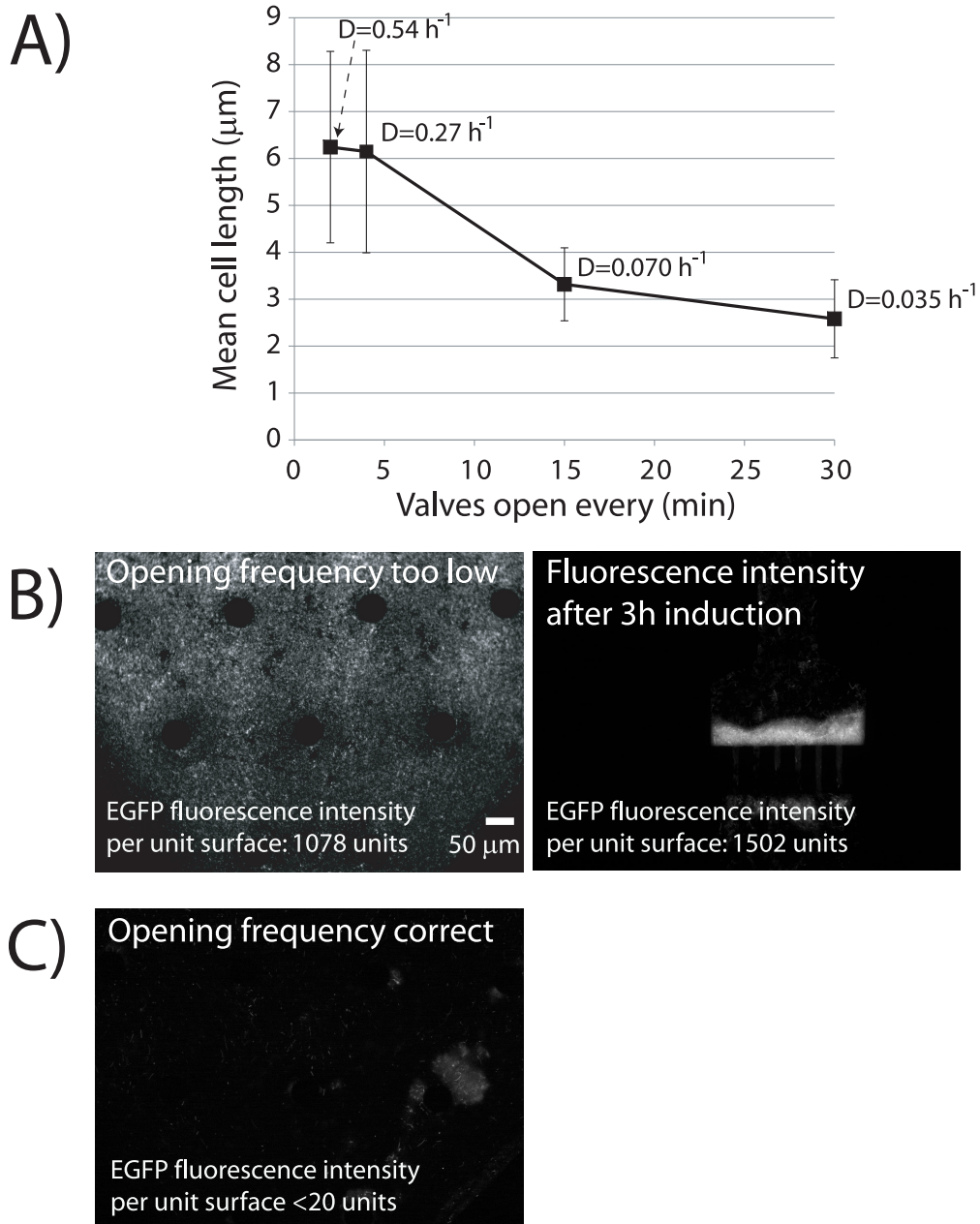


Figure 4.8: A) Mean cell length (on 100 values) of cells maintained 20 h on chip in function of the opening frequency. B) Fluorescence picture (exposure time of 66 ms) of the cells maintained 20 h in the chamber with an opening frequency too low (every 15 minutes or more, left). Typical fluorescence intensity level of cells exposed to 50 µg/L of arsenite (right). When the background fluorescence level of the cells in the chamber becomes too close to the one corresponding to induced cells, they can not be used as a biosensor anymore, as their background would mask the arsenic response. C) Fluorescence picture (exposure time of 66 ms) of the cells maintained 20 h in the chamber with a suitable opening frequency (every 4 minutes).

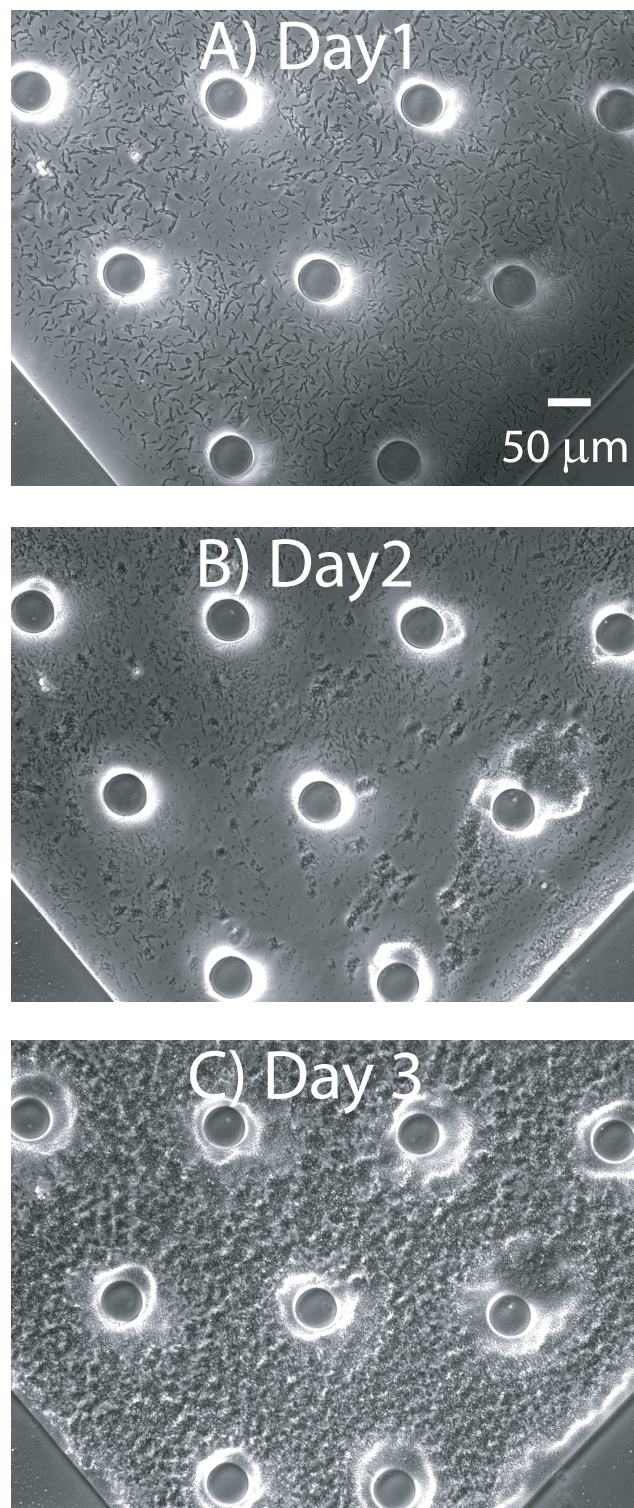


Figure 4.9: Images of cells in the microchamber on day 1 (A), 2 (B) and 3 (C) with a valves opening frequency and time of  $1/4 \text{ min}^{-1}$  and 120 ms respectively.

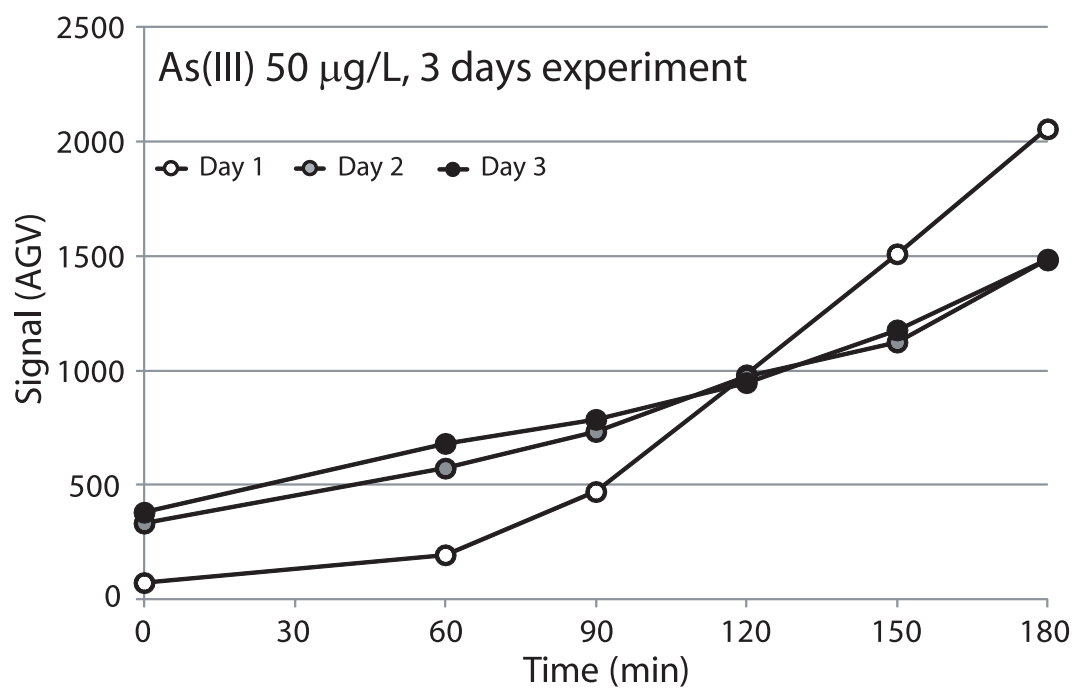


Figure 4.10: Induction with arsenite (50 µg/L) of cells maintained in the microchamber with a valves opening frequency and time of 1/4 min<sup>-1</sup> and 120 ms respectively for 1 (Figure 4.9 A), 2 (Figure 4.9 B) and 3 days (Figure 4.9 C).

Cells strain	Experiment time (days)	Driving $P^a$ (bar)	Opening $f^b$ ( $\text{min}^{-1}$ )	Opening duration <sup>c</sup> (ms)	$D^d$ ( $\text{h}^{-1}$ )	Background fluorescence	Cells sticking / Observations
1598	3	0.3	1/30	180	0.035	After 1 day it masks the arsenite response.	Cells tends to stick to each other and to the chip walls and to form a biofilm.
1598	3	0.3	1/15	120	0.070	After 1 day it starts to make the arsenic response hardly visible	Cells tends to stick to each other and to the chip walls and to form a biofilm but some non-sticky individual cells were observed.
1598	3	0.3	1/4	120	0.270	Arsenite response clearly visible after 3 days.	During the first day and a half most of the cells are non-sticky individual cells but after they start to stick to each other and to the chip walls and to form a biofilm.
1598	3	0.3	1/2	120	0.540	Arsenite response clearly visible after 3 days.	Most of the cells are non-sticky individual cells. Cells accumulations against the filter takes too long (>2 h) because of the small number of cells in the chamber ( $D$ too high).

Table 4.1: Chemostat parameters tested. a) Pressure applied to the nutrients inlet driving the nutrients solution and cells outflow. b) Opening frequency of the chamber valves. c) Time during which the chamber valves are open. d) Reactor apparent dilution rate.

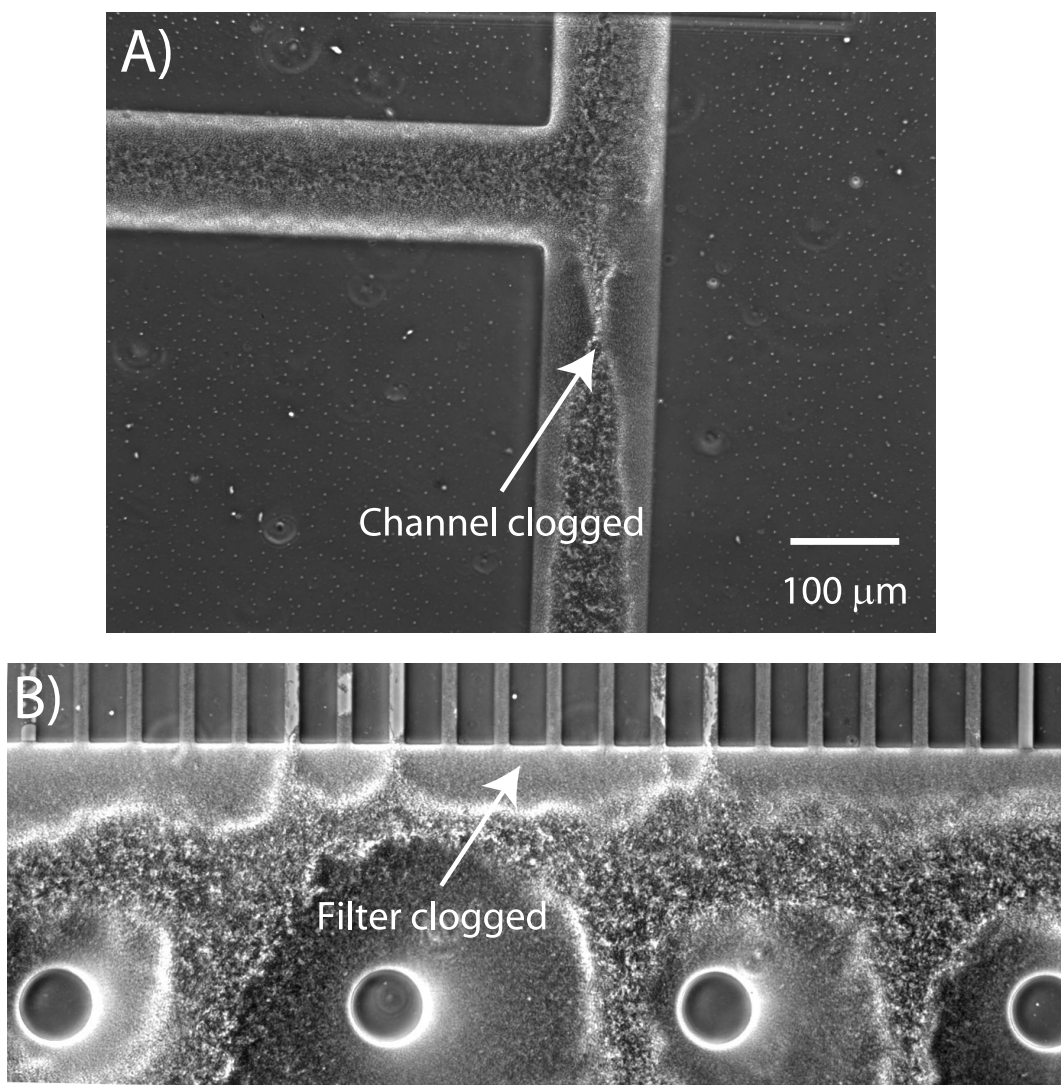


Figure 4.11: Clogging of a chip channel (A) and of the chamber filter in a 3 days experiment without adding Triton X-100 and with  $1/4 \text{ min}^{-1}$  and 120 ms of valves opening time and frequency respectively.

### 4.5.3 Nutrient medium optimization

In order to prevent sticking of the cells to the chemostat walls and flow lanes, we tested the addition of low concentrations of a detergent into the nutrient solution. After having verified that concentrations of Triton X-100  $<0.1\%$  have very little effect on batch growth rates of *E. coli* 1598 cells and on their inducibility (data not shown), we added to the microchemostat

nutrients medium 0.1% of this detergent. In this case, as illustrated in Figure 4.12, using the optimized parameters values previously determined (*i.e.*  $1/4 \text{ min}^{-1}$  and 120ms), the sticking of the cells was drastically reduced, the cells maintaining on chip was possible for several days (6 days) and we noticed that their number in the chamber was almost constant (Figure 4.12), suggesting that we could obtain steady-state continuous growth conditions. Video-imaging of the valves during chamber opening suggested qualitatively that the amount of cells released during every cycle opening remained more or less constant during the whole experiment. The mean cell length of the cells under those conditions remained constant over time and close to  $6.2 \pm 0.2 \mu\text{m}$  (Figure 4.13), which is very close to the mean cell length measured at the early phase of growth at the previous nutrient medium ( $6.1 \pm 2.1 \mu\text{m}$ ). Assuming that the chemostat on average is operated at  $0.27 \text{ h}^{-1}$ , the approximate generation time of cells in the reactor is 2.6 h (Equation 4.20). Obviously, as the cells do not stick anymore, the number of cells in the chamber is much lower when compared to the case without the addition of Triton X-100, but this amount is still enough to perform a measurement (the accumulation time was of ca. 1.5 h). Figure 4.14 shows the induction curve of cells maintained 6 days on chip and exposed to  $50 \mu\text{g/L}$  of arsenite.



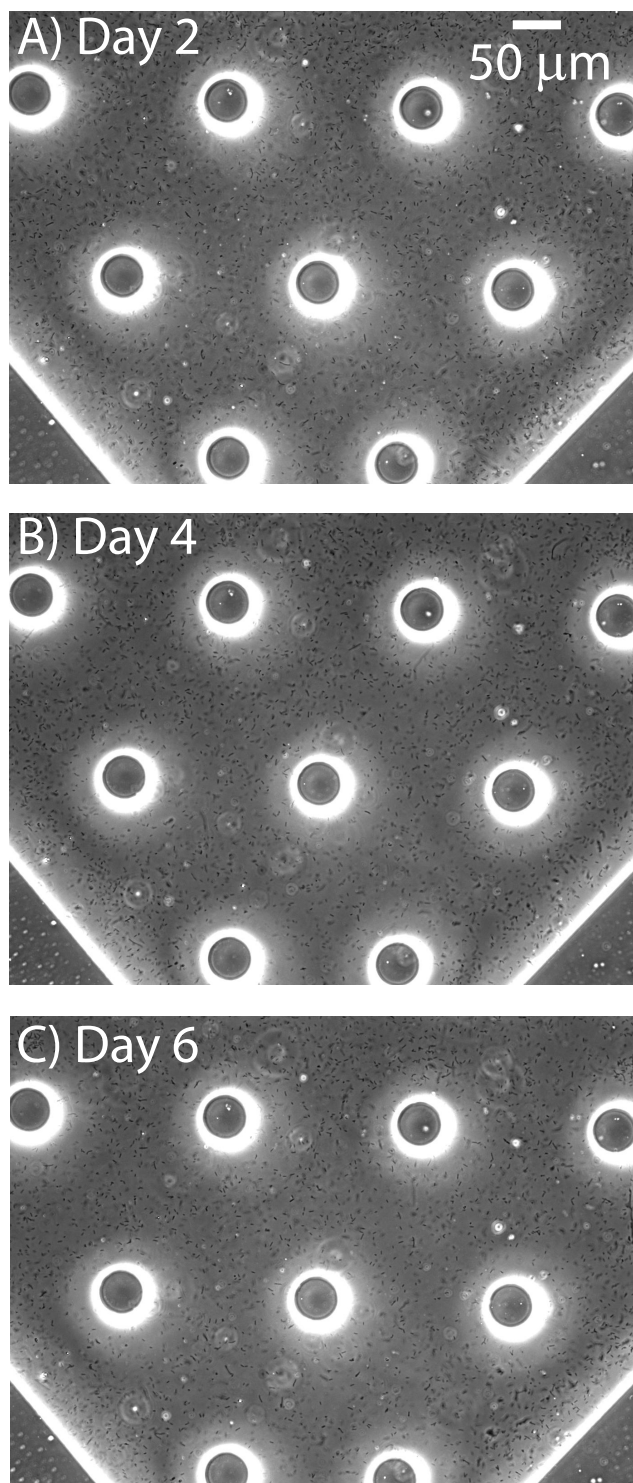


Figure 4.12: Images of cells in the microchamber on day 2 (A), 4 (B) and 6 (C) with the addition of Triton X-100 and a valves opening frequency and time of  $1/4 \text{ min}^{-1}$  and 120 ms respectively.



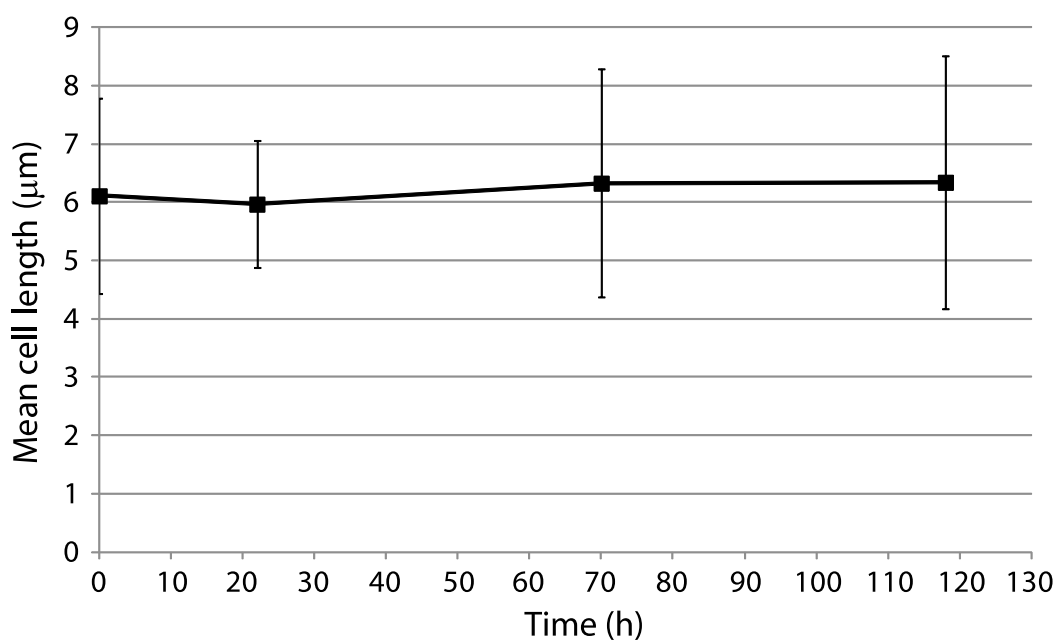


Figure 4.13: Mean cells length (on 100 values) of the cells in the chamber for different days with the addition of Triton X-100 and a valves opening frequency and time of  $1/4 \text{ min}^{-1}$  and 120 ms respectively.

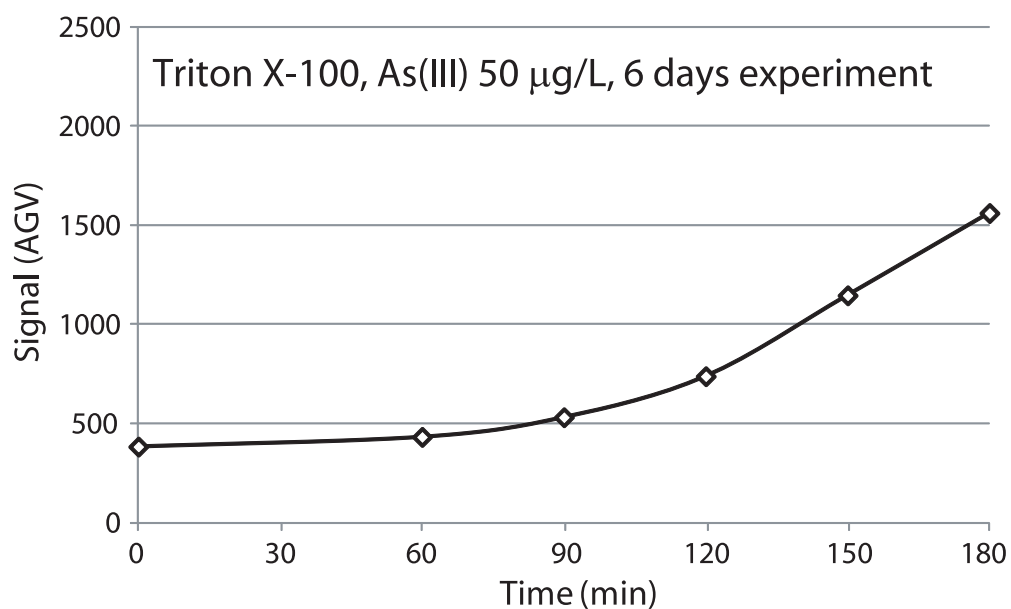


Figure 4.14: Induction with arsenite ( $50 \mu\text{g/L}$ ) of cells maintained in the microchamber for 6 days with the addition of Triton X-100 and with a valves opening frequency and time of  $1/4 \text{ min}^{-1}$  and 120 ms respectively (4.12 C).

### 4.5.4 Cellular physiology in the microchemostat

In order to further examine the physiology of the *E. coli* reporter cells in the reactor, we repeated continuous growth with an *E. coli* strain (strain 4224) in which expression of unstable EGFP (half life  $\approx 40$  min [Andersen *et al.*, 1998]) is coupled to the *rrnB1* ribosomal promoter (chamber valves frequency and opening time of  $1/4 \text{ min}^{-1}$  and 120 ms, addition of Triton X-100). When these reporter cells are actively growing the *rrnB1* promoter is turned on and EGFP fluorescence increases. In contrast, in stationary phase cells the promoter is silent and EGFP fluorescence will decrease through degradation. When averaged across the whole microchemostat area we observed that the EGFP fluorescence diminished after inoculation and then remained more or less stable during the next 2 days (Figure 4.15 A). Visual observation of cells in the microchemostat area suggested that this is probably due to a wash-out of cells after inoculation. Afterwards, the number of cells in the reactor remained more or less constant and EGFP fluorescence slowly increased between day 2 and day 3. This suggested that the cells are actively growing and dividing, and the EGFP production rate is higher than the degradation rate. When in- and outflow were halted (as during an arsenic bioassay) EGFP fluorescence stabilized and started to decrease after 2 h, indicating that cells face nutrient starvation and enter into stationary phase. This step is reversible as soon as nutrient in- and outflow is resumed, and EGFP fluorescence will increase at the same rate as before. This suggests that cells again resume exponential growth.

To verify that there are no zones in the reactor where cells accumulate and have less supply of nutrients, we divided the fluorescence image of the reactor chamber at day 3 in rectangles and we verified that the average fluorescence signal per unit area of each rectangle is not significantly different from the one of the chamber (Chi-square test with a confidence interval of 95%, Figure 4.15 B)

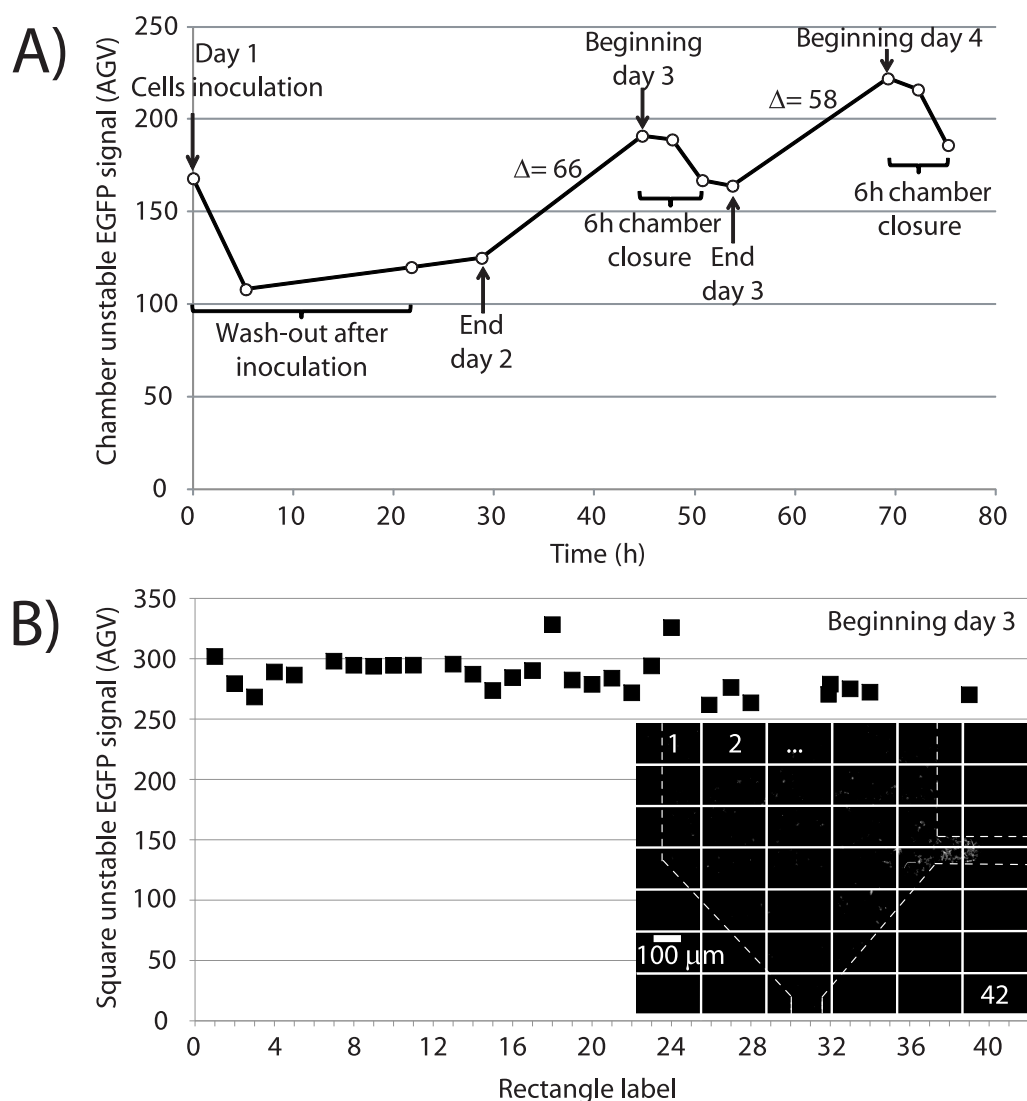


Figure 4.15: Results obtained with a strain constitutively expressing an unstable GFP (4224) in a 4 days experiment (parameters values of the chamber valves:  $1/4 \text{ min}^{-1}$  and 120 ms, addition of Triton X-100). A) Fluorescent signal per unit area from the overall chamber image (exposure time 600 ms, image was acquired at 100-fold magnification). After a stabilization phase (ca. 20h), during the normal chemostat functioning the signal is constantly increasing, while during the chamber valves closure it decreases. B) Fluorescence image of the chamber (exposure time 600 ms) at day 3. We divided the chamber in rectangles (image was acquired at 100-fold magnification) and we verified that the average fluorescence signal per unit area of each rectangle is not significantly different from the one of the chamber (Chi-square test with a confidence interval of 95%). We took into consideration just the rectangles overlapping the chamber.

### 4.6 Discussion

As the channels need to be rounded in order to be closed by the deflection of the upper channel [Unger *et al.*, 2000], it was not possible to construct their negative with silicon and thus we had to fabricate their negative by structuring a photoresist (AZ512) previously deposited on silicon. We found the adhesion of this resist on silicon good when compared to other resists, but the mold can be used less times to fabricate the corresponding PDMS layer with respect to a mold entirely made by silicon. However, in this case we do not have the problem of the required minimum filter wall length due to the downwards transfer of the filter profile as in the case of the previously developed single cells device (Figure 3.3).

From a design point of view, the next chip generation should contain a valve decoupling the chamber from the measurement zone. In fact, with the current design, when we take a measurement, the chamber needs to stay closed to avoid arsenic entering into it, the cells do not receive nutrients, and their background signal increases. Normally, when we restart the chamber valves opening and closing, the cells background signal lower itself again, but an additional valve after the channel going to the waste outlet (Figure 4.6) would completely solve this problem. Furthermore, from an application point of view, it would be necessary to have a second measurement zone using the cells coming from the same chamber in order to be able to perform a control measurement.

As showed in Section 1.2.5, the maintenance of chemostatic conditions on chip has been demonstrated by several research groups [Balagaddé *et al.*, 2005; Groisman *et al.*, 2005; Zhang *et al.*, 2006; Cookson *et al.*, 2005; Luo *et al.*, 2010; Edlich *et al.*, 2010; Lee *et al.*, 2011]. However, to our knowledge, no microfluidic device has been studied in which cells can be maintained in physiologically active state by continuous growth and at the same time exposed to a target compound.

When compared to the beads system, the chemostat on chip presents the advantage that it can be maintained at room temperature, thus eliminating the need of a freezer, and that allows multiple measurements on the same device. Furthermore, more important, as there is a continuous supply of fresh cells, the problem of the signal decrease with the time of storage presented by the beads system should in principle be solved, which is extremely important from an application point of view. However, because of a lack of robustness, we could not perform experiments that last more than one week and we can not confirm (or not) this

assumption, while with the beads system we know that measurements can be performed during one month. In fact, we had problems of water evaporation in the valves channels, which translated in air bubbles passing from the valves channels to the flow channels, and in the sealing of the solenoid valves connections, which resulted in air leakage and in the consequent depletion of the compressed air bottle. It has also to be noted that because of the integration of the PDMS valves, the microfabrication of the the chemostat on chip and the implementation of the setup surrounding it is less straightforward than one of the beads chip.

## 4.7 Conclusions and outlook

### 4.7.1 Summary of results

We redesigned the microfluidic chip in such a way as to create a nL-chemostat reactor for the reporter cells with integrated valves operated by pressurized channels in a second PDMS layer. We demonstrated how cells can be continuously grown for up to 1 week in a miniaturized reactor on the cartridge and remain in physiologically active state (exponential growth). We further showed how part of the reporter cell biomass from the reactor can be released and transferred to a measurement zone where the cells can be trapped by a filter and exposed to an aqueous sample containing arsenic. The filter can be cleaned from cells and the procedure can be repeated for a new measurement.

### 4.7.2 Perspectives

The system we developed represents an important demonstration for an automated bioreporter device that can potentially be used as basis in other biosensor platforms. However, in the optics of an in-field application, it is necessary to develop an optical detection system and to construct an instrument housing the microfluidic cartridge, and the robustness of the cartridge itself needs to be improved so that a long term function (one month) can be reached.



# 5 Arsenite transport effect on the bioreporter signal production

## 5.1 Introduction

Whereas the previously developed filter wall for reporter cells served its purpose as signal concentrator, no arsenic transport effect was observed. In order to investigate the relation between target compound transport and reporter signal production, we exposed cells stacked against a filter wall to aqueous solutions with different arsenite concentrations at different flow rates. We noticed that extensive gradients of reporter signal intensity formed as a function of distance to the inflowing sample, of the arsenite concentration and of flow rate. Therefore, we attempted to understand the nature of these gradients by a modeling approach. This chapter focuses on this investigation and aims to give a better understanding on the mechanisms occurring in the bioreporter cells in the presence of arsenite.

## 5.2 Materials and methods

### 5.2.1 Microfluidic chip design and micofabrication

The microfluidic chip is composed of a two-layered polydimethylsiloxane (PDMS) block bonded on a transparent glass slide with thickness of 1 mm (Figure 5.1 B). The (lower) layer contains two inflow channels converging to a filter (Figure 5.1 A). The flow channels have a height of 20  $\mu\text{m}$  and width of 100  $\mu\text{m}$ , whereas the filter outlet channels were designed with a height of 600 nm, obstructing *E. coli* cell passage ( $\varnothing$ 1  $\mu\text{m}$ , length 2-5  $\mu\text{m}$ ) but allowing liquid flow. The top (control) layer contains a set of pressure-controlled valves, which can open and

## Chapter 5. Arsenite transport effect on the bioreporter signal production

close the inflow channels in the microfluidics layer. With this device it is thus possible to first accumulate the required amount of cells and then expose them to the arsenic solution. The chip fabrication and the control and working principle of the PDMS valves are the same as in the case of the chemostat on chip and are described in Sections 4.4.1 and 4.4.2.

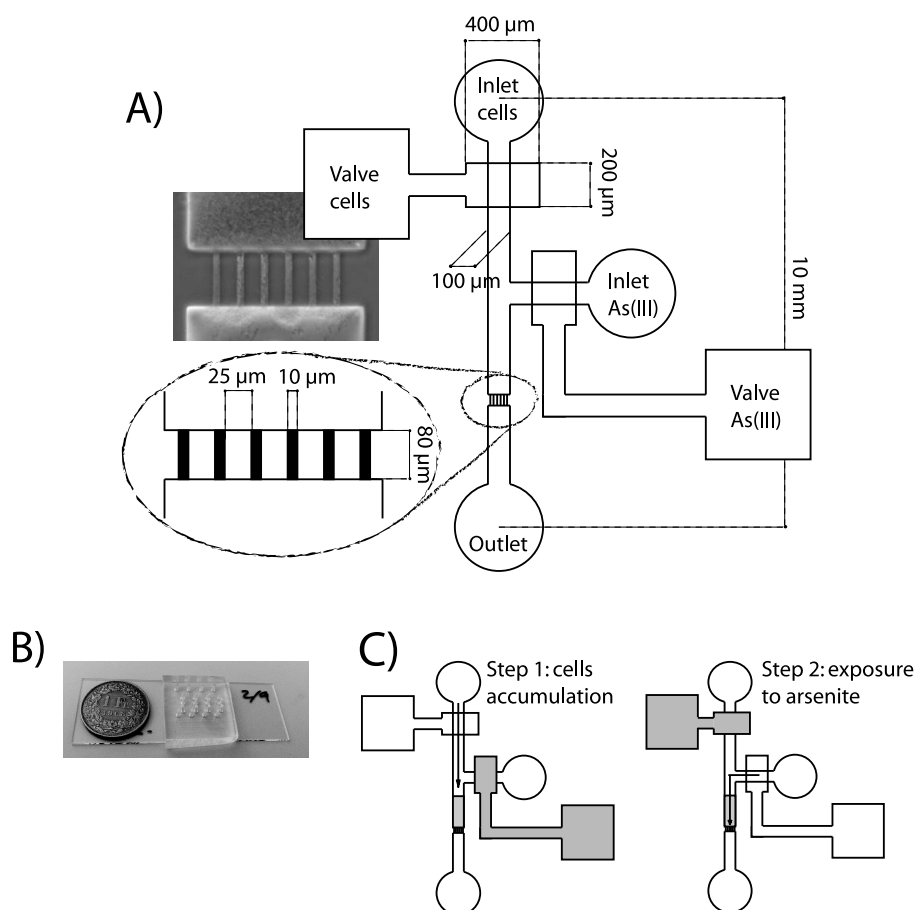


Figure 5.1: Working principle of the microfluidic chip. A) The chip is composed of two crossing channels, one for the arsenite solution and one for the cells, each controlled by a valve. The joining channel contains a filter, which traps the cells (image was acquired at 200-fold magnification), while allowing flow through the holes. In this way it is possible to first accumulate the desired amount of cells and then expose them to the arsenite solution. B) The chip is contained in a PDMS block bonded on a glass slide. C) Experiment steps. The first step consists in closing the arsenite valve and opening the cells valve so that the cells accumulate against the filter. The second one consists in closing the cells valve and opening the arsenite valve so that the accumulated cells are exposed to the arsenite solution.



### 5.2.2 Bioreporter strain

To test the arsenic transport effect, the previously described *E. coli* DH5 $\alpha$  strain 1598 (pPROBE-arsR-ABS) is employed, while as a control for constitutive EGFP production strain 2386 is used.

### 5.2.3 Reporter cells preparation

Starting from a single colony, *E. coli* DH5 $\alpha$  strain 1598 (pPROBE-arsR-ABS) or 2386 is grown in Luria-Bertani (LB) medium in the presence of 50  $\mu\text{g}/\text{mL}$  kanamycin at 37°C for 18 h and with 180 rpm agitation of the culture flask. The bacterial culture is then 100-fold diluted into fresh LB medium plus kanamycin and incubated for a further 2 h at 37°C and with 180 rpm agitation. At a culture turbidity at 600 nm of between 0.130 and 0.200 (representative for early exponential phase), cells from 8 mL of culture are harvested by centrifugation at 5000 rpm for 6 min and room temperature. The cell pellet is then resuspended into 50  $\mu\text{L}$  of MOPS medium. The final concentration of cells in the suspension equals about  $2 \cdot 10^{10}/\text{mL}$ .

### 5.2.4 Microchip bioreporter induction

Bioreporter cells are loaded in the cavity by opening the valve for the cell inflow line, pipetting the bioreporter cell suspension (7  $\mu\text{L}$ ) in the inlet reservoir and applying a pressure of 0.3 bar to drive the flow of cells towards the filter wall (Figure 5.1 C, left). Once the required amount of cells is accumulated, the cell inflow valve is closed and the arsenite sample is connected to the sample inlet. Samples are introduced by means of a 50  $\mu\text{L}$  syringe mounted on a syringe pump (Harvard, Pump 22 Multiple Syringe Pump) connected to the chip inlet with a 1.06 mm diameter PTFE tubing (Fisher Scientific). Cells are exposed to the arsenite sample by opening the sample valve and flushing the sample through the filter at flow rates of 0.1, 0.5, 1.0 or 2.0  $\mu\text{L}/\text{h}$  (Figure 5.1 C, right). Two arsenite concentrations are tested (10 and 50  $\mu\text{g}$  As(III)/L) and compared to a control of MOPS only. Arsenite solutions are prepared by making appropriate dilutions of a 50 mM stock solution of sodium arsenite ( $\text{NaAsO}_2$ , Merck) in MOPS medium.

### 5.2.5 Quantification of EGFP fluorescence

Reporter cells are exposed for up to 3 h at room temperature under constant flow. EGFP fluorescence from the reporter cells in the cavity of the microfluidic chip is imaged using a Leica DFC320 cooled black and white charge-coupled device camera (Leica Microsystem CMS GmbH, Wetzlar, Germany) mounted on a Leica DMI6000B inverted epifluorescence microscope. Cells are imaged every 20 minutes during incubation and as a function of distance to the filter outlet channels using 100-fold magnification. Images are recorded in 16-bit TIFF files at an exposition time of 66 ms (Leica AF6000), both for phase-contrast and for EGFP fluorescence (BP470/40 filter, Leica). Images are exported and the signal intensity profile as a function of distance is determined using ImageJ (National Institutes of Health). A moving average on 9 points is applied to average the signal intensity profiles.

### 5.2.6 Modeling

The developed model describes the EGFP production by the reporter cells as a function of arsenite flux through the flow channel and cell layers stacking on the filter. The cell layers are separated in 5  $\mu\text{m}$  thick slices and both arsenite influx and efflux per slice, and EGFP production rate per slice are calculated. The EGFP production rate per slice is taken as the sum of production from individual bioreporter cells. The individual EGFP production per cell is modeled from a simplified biological mechanism of arsenite-influx into and efflux from the cell, plus ArsR/arsenite-dependent induction of ArsR/EGFP production from the reporter circuit and of the ArsB efflux pump (Figure 5.2). We used "discrete" modeling, meaning that at each time-step the cell can take up, produce and export only an integer number of molecules or proteins. Because of the fixed cellular volume and discrete modeling, we translated all equations to molecules per cell instead of concentrations (mol/L), as indicated. In order to take into account the fact that, due to the applied pressure, the PDMS channels expand (as explained in section 4.4.1), we introduced a so-called expansion factor, which multiply the designed channels height and width. The detailed modeling steps are described hereafter.

1. Arsenite influx is thought to be mediated by unspecific glycerol channels, whose number per cell is assumed to be constant. The arsenite influx rate  $V_{As,in}$  (molecules per second per cell), can thus be described by Michaelis-Menten kinetic, and it is dependent on the external arsenite concentration  $[As_{out}]$ :

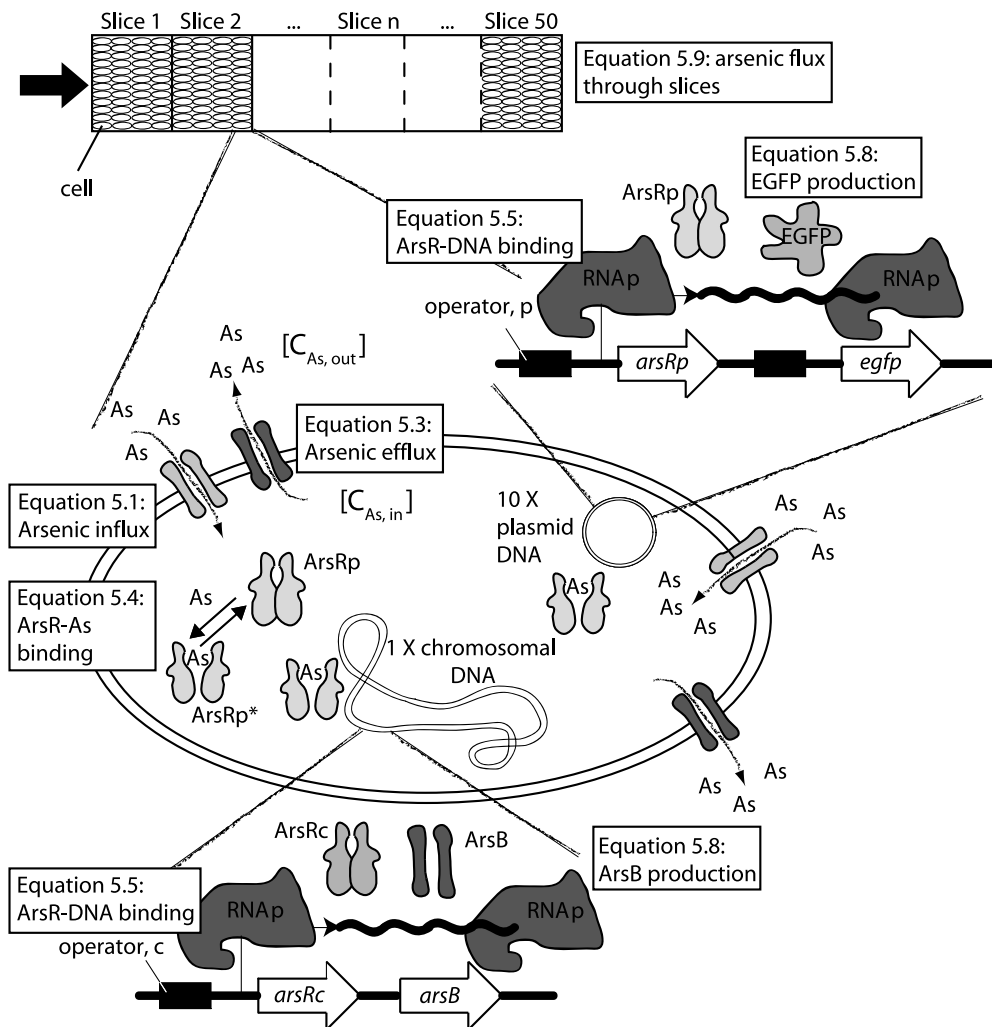


Figure 5.2: Schematic of the model. We divided the microfluidic channel in slices of  $5\ \mu\text{m}$  and we consider that the cells contained in the same slice see the same arsenite flow rate and concentration. Each cell captures and gives out a certain number of arsenite molecules (Equation 5.1 and 5.3) and, depending on its internal arsenite concentration, produces a certain amount of EGFP molecules (Equation 5.8), which determines the fluorescence signal. The flux of arsenite molecules coming to the considered slice is the flux coming to the previous slice minus the number of molecules it takes in and plus the number of molecules it gives out (Equation 5.9).

$$V_{As,in} = V_{As,in,max} \frac{[As_{out}]}{[As_{out}] + K_{m,in}} \quad (5.1)$$

where  $V_{As,in,max}$  is the maximum influx rate and  $K_{m,in}$  is the external arsenite concentration at which the uptake rate is half of  $V_{As,in,max}$ .

2. Arsenite efflux from the cell is governed by a specific efflux protein ArsB and efflux kinetics ( $V_{As,out,MM}$ ) can be described again by Michaelis-Menten kinetics:

$$V_{As,out,MM} = V_{As,out,max} \frac{[As_{in}]}{[As_{in}] + K_{m,out}} \quad (5.2)$$

where  $V_{As,out,max}$  is the maximum efflux rate,  $K_{m,out}$  is the concentration of arsenite present in the cell ( $[As_{in}]$ ) at which the reaction rate is half of  $V_{As,out,max}$ . In contrast to arsenite influx, the actual arsenite efflux rate  $V_{As,out}$  is a function of the intracellular arsenite concentration, but is also dependent on the number of ArsB pumps per cell  $[ArsB]$ , which are inducible in an ArsR/arsenite dependent manner:

$$V_{As,out} = V_{As,out,MM} \frac{[ArsB]}{[ArsB_{max}]} \quad (5.3)$$

where  $[ArsB_{max}]$  is the maximum number of ArsB molecules per cell.

3. ArsR/arsenite dependent induction is governed by the intracellular arsenite concentration. For simplicity we assume that the gene products of *arsR* on the reporter plasmid (approximately 10 copies) and of the chromosomal *arsR* (1 copy) behave similarly. The repression/derepression cycle by ArsR on  $P_{ars}$  can be described by two equilibria. The first is the dimerization and binding of arsenite to ArsR:



with an equilibrium constant  $K_{d,1}$ . The second describes the binding and dissociation of ArsR dimers to the operator DNA:



with an equilibrium constant  $K_{d,2}$ , where  $[ArsR_d]$  is the concentration in molecules per

cell of ArsR-dimer and  $[DNAArsR_d]$  is the concentration in molecules per cell of ArsR-dimer bound to the operator-*DNA*. Consequently,  $[AsArsR_d]$  is the concentration in molecules per cell of ArsR-dimer that has bound *As*; this results in its dissociation from the *DNA* operator. The model further assumes that when  $ArsR_d$  is bound to its operator *DNA*, transcription and production of ArsR or ArsB does not occur. Reactions 5.4 and 5.5 can be rewritten and combined for  $[ArsR_d]$ :

$$[ArsR_d] = K_{d,1} \frac{[AsArsR_d]}{[As_{in}]} \quad (5.6)$$

and

$$[ArsR_d] = K_{d,2} \frac{[DNAArsR_d]}{[DNA]} \quad (5.7)$$

producing:

$$\frac{[AsArsR_d]}{[DNAArsR_d]} = \frac{K_{d,2}}{K_{d,1}} \frac{[As_{in}]}{[DNA]} \quad (5.8)$$

Equation 5.8 gives the equilibrium ratio between the concentration of unbound  $ArsR_d$  molecules and  $ArsR_d$  bound to *DNA*. Since both *K*-values are constant and the number of *DNA* binding sites per cell is constant (=11), this ratio is only dependent on the intracellular arsenite concentration. For modelling purposes, we translate this ratio into a time fraction; the fraction of time per cell during which  $ArsR_d$  is unbound versus bound to its operator *DNA*.

4. The production of ArsR, EGFP and ArsB can be modeled from the ArsR/arsenite dependent feedback loops. Thus, when  $ArsR_d$  is bound to the operator *DNA* there is no production of ArsR, EGFP and ArsB, whereas when the operator *DNA* is free the production of ArsR, EGFP and ArsB occurs at the maximum production rate (10 per minute for ArsR and 0.1 per minute for ArsB). We further assume that the measured fluorescent signal is proportional to the number of EGFP molecules produced.
5. Finally, by calculating the number of arsenite molecules entering, binding to  $ArsR_d$ , and exiting from each cell, and multiplying these values by an estimated packed number of cells per slice ( $n = 2 \cdot 10^4$ ), we obtain the arsenite influx, "loss" and efflux per slice. The arsenite influx in slice<sub>*n*</sub> is thus a function of the influx to slice<sub>*n-1*</sub> and the internal uptake

and efflux in and from cells of slice<sub>n-1</sub>:

$$As_{influx, slice\ n} = As_{influx, slice\ (n-1)} - As_{uptake, slice\ (n-1)} + As_{efflux, slice\ (n-1)} \quad (5.9)$$

We translated all reactions into a Matlab code and we nested two "forward" loops: the first one controls the time, which, at each iteration, is increased by 1 s. The second loop, contained within the first one, controls the space dimension and at each iteration considers the next slice. For every time step we calculate how many arsenite molecules are flowing in and out per slice, and how many EGFP molecules are produced in each slice. Then we increase the time by one time-step and repeat the calculations.

The developed Matlab code can be found in Appendix A.

### 5.3 Results

#### 5.3.1 Microfluidic chip

For flow rates smaller than 2  $\mu\text{L}/\text{h}$ , the 600 nm PDMS pores act as an effective filter trap for the cells whereas the aqueous solution passes through. By applying a pressure of ca. 0.3 bar to the flow channel and with a cells concentration of  $2 \cdot 10^{10}/\text{mL}$ , we found that the waiting time to accumulate the necessary amount of reporter cells, that is filling a volume of  $20 \times 100 \times 250 \mu\text{m}^3$ , is ca. 30 minutes.

#### 5.3.2 Bioreporter signal development as function of arsenite flux

We exposed the *E. coli* reporter cells to aqueous concentrations of 0, 10 and 50  $\mu\text{g As(III)}/\text{L}$ , and at flow rates between 0.1 and 2  $\mu\text{L}/\text{h}$  for periods of up to 200 min. Averaged reporter signal intensity profiles after 200 min exposure time (Figure 5.3 A and B), show a strong fluorescence gradient along the distance over the cell layers, with low fluorescence close to the filter pores and highest fluorescence in the cell layers exposed "first" to the arsenite sample. This suggests that cells furthest away from the arsenite inflow did not receive any arsenite during the duration of exposure and did not derepress the EGFP reporter circuit. Conversely, cells closest to the arsenite inflow "source" became derepressed first and started accumulating EGFP. In order to exclude that the observed gradient was due to nutrient depletion, lack of

oxygen for EGFP maturation or to a cell density packing effect (higher local density of cells causing more apparent fluorescence), we repeated the same experiment using a *E. coli* strain constitutively producing the EGFP protein (number 2386). In this case no gradient but a homogeneous fluorescence signal was measured along distance (Figure 5.3 D), indicating that the previously observed gradient formation with the arsenite bioreporter strain 1598 must have been the result of an arsenite gradient forming along distance. This was contrary to our expectations of the arsenite derepression mechanism, which dictates that cells are "inert" for arsenite, meaning it only flows in and is pumped out without being retained. Moreover, at an exposure duration of 200 min the front of the arsenite inflow moves  $1.5 \cdot 10^5 \mu\text{m}$  in the flow channels, which would be largely sufficient to transport arsenite to all cells in the filter zone. We thus speculated that the cause of an arsenite gradient was local arsenite depletion by the cells. If the cells closest to the sample inflow would somehow "store" the arsenite in the cells, this would gradually deplete arsenite from the sample flow and there would not be enough for downstream cells to derepress the reporter construct and develop fluorescence.

Interestingly, the gradients were dependent on the arsenite concentration and on the sample flow rate. We observed that for the same arsenite concentration the fluorescence zone length linearly increased with the flow rate (Figure 5.3 A, Table 5.1), but not the maximum fluorescence intensity. In contrast, the maximum intensity increased with higher arsenite concentrations, and at  $50 \mu\text{g/L As(III)}$  the maximum fluorescence of the reporter cell layers was 4 times higher than at  $10 \mu\text{g/L As(III)}$  (Figure 5.3 A, Table 5.1). Reporter signal development was also faster at higher As(III) concentration. Whereas at  $10 \mu\text{g As(III)/L}$  the fluorescence signal started to develop after 140-160 minutes perfusion, this only took 60-80 min at  $50 \mu\text{g As(III)/L}$  (Figure 5.4). The ratio between the maximum values for different concentrations as well as the times needed for the signals to develop are in agreement with experiments performed with a combination of flow rates and amounts of cells for which no gradient is observed (Section 3.3.2).

Using the determined fluorescence zone length, we calculated the storage capacity of one cell. We found that it is independent on the flow rate and, surprisingly, that it is higher for a concentration of  $10 \mu\text{g/L As(III)}$  than for a concentration of  $50 \mu\text{g/L As(III)}$ . In fact, in the first case it is  $8.4 \cdot 10^{-2} \pm 1.2 \cdot 10^{-2}$  fg, while for a concentration of  $50 \mu\text{g/L}$  it is of  $4.3 \cdot 10^{-2} \pm 2.3 \cdot 10^{-3}$  fg.

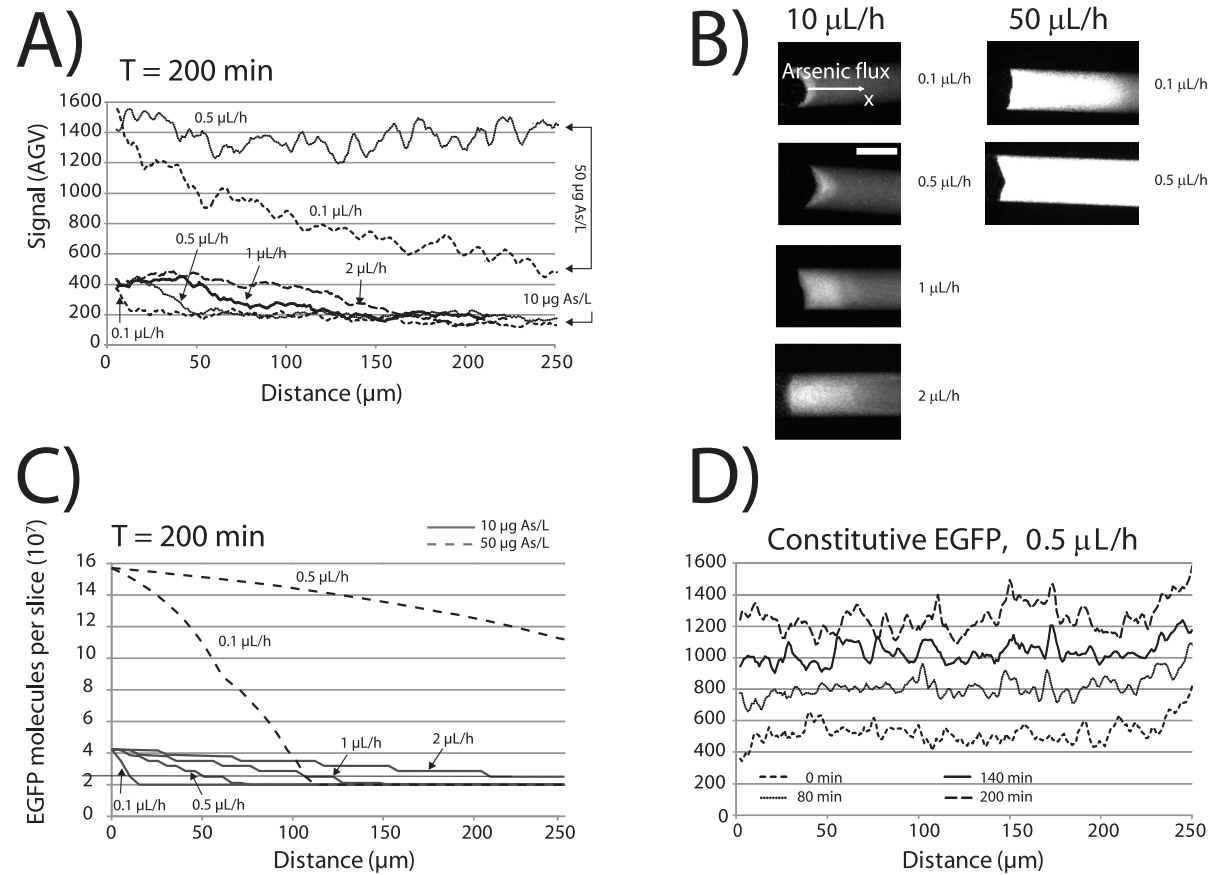


Figure 5.3: A) Fluorescence intensity profiles for arsenite concentrations of 10 and 50  $\mu\text{g/L}$  and for flow rates of 0.1, 0.5, 1 and 2  $\mu\text{L/h}$  (moving average on 9 points). Measurements were repeated twice. B) Fluorescence images of the cells exposed to the different arsenite flow rates and concentrations after 200 minutes (same gray level scale for all pictures, images were acquired at 100-fold magnification) Scale bar, 100  $\mu\text{m}$ . C) Modeled fluorescence intensity profiles for arsenite concentrations of 10 and 50  $\mu\text{g/L}$  and for flow rates of 0.1, 0.5, 1 and 2  $\mu\text{L/h}$ . D) Fluorescence intensity profiles at different times obtained using a constitutive EGFP strain (moving average on 9 points). The flow rate was set to 0.5  $\mu\text{L/h}$ .



As(III) concentration ( $\mu\text{g/L}$ )	Flow rate ( $\mu\text{L/h}$ )	Measured	Modeled	Error (%) <sup>c</sup>
		<b>Fluorescence zone length (<math>\mu\text{m}</math>)<sup>a</sup></b>		
10	0.1	7	8	13
	0.5	30	40	25
	1	59	79	22
	2	121	155	22
50	0.1	109	73	49
		<b>50 to 10 <math>\mu\text{g/L}</math> ratio<sup>b</sup></b>		
		3.75	3.72	1

Table 5.1: a) With a constant arsenite concentration, the fluorescence zone length, defined as all the points above the threshold set as half of the curve maximum value, linearly increases with the flow rate. b) The maximum intensity of the fluorescence zone length increases with the arsenite concentration: passing from 10  $\mu\text{g/L}$  As(III) to 50  $\mu\text{g/L}$  As(III) it becomes 4 times higher. c) Percentage error of the measured curves with respect to the modeled curves.

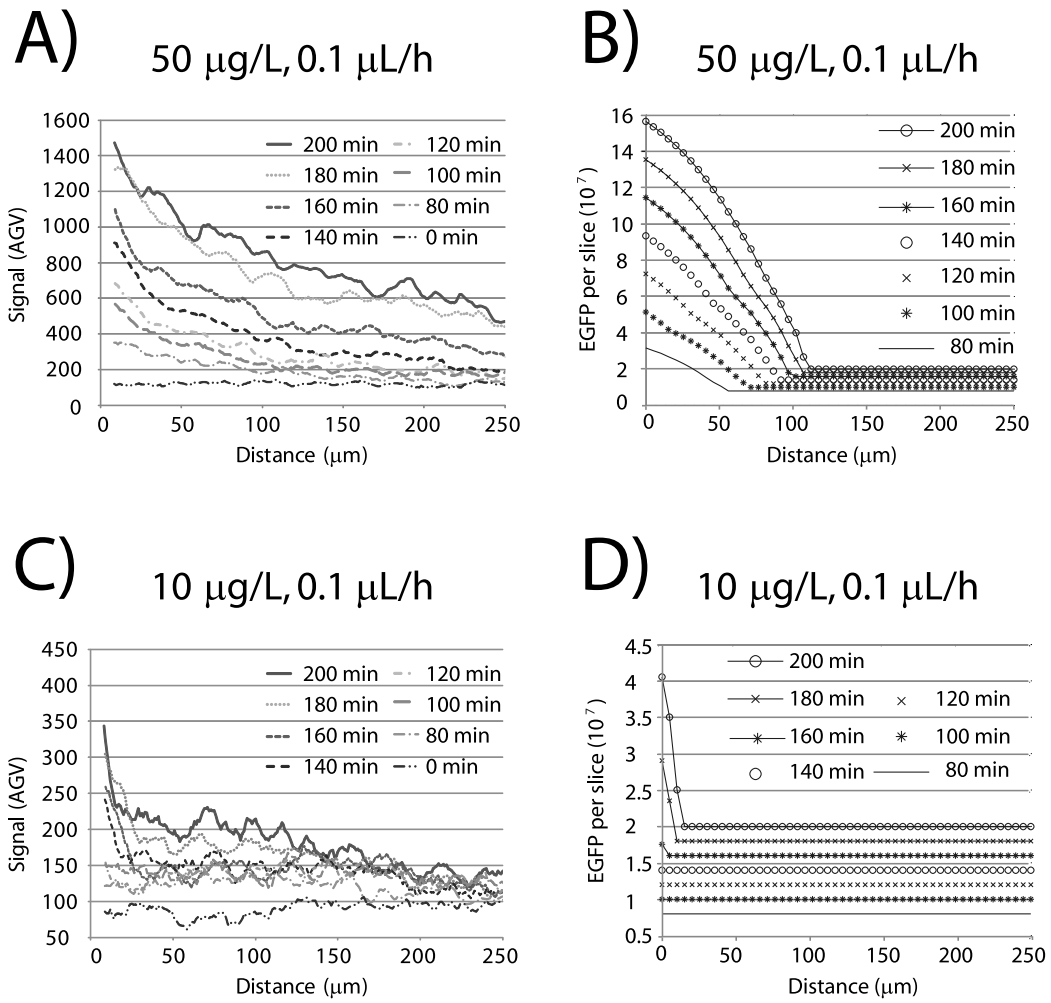


Figure 5.4: Time evolution of the experimental (A and C) and modeled (B and D) signals.

### 5.3.3 Model

Table 5.2 summarizes the nominal values for the various equation parameters, with which we obtained the predictive EGFP production gradients shown in Figure 5.3 C. The expansion factor describes the fact that with the applied flow rates (and thus the pressure) the PDMS channels expands. Its value was chosen considering that for the range of flow rates applied (and thus pressures) we already see some cells, whose diameter is 1  $\mu\text{m}$ , escaping from the filter holes, which were designed with a height of 600 nm. The values of the arsenite influx parameters, i.e.  $K_{m,in}$ ,  $\text{in}$  and  $V_{As,in,max}$ , were chosen by tuning them around the data acquired from [Gronigen, 2009] to obtain the best match between the experimental and the model curves. The values of the efflux parameter were chosen assuming that the arsenite efflux has to be lower than the arsenite influx. Concerning the ones related to EGFP production: the DNA copies number is known and the ArsR production value was tuned around a value that seems to be reasonable. The value of the  $K_{d,2}/K_{d,1}$  ratio is significantly different from what was previously determined [Chen and Rosen, 1997; Gronigen, 2009], but only with this value we can obtain a good correspondence between the experimental and the model results.

The model matches well with the experimental results: the error on the fluorescence zone length is always less than 50% and the one on its intensity is 1% (Table 5.1). Furthermore, there is a good correspondence also in the signals time evolutions (Figure 5.4): the modeled signals start to develop after 160 minutes for a concentration of 10  $\mu\text{g/L}$  and after 60 minutes for a concentration of 50  $\mu\text{g/L}$ , while the measured ones after 140-160 minutes for a concentration of 10  $\mu\text{g/L}$  and after 60-80 minutes for a concentration of 50  $\mu\text{g/L}$ .

Figure 5.5 shows the model sensitivity analysis: we doubled and divided by 2 the nominal value of model parameters and we traced the resulting curves. Increasing (respectively decreasing) the maximum rate at which the cell can take in the arsenite molecules, i.e.  $V_{As,in,max}$ , increases (respectively decreases) the number of EGFP molecules produced. This is explained by the fact that if there are more (less) arsenite molecules entering the cell per unit time, after a certain amount of time there are also more (less) arsenite molecules in the cell (Equation 5.1) and thus more (less) unbound ArsR<sub>d</sub> (Equation 5.8), which translates in more (less) EGFP produced. The curves for the 10  $\mu\text{g/L}$  As(III) and the 50  $\mu\text{g/L}$  As(III) are differently affected by these changes: in the case of an arsenite concentration of 10  $\mu\text{g/L}$  the increase (decrease) is, in proportion, higher and we observe that the curve slope becomes steeper (less steep), which is not the

## Chapter 5. Arsenite transport effect on the bioreporter signal production

---

case for the 50  $\mu\text{g/L}$  As(III). The effect of changing the  $K_{m,in}$  value is similar to the effect of changing the  $V_{As,in,max}$  value and this is explained by the fact that if the external concentration needed to have an arsenite import rate which is half of the maximum decreases (increases), the number of arsenite molecules entering the cell per unit time increases (decreases) and so does the number of EGFP molecules produced. If the number of plasmids increases (decreases), there are two phenomena occurring at the same time: according to Equation 5.8, the time during which the *DNA* plasmids are free to produce EGFP molecules decreases (increases), but on the other hand during this time the EGFP production rate is higher (lower) because of the higher (lower) number of plasmids. In the case of an arsenite concentration of 50  $\mu\text{g/L}$ , this higher (lower) production rate seems to play a major role, while for an arsenite concentration of 10  $\mu\text{g/L}$  the decrease in the EGFP production time has also to be taken into account. If the *ArsR* production rate increases (decreases), the number of EGFP molecules produced increases (decreases) as well. This is due to the fact that the EGFP production is coupled to the *ArsR* production (Figure 5.2). Again, the effect on the 10  $\mu\text{g/L}$  As(III) curve is not the same as the one on the 50  $\mu\text{g/L}$  As(III): in the case of an arsenite concentration of 10  $\mu\text{g/L}$  the increase (decrease) is, in proportion, higher and we observe that the curve slope becomes steeper (less steep), which is not the case for the 50  $\mu\text{g/L}$  As(III). Changing the value of the efflux parameters has no effect on the outcome (data not shown).

In order to further test our model, we plotted the fluorescence intensities of the first layer of cells as function of time and arsenite concentration (Figure 5.6 B). These curves should correspond to the ones obtained in the experiments in which the arsenite flow rate was sufficiently high or the number of cells exposed sufficiently low to prevent the gradients formation (Chapter 3, Figure 5.6 A). We observe that our model predict well the experimental behavior in terms of ratios between the endpoints of the different concentrations curves (the error on the endpoint ratios is always less than 20%). However, from a qualitative point of view, we observe that in the experimental curves it is the rate of signal increase rather than the time delay before the signal starts to develop that it is more affected by a change in the arsenite concentration, while in the modeled curves it seems to be the inverse.

<b>Arsenite flow</b>	<b>Value</b>	<b>Unit</b>
As(III) concentration	0, 10 and 50	μg/L
As(III) flow rate	0.1, 0.5, 1 and 2	μL/h
<b>Geometry</b>	<b>Value</b>	<b>Unit</b>
Channel length	250	μm
Channel height	20	μm
Channel width	100	μm
Slice length	5	μm
Cell diameter	1	μm
Cell length	2	μm
Expansion factor	1.7	-
<b>Influx</b>	<b>Value</b>	<b>Unit</b>
$K_{m,in}$	$1.6 \cdot 10^{-6}$	moles/L
$V_{As,in,max}$	125	molecules/(s · cell)
<b>Efflux</b>	<b>Value</b>	<b>Unit</b>
$K_{m,out}$	$5 \cdot 10^6$	molecules/cell
$V_{As,out,max}$	10	molecules/(s · cell)
ArsB production rate	$1.7 \cdot 10^{-3}$	molecules/(s · cell)
<b>EGFP production</b>	<b>Value</b>	<b>Unit</b>
$[DNA_{total}]$	11	molecules/cells
$[DNA_{plasmids}]$	10	molecules/cells
$[DNA_{chromosomal}]$	1	molecules/cells
$K_{d,2}/K_{d,1}$	$4.03 \cdot 10^{-5}$	-
ArsR production rate	$1.7 \cdot 10^{-1}$	molecules/(s · cell)

Table 5.2: Nominal values of the parameters used in the model.

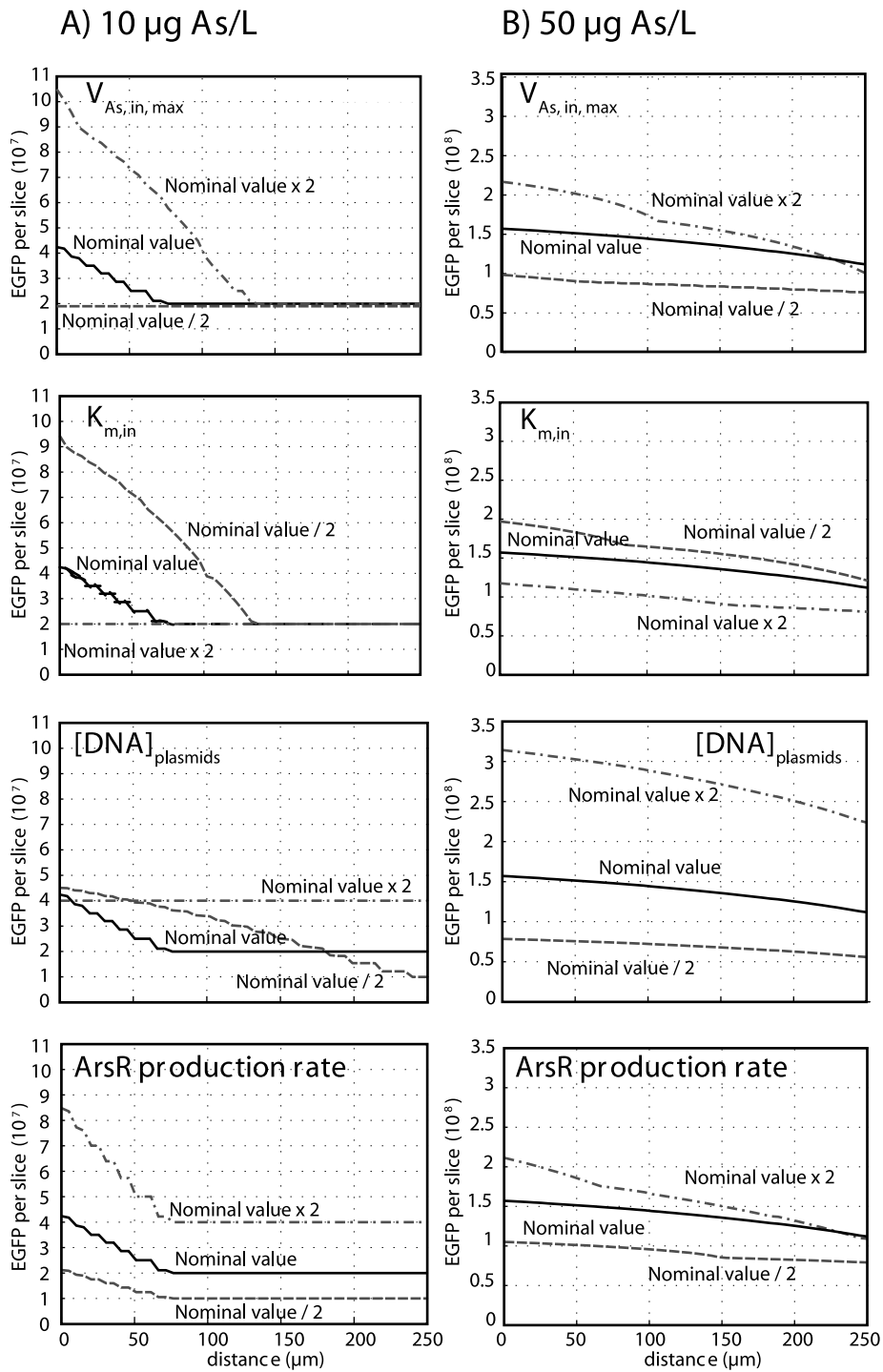


Figure 5.5: Effect on the model curves of varying the different parameters for a concentration of 10 and 50 µg/L and a flow rate of 0.5 µL/h.

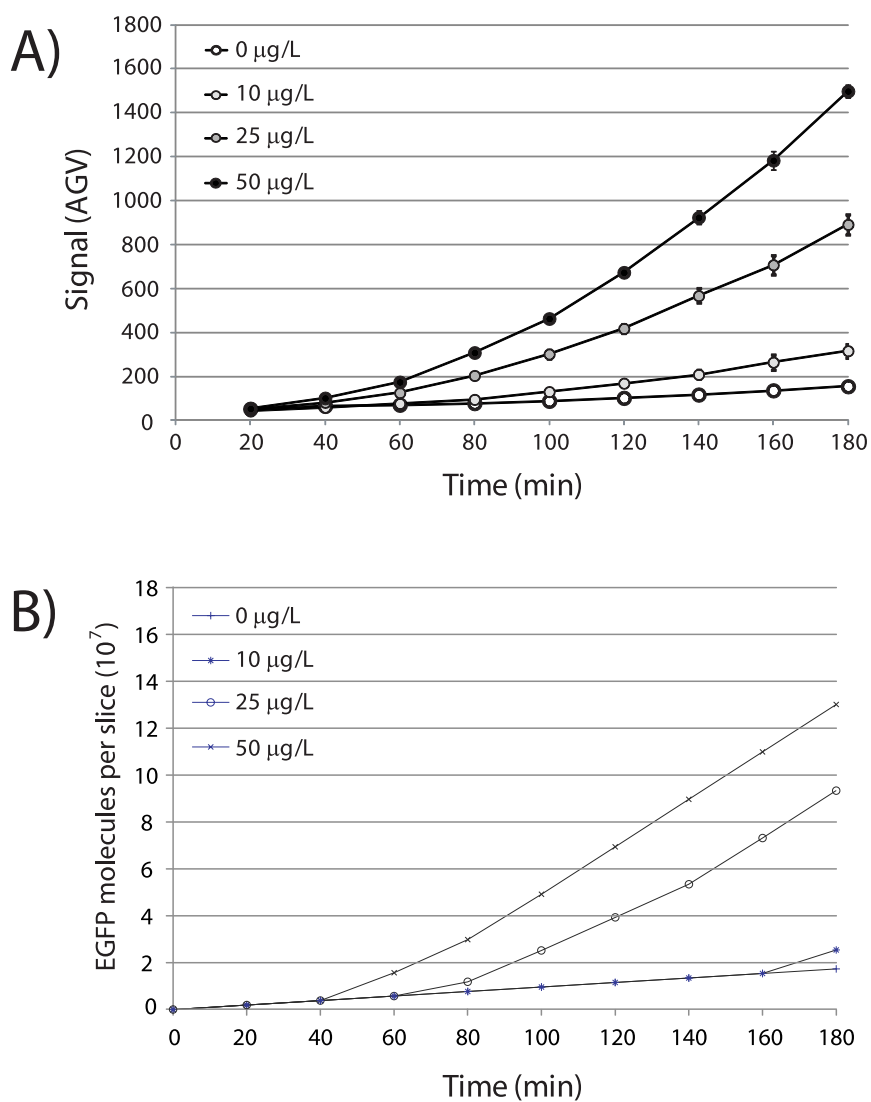


Figure 5.6: A) Experimental fluorescence intensities of trapped bioreporter cells as function of time and arsenite concentration in the case in which no gradients were observed (Chapter 3). B) Modeled fluorescence intensities of the first layer of the trapped bioreporter cells as function of time and arsenite concentration.

### 5.4 Discussion

As the observed gradients indicate that the reporter cells are able to store part of the incoming arsenite molecules (the storage capacity per cell in the case of an external arsenic concentration of 10  $\mu\text{g/L}$  is  $8.4 \cdot 10^{-2}$  fg), they could be used not only as a sensor but also as scavenger. However, to clean 1 L of water contaminated with 10  $\mu\text{g/L}$  of As(III), one would require  $1.2 \cdot 10^{11}$  cells, which is more than 5 orders of magnitude than the amount of cells that can be accumulated with this device, and a system able to handle volumes of water in the liter scale in a reasonable amount of time.

It is also interesting to notice that, at least for arsenite concentrations less than 50  $\mu\text{g/L}$ , the efflux pumps do not play a significant role, which means that all the arsenite taken in the cell stays in the cell.

In order to use accumulated bioreporter cells as a sensor, we need a detection area which is dependent only on the arsenite concentration. For this purpose an accumulated amount of cells of  $100 \times 100 \times 20 \mu\text{m}^3$  and a flow rate of 1-2  $\mu\text{L/h}$  seem to be adequate. In fact, a higher amount of accumulated cells would require a higher flow rate (to avoid fluorescent gradients) and we observed that for flow rates  $>2 \mu\text{L/h}$  cells start to pass through the filter pores.

### 5.5 Conclusions and outlook

#### 5.5.1 Summary of results

Thanks to the developed device in which it is possible to first accumulate a defined amount of bioreporter cells and then expose them to different arsenite concentrations and flow rates, we could observe extensive gradients of reporter signal intensity as a function of distance to the inflowing sample, of the arsenite concentration and the flow rate. In order to understand the nature of these gradients, we developed a model for the bioreporter cell defense mechanism against arsenic. The experimental results and the corresponding model suggested that the reporter cells - contrary to current belief - are not "inert", but store part of the arsenic in the cells, and that the storage capacity is inducible and dependent on the arsenite exposure concentration. We also found that for low arsenite concentrations ( $\leq 50 \mu\text{g/L}$ ) the role of the efflux pumps is negligible. In addition, we could also determine the best parameters, in terms of arsenite flow rate and number of cells accumulated, for a practical application of this device



as a biosensor.

### 5.5.2 Perspectives

It would be interesting to see if the model is able to correctly predict the behavior of engineered *E. coli* strains in which the mechanisms of response to arsenite are different, as for example the strain with the absence of the efflux pumps or the one in which there is no feedback loop.



## 6 Conclusion and outlook

This final chapter puts a conclusion to the dissertation. We first summarize our technical, experimental and modeling achievements: the miniaturized microfluidic system, the on chip active maintenance of bioreporter cells and the conditions for an optimal signal-to-noise ratio. Future directions of research on this topic are then presented in an outlook section.

### 6.1 Summary of results

#### 6.1.1 Miniaturized microfluidic system

The primary goal of this work was to design and construct a miniaturized microfluidic system in which the bioreporter cells could be exposed to aqueous arsenic samples and which allowed direct detection of the reporter signal produced. We provided two alternatives to trap, accumulate and expose bioreporter cells to arsenic aqueous samples and to obtain an easy read-out of the signal. The first one consists in a beads device, which is able to trap and accumulate in a microcage bioreporter cells embedded in 40-70  $\mu\text{m}$  agarose beads. The microcage allows the exposure of the reporter cells to arsenic and permits signal amplification as a result of hundreds of beads accumulating at one position, while the replicate flow-lines increase the accuracy of the measurement. With this system, we were able to reliably and reproducibly discriminate arsenite concentrations in the range of 0-100  $\mu\text{g/L}$  in less than 200 min with a detection limit of 1-1.6  $\mu\text{g As/L}$ , which is well below the current drinking water limit of 10  $\mu\text{g As/L}$ . The second option that we proposed is the use of single cells by employing a filter wall instead of a cage. In terms of performance in detecting arsenic (minimum detec-

tion limit, sensitivity, relative standard deviation, time needed to discriminate the different concentrations) there is no significative difference between these two systems, but in this second case, a valves system needs to be integrated in order to accumulate a constant amount of cells, making the fabrication of the device and the implementation of the setup surrounding it less straightforward. However, this alternative reveals all its potential in the integration of a chemostat on chip and in the possibility to actively maintain cells on chip.

### 6.1.2 On chip actively maintenance of bioreporter cells

The second objective of this work was to actively maintain cells on chip for one week. We found that EGFP signal development remained highly reproducible for bioreporter cells embedded in agarose beads frozen inside the chip at  $-80^{\circ}\text{C}$ , whereas it decreased for prolonged storage periods at  $-20^{\circ}\text{C}$ . In the optics of an in-field application, only the  $-20^{\circ}\text{C}$  storage option can be taken into account and in this case beads can be prefilled and stored up to one month before use in the microfluidic cartridge with satisfactory performance in terms of discriminating concentrations of 0, 10 and  $50\ \mu\text{g As/L}$ . To overcome this signal decrease, we tried a chemostat on chip approach. With this method, we could demonstrate that we are able to maintain cells in physiologically active state on chip for up to 1 week. Even if, due to a lack of robustness of the system, we were not able to perform longer experiments, we showed that it is possible to have a biosensor in which the sensitive element not only can survive for a certain amount of time but is continuously renewed. This could lead, in an improved device, to the complete overcoming of the signal decrease experienced with frozen beads. Furthermore, the chemostat on chip can be maintained at room temperature, thus eliminating the need of a freezer.

### 6.1.3 Arsenite transport effects and conditions for an optimal signal-to-noise ratio

Another aspect we wanted to explore with this work was under which conditions, in terms of arsenic flow rate and number of cells exposed, the bioreporter cells express the maximum signal-to-noise ratio. Thanks to the single cells device with the integrated valves on it, we were able to expose a fixed amount of cells to different arsenic fluxes and we could observe extensive gradients of reporter signal intensity as a function of distance to the inflowing sample, of the arsenite concentration and the flow rate. From a practical application point of view, with these measurements we could determine in which range the number of cells accumulated and the

flow rate have to be in order to obtain the maximum signal intensity for a given concentration. Furthermore, we tried to understand the nature of these gradients by developing a model for the bioreporter cell defense mechanism against arsenic. This model suggested that reporter cells are not "inert" on the target molecule, but store part of the arsenic in the cells, and that for low arsenite concentrations (<50 µg/L) the role of the efflux pumps is negligible. Furthermore, results indicated that this storage capacity is inducible and dependent on the arsenite exposure concentration.

## 6.2 Perspectives

### 6.2.1 Technical improvements

In terms of microfluidic cartridge, the major technical improvements to be achieved are in the chemostat on chip design. As discussed in Section 4.6, a second measurement zone using cells coming from the same chamber, would allow to have a control measurement, which is indispensable for an application point of view. Furthermore, a valve decoupling the measurement zone from the growing chamber would also be necessary to avoid the interference between these two units. The robustness of the system has also to be improved in order to have a more reliable device able to function for longer periods of time. What it is also required to render feasible the use of this biosensor in the field is the finalization of the opto-electronic device (ReaderLab) by the HES-SO team, which should allow the signal read-out directly on the microfluidic cartridge and its housing. A point that remains still challenging is the chip connections to the outside world: in both beads and chemostat on chip devices, to perform a measurement one has to fix (or detach and re-fix) the tubings connecting the arsenic sample to the arsenic inlet. This is a critical operation as it can unintentionally lead to an excessive pressure applied on the PDMS block which, because of the PDMS flexibility, translates in the displacement of the cells or beads in undesired positions.

### 6.2.2 From the laboratory to the in-field situation

The developed whole-cell living bacterial biosensor shows satisfactory performance in terms of discriminating concentrations of 0, 10 and 50 µg/L of arsenic, is potentially utilizable by a user who is not familiar with the laboratory techniques, and is promising with regards to long term cells maintenance. Concerning the costs, the silicon molds are relatively inexpensive

with one silicon mold serving for the manufacturing of more than one hundred chips, and also from the biological point of view they are extremely low because with 0.2 mL of cell culture one can fill more than 40 chemostats on chip or produce a batch of beads sufficient for more than 20 chips. A sensor for the in-field detection of arsenic in developing countries must not only be reliable, but also be affordable and easy to maintain and it should be able to be produced in situ. Thus, even if more research effort is required - in particular in the development of an optical detection system and in the construction of an instrument housing the microfluidics cartridge - before we will be able to use our device in the field, I believe it constitutes a crucial step forward in the direction of a sensor usable for the in-field detection of arsenic in developing countries. When compared to the current in-field arsenic measurement techniques (Section 1.2.1.5), our device does not present the reliability issue shown by the colorimetric assays, does not require sample preparation as in the case of the portable XRF devices, and it does not show interference problems as in the case of the ASV systems [Trang *et al.*, 2005]. In the case of the beads system, the biggest source of uncertainty is the decrease in reporter signal development over storage time, but this issue can be easily solved by running a calibration measurement in one of the PDMS blocks of the chip. Of course, a very promising way is also the use of the lyophilized bacteria, which can be stored at 4°C until use and showed impressive in-field results [Siegfried *et al.*, 2012], although the use of a portable luminometer it is still required [Siegfried *et al.*, 2012].

### 6.2.3 Other applications

As in principle diverse biological recognition mechanisms can be coupled to reporter genes [Daunert *et al.*, 2000; Keane *et al.*, 2002], the developed device could serve for the detection of other pollutants or toxicity [Ron, 2007]. Of course the sample needs to be in aqueous phase and the chip needs to be adapted depending on the characteristics of the cells used (size, stickness) and the type of reporter signal produced (colour, light, fluorescence or electrochemical).

# Bibliography

- C. Abernathy, R.L. Calderon, and W.R. Chappell. *Arsenic exposure and health effects*. Elsevier Science Ltd., 1999.
- M. G. M. Alam, G. Allinson, F. Stagnitti, A. Tanaka, and M. Westbrooke. Arsenic contamination in bangladesh groundwater: a major environmental and social disaster. *International Journal of Environmental Health Research*, 12(3):235–253, 2002.
- M. Amini, K. C. Abbaspour, M. Berg, L. Winkel, S. J. Hug, E. Hoehn, H. Yang, and C. A. Johnson. Statistical modeling of global geogenic arsenic contamination in groundwater. *Environ. Sci. Technol.*, 42(10):3669–3675, 2008.
- J. B. Andersen, C. Sternberg, L. K. Poulsen, S. P. Bjørn, M. Givskov, and S. Molin. New unstable variants of green fluorescent protein for studies of transient gene expression in bacteria. *Appl. Environ. Microbiol.*, 64(6):2240–2246, 1998.
- H. Andersson and A. van den Berg. Microfluidic devices for cellomics: a review. *Sensors and Actuators B: Chemical*, 92(3):315–325, 2003.
- Y. Arai, R. Yasuda, K. Akashi, Y. Harada, H. Miyata, K. Kinoshita Jr., and H. Itoh. Tying a molecular knot with optical tweezers. *Nature*, 399(466):446–448, 1990.
- A. Ashkin, J. M. Dziedzic, and T. Yamane. Optical trapping and manipulation of single cells using infrared laser beams. *Nature*, 330(6150):769–771, 1987.
- F. K. Balagaddé, L. You, C. L. Hansen, F. H. Arnold, and S. R. Quake. Long-term monitoring of bacteria undergoing programmed population control in a microchemostat. *Science*, 309(5731):137–140, 2005.
- H. T. Banks. *Modeling and Control in the Biomedical Sciences*, volume 6 of *Lecture Notes in Biomathematics*. Springer-Verlag, 1975.

## Bibliography

---

- H. T. Banks and Marie Davidian. Introduction to the chemostat. Technical report, North Carolina State University, 2009.
- B. Baumann and J. R. van der Meer. Analysis of bioavailable arsenic in rice with whole cell living bioreporter bacteria. *J. Agric. Food Chem.*, 55(6):2115–2120, 2007.
- D. J. Beebe, J. S. Moore and J. M. Bauer, Q. Yu, R. H. Liu, C. Devadoss, and B.-H. Jo. Functional hydrogel structures for autonomous flow control inside microfluidic channels. *Nature*, 404(6778):588–590, 1999.
- S. Belkin. Microbial whole-cell sensing systems of environmental pollutants. *Current Opinion in Microbiology*, 6(3):206–212, 2003.
- H. Ben-Yoav, A. Biran, R. Pedahzur, S. Belkin, S. Buchinger, G. Reifferscheid, and Y. Shacham-Diamand. A whole cell electrochemical biosensor for water genotoxicity bio-detection. *Electrochimica Acta*, 54(25):6113–6118, 2009.
- S. N. Bhatia, M. L. Yarmush, and M. Toner. Controlling cell interactions by micropatterning in co-cultures: hepatocytes and 3T3 fibroblast. *J. Biomed. Mater. Res.*, 32(2):189–199, 1997.
- J. Bjerketorp, S. Hakansson, S. Belkin, and KJ Jansson. Advances in preservation methods: keeping biosensor microorganisms alive and active. *Current Opinion in Biotechnology*, 17(1):43–49, 2006.
- E. K. Bolton, G. S. Sayler, D. E. Nivens, J. M. Rochelle, S. Ripp, and M. L. Simpson. Integrated CMOS photodetectors and signal processing for very low-level chemical sensing with the bioluminescent bioreporter integrated circuits. *Sens. Act. B: Chem.*, 85:179–185, 2002.
- T. Braschler, R. Johann, M. Heule, L. Metref, and P. Renaud. Gentle cell trapping and release on a microfluidic chip by *in situ* alginate hydrogel formation. *Lab on a Chip*, 5(5):553–559, 2005.
- N. Buffi, D. Merulla, J. Beutier, F. Barbaud, S. Beggah, H. van Lintel, P. Renaud, and J. R. van der Meer. Development of a microfluidics biosensor for agarose-bead immobilized escherichia coli bioreporter cells for arsenite detection in aqueous samples. *Lab on a Chip*, 11(14):2369–2377, 2011a.



- N. Buffi, D. Merulla, J. Beutier, F. Barbaud, S. Beggah, H. van Lintel, P. Renaud, and J. R. van der Meer. Miniaturized bacterial biosensor system for arsenic detection holds great promise for making integrated measurement device. *BioengineeredBugs*, 5(2):296–298, 2011b.
- A. Campion and P. Kambhampati. Surface-enhanced Raman scattering. *Chemical Society Reviews*, 27(4):241–250, 1998.
- Center of micronanotechnology (CMI) at Swiss Federal Institute of Technology (EPFL). Manual for Alcatel 601 E, July 2012. URL <http://cmi.epfl.ch/etch/601E.php>.
- Y. Changqing, L. Cheuk-Wing, J. Shenglin, and Y. Mengsu. Microfluidics technology for manipulation and analysis of biological cells. *Anal. Chim. Acta*, 560(1-2):1–23, 2006.
- Y. Chen and B. P. Rosen. Metalloregulatory properties of the arsd repressor. *Journal of Biological Chemistry*, 272(22):14257–14262, 1997.
- S. K. Cho. Creating, transporting, cutting, and merging liquid droplets by electrowetting-based actuation for digital microfluidic circuits. *Microelectromechanical Systems*, 12(1):70–80, 2003.
- S. Cookson, N. Ostroff, W. L. Pang, D. Volfson, and J. Hasty. Monitoring dynamics of single-cell gene expression over multiple cell cycles. *Molecular Systems Biology*, 1(2005.0024), 2005.
- C. G. Cooney, C.-Y. Chen, M. R. Emerling, A. Nadim, and J. D. Sterling. Electrowetting droplet microfluidics on a single planar surface. *Microfluidics and Nanofluidics*, 2(5):435–446, 2006.
- B. M. Cullum, J. Mobley, Z. Chi, D. L. Stokes, G. H. Miller, and Tuan Vo-Dinh. Development of a compact, handheld Raman instrument with no moving parts for use in field analysis. *Review of Scientific Instruments*, 71(4):1602–1607, 2000.
- A. A. Darhuber, J. Z. Chen, J. M. Davis, and S. M. Troian. A study of mixing in thermocapillary flows on micropatterned surfaces. *Phil. Trans. R. Soc. Lond. A*, 362(1818):1037–1058, 2004.
- S. Daunert, G. Barrett, J. S. Feliciano, R. S. Shetty, S. Shrestha, and W. Smith-Spencer. Genetically engineered whole-cell sensing systems: coupling biological recognition with reporter genes. *Chemical Reviews*, 100(7):2705–2738, 2000.
- E. Delamarche, D. Juncker, and H. Schmid. Microfluidics for processing surfaces and miniaturizing biological assays. *Advanced Materials*, 17(24):2911–2933, 2005.

## Bibliography

---

- E. Diesel, M. Schreiber, and J. R. van der Meer. Development of bacteria-based bioassays for arsenic detection in natural waters. *Anal. Bioanal. Chem.*, 394(3):687–693, 2009.
- J. I. Drever. *The geochemistry of natural waters: surface and groundwater environments*. Prentice Hall, 2002.
- A. Edlich, V. Magdanz, D. Rasch, S. Demming, S. A. Zadeh, R. Segura, R. Radespiel C. Kämhler, S. Bümttgenbach, E. Franco-Lara, and R. Krull. Microfluidic reactor for continuous cultivation of *Saccharomyces cerevisiae*. *Biotechnology Progress*, 26(5):1259–1270, 2010.
- U.S. EPA. SW-846. Technical report, U.S. Environmental Protection Agency, 1994. URL <http://www.epa.gov/epaoswer/hazwaste/test/sw846.htm>.
- U.S. EPA. Verifications: X-ray fluorescence analyzers (field portable). Technical report, U.S. Environmental Protection Agency, Environmental Technology Verification Program, 1997.
- B. E. Erickson. Field kits fail to provide accurate measure of arsenic in groundwater. *Environ. Sci. Technol.*, 37(1):35–38, 2003.
- M. Evander, L. Johansson, T. Lilliehorn, J. Piskur, M. Lindvall, S. Johansson, M. Almqvist, T. Laurell, and Johan Nilsson. Noninvasive acoustic cell trapping in a microfluidic perfusion system for online bioassays. *Anal. Chem.*, 79(7):2984–2991, 2007.
- R. Feeney and S. P. Kounaves. On-site analysis of arsenic in groundwater using a microfabricated gold ultramicroelectrode array. *Anal. Chem.*, 72(10):2222–2228, 2000.
- S. Fendorf, H. A. Michael, and A. van Geen. Spatial and temporal variations of groundwater arsenic in South and Southeast Asia. *Science*, 328(5982):1123–1127, 2012.
- D. O. Fesenko, T. V. Nasedkina, A. V. Chudinov, D. V. Prokopenko, R. A. Yurasov, and A. S. Zasedatelev. Alginate gel biochip for real-time monitoring of intracellular processes in bacterial and yeast cells. *Mol. Biol.*, 39(1):84–89, 2005.
- B. T. Fisher, A. H. Howard, S. G. Buckley, and D. W. Hahn. Temporal gating for the optimization of laser-induced breakdown spectroscopy detection and analysis of toxic metals. *Applied Spectroscopy*, 55(10):319A–350A, 2001.
- M. J. D. San Francisco, C. L. Hope, J. B. Owolabi, L. S. Tisa, and B. P. Rosen. Identification of the metalloregulatory element of the plasmid-encoded arsenical resistance operon. *Nucleic Acid Res.*, 18(3):619–624, 1990.

- Ashok Gadgil. Drinking water in developing countries. *Annual Review of Energy and the Environment*, 23:253–286, 1998.
- H. Garelick and H. Jones. Mitigating arsenic pollution: bridging the gap between knowledge and practice. *Chemistry International*, 30(4):7–12, 2008.
- S. G. Gilbert. *A small dose of toxicology - The health effects of common chemicals*. Healthy World Press, 2012.
- A. Groisman, C. Lobo, H. Cho, J. K. Campbell, Y. S. Dufour, A. M. Stevens, and A. Levchenko. A microfluidic chemostat for experiments with bacterial and yeast cells. *Nature Methods*, 2(9):685–689, 2005.
- IGEM Team Gronigen. Heavy metals scavengers with a vertical gas drive, 2009. URL <http://2009.igem.org/Team:Groningen>.
- F. X. Han, Y. Su, D. L. Monts, M. J. Plodinec, A. Banin, and G. E. Triplett. Assessment of global industrial-age anthropogenic arsenic contamination. *Naturwissenschaften*, 90(9):395–401, 2003.
- K.-H. Han and B. Frazier. Continuous magnetophoretic separation of blood cells in microdevice format. *J. Appl. Phys.*, 96(10):5797–5803, 2004.
- M.-J. Han, J. Hao, Z. Xu, and X. Meng. Surface-enhanced raman scattering for arsenate detection on multilayer silver nanofilms. *Anal. Chim. Acta*, 692(1-2):96–102, 2011.
- H. M. Hertz. Standing-wave acoustic trap for nonintrusive positioning of microparticles. *J. Appl. Phys.*, 78:4845–4849, 1995.
- A. Hierlemann, O. Brand, C. Hagleitner, and H. Baltes. Microfabrication techniques for chemical biosensors. *Proceedings of the IEEE*, 91(6):839–863, 2003.
- M.F. Hossain. Arsenic contamination in Bangladesh - An overview. *Agriculture, Ecosystems & Environment*, 113(1-4):1–16, 2006.
- Y.-M. Huang and C.-W. Whang. Capillary electrophoresis of arsenic compounds with indirect fluorescence detection. *Electrophoresis*, 19(12):2140–2144, 1998.
- D. Q. Hung, O. Nekrassova, and R. G. Compton. Analytical methods for inorganic arsenic in water: a review. *Talanta*, 64(2):269–277, 2004.

## Bibliography

---

- A. Hussam, M. Alauddin, A.H. Khan, S.B. Rasul, and A.K.M. Munir. Evaluation of arsine generation in arsenic field kit. *Environ. Sci. Technol*, 33(20):3686–3688, 1999.
- C. K. Jain and I. Ali. Arsenic: occurrence, toxicity and speciation techniques. *Water Research*, 34(17):4304–4312, 2000.
- H.-F. Ji, E. Finot, R. Dabestani, T. Thundat, G. M. Brown, and P. F. Britt. A novel self-assembled monolayer (SAM) coated microcantilever for low level caesium detection. *Chemical Communications*, 6:457–458, 2000.
- R. M. Johann. Cell trapping in microfluidic chips. *Anal. Bioanal. Chem.*, 385(3):408–412, 2006.
- Rajmohan Joshi. *Biosensors*. Gyan Books, 2006.
- D. E. Kataoka and S. M. Troian. Patterning liquid flow on the microscopic scale. *Letters to Nature*, 402(6763):794–797, 1999.
- A. Keane, P. Phoenix, S. Ghoshal, and Peter C. K. Lau. Exposing culprit organic pollutants: A review. *Journal of Microbiological Methods*, 49(2):103–119, 2002.
- A. Khademhosseini, J. Yeh, G. Eng, K. Y. Suh, J. A. Burdick, and R. Langer. Molded polyethylene glycol microstructures for capturing cells within microfluidic channels. *Lab on a Chip*, 4(5):425–430, 2004.
- J. M. H. King, P. M. DiGrazia, B. Applegate, R. Burlage, J. Sanseverino, P. Dunbar, F. Larimer, and G. S. Sayler. Rapid, sensitive bioluminescent reporter technology for naphthalene exposure and biodegradation. *Science*, 249(4970):778–781, 1990.
- D. G. Kinniburgha and W. Kosmus. Arsenic contamination in groundwater: some analytical considerations. *Talanta*, 58(1):165–180, 2002.
- B. J. Kirby. *Micro- and nanoscale fluid mechanics - Transport in microfluidic devices*. Cambridge University Press, 2010.
- K. Kneipp. Surface-enhanced Raman scattering. *Physics Today*, 60(11):40–47, 2007.
- W.-G. Koh, L. J. Itle, and M. V. Pishko. Molding of hydrogel microstructures to create multiphenotype cell microarrays. *Anal. Chem*, 75(21):5783–5789, 2003.

- K. Kojima, H. Morihuchi, A. Hattori, T. Kaneko, and K. Yasuda. Two-dimensional network formation of cardiac myocytes in agar microculture chip with 1480 nm infrared laser photo-thermal etching. *Lab on a Chip*, 3(4):292–296, 2003.
- C. S. S. R. Kumar, editor. *Microfluidic devices in nanotechnology - fundamental concepts*. Wiley, 2010.
- S. Laschi, G. Bagni, I Palchetti, and M. Mascini. As(III) voltammetric detection by means of disposable screen-printed gold electrochemical sensors. *Anal. Lett.*, 40(16):3002–3013, 2008.
- C. H. Lee, K.C. Jiang, P. Jin, and P.D. Prewett. Design and fabrication of a micro Wankel engine using MEMS technology. *Microelectronic Engineering*, 73-74:529–534, 2004.
- J. H. Lee, R. J. Mitchell, B. C. Kim and D. C. Cullen, and M. B. Gu. A cell array biosensor for environmental toxicity analysis. *Biosens. Bioelectr.*, 21(3):500–507, 2005.
- K. S. Lee, P. Boccazzi, A. J. Sinskey, and R. J. Ram. Microfluidic chemostat and turbidostat with flow rate, oxygen, and temperature control for dynamic continuous culture. *Lab on a Chip*, 11(10):1730–1739, 2011.
- T. Lilliehorn, U. Simu, M. Nilsson, M. Almqvist, T. Stepinski, T. Laurell, J. Nilsson, and S. Johansson. Trapping of microparticles in the near field of an ultrasonic transducer. *Ultrasonics*, 43(5):293–303, 2005.
- X. Liu, K. J. Germaine, D. Ryan, and D. N. Dowling. Whole-cell fluorescent biosensors for bioavailability and biodegradation of polychlorinated biphenyls. *Sensors*, 10:1377–1398, 2010.
- X. Luo, K. Shen, C. Luo, H. Ji, Q. Ouyang, and Y. Chen. An automatic microturbidostat for bacterial culture at constant density. *Biomedical Microdevices*, 12(3):499–503, 2010.
- M. Madou, J. Zoval, G. Y. Jia, H. Kido, J. Kim, and N. Kim. Lab on a CD. *Annual Review of Biomedical Engineering*, 8:601–628, 2006.
- Alexander Maksik. *You deserve nothing*. John Murray, 2011.
- S. McKelvey. Malthusian growth model. Technical report, Saint Olaf College, Department of Mathematics, Northfield, Minnesota, 1995.

## Bibliography

---

- Dan Melamed. Monitoring arsenic in the environment: a review of science and technologies. *Anal. Chim. Acta*, 532(1):1–13, 2005.
- Y. Mengsu, L. Cheuck-Wing, and Y. Jun. Cell docking and on-chip monitoring of cellular reactions with a controlled concentration gradient on a microfluidic device. *Anal. Chem.*, 74(16):3991–4001, 2002.
- R. Nickson, J. McArthur, W. Burgess, K.M. Ahmed, P. Ravenscroft, and M. Rahman. Arsenic poisoning of Bangladesh groundwater. *Nature*, 395(6700):338, 1998.
- J. Nilsson, M. Evander, B. Hammarstöm, and T. Laurell. Review of cell and particle trapping in microfluidic systems. *Anal. Chim. Acta*, 649(7):141–157, 2009.
- D. E. Nivens, T. E. McKnight, S. A. Moser, S. J. Osbourn, M. L. Simpson, and G.S. Sayler. Bioluminescent bioreporter integrated circuits: potentially small, rugged and inexpensive whole-cell biosensors for remote environmental monitoring. *Journal of Applied Microbiology*, 96(1):33–46, 2003.
- D. K. Nordstrom. Worldwide occurrences of arsenic in groundwater. *Science*, 296(5576):2143–2144, 2002.
- A. Novick and L. Szilard. Description of the chemostat. *Science*, 112(2920):715–716, 1950.
- J. Ouellette. A new wave of microfluidic devices. *The Industrial Physicist*, 9(4):14–17, 2003.
- M. C. Park, J. Y. Hur, J.-R. Kim, K.-H. Cho, K. W. Kwon, M. K. Kwak, H. S. Cho, and S.-Y. Hwang. Receding meniscus induced docking of yeast cells for quantitative single-cell analysis. In *Twelfth International Conference on Miniaturized Systems for Chemistry and Life Sciences*, San Diego, California, USA, October 2008.
- S. Pennathur. Flow control in microfluidics: are the workhorse flows adequate? *Lab on a Chip*, 8(3):383–387, 2008.
- H. A. Pohl. *Dielectrophoresis the behavior of neutral matter in nonuniform electric fields*. Cambridge University Press, Cambridge, 1978.
- P. J. Pottes, M. H. Ramsey, and J. Carlisle. Portable X-ray fluorescence in the characterization of arsenic contamination associated with industrial buildings at a heritage arsenic works near redruth, cornwall, UK. *J. Environ. Monit.*, 4:1017–1024, 2002.

- J. R. Premkumar, R. Rosen, S. Belkin, and O. Lev. Sol-gel luminescence biosensors: encapsulation of recombinant *E. coli* reporters in thick silicate films. *Anal. Chim. Acta*, 462(1):11–23, 2002.
- A. Prindle, Ph. Samayoa, I. Razinkov, T. Danino, L. S. Tsimring, and J. Hasty. A sensing array of radically coupled genetic "biopixels". *Nature*, 481:39–44, 2012.
- M. M. Rahman, D. Mukherjee, M. K. Sengupta, U. K. Chowdhury, Di. Lodh, C. R. Chanda, S. Roy, M. Selim, Q. Quamruzzaman, A. H. Milton, S. M. Shahidullah, Md. T. Rahman, and D. Chakraborti. Effectiveness and reliability of arsenic field testing kits: are the million dollar screening projects effective or not? *Environmental Science & Technology*, 36(24):5385–5394, 2002.
- M. B. Rasmussen, L. B. Oddershede, and H. Siegumfeldt. Optical tweezers cause physiological damage to *Escherichia coli* and *Listeria Bacteria*. *Appl. Environ. Microbiol.*, 74(8):2441–2446, 2008.
- S. B. Rasul, A. K. M. Munir, Z. A. Hossain, A. H. Khan, M. Alauddin, and A. Hussam. Electrochemical measurement and speciation of inorganic arsenic in groundwater of Bangladesh. *Talanta*, 58(1):33–43, 2002.
- P. Ravenscroft, H. Brammer, and K. Richards. *Arsenic pollution: a global synthesis*. Wiley-Blackwell, 2009.
- A. Revzin, R. J. Russel, V. K. Yadavalli, W.-G. Koh, C. Deister, D. D. Hile, M. B. Mellott, and M. V. Pishko. Fabrication of poly(ethylene glycol) hydrogel microstructures using photolithography. *Langmuir*, 17(18):5440–5447, 2001.
- F. F. Roberto, J. M. Barnes, and D. F. Bruhn. Evaluation of a GFP reporter gene construct for environmental arsenic detection. *Talanta*, 58(1):181–188, 2002.
- E. Z. Ron. Biosensing environmental pollution. *Current Opinion in Biotechnology*, 18(3): 252–256, 2007.
- A. Rosenthal and J. Voldman. Dielectrophoretic traps for single-particle patterning. *Biophysical Journal*, 88(3), 2005.
- K.-Y. San. Bioreactors in biochemical and metabolic engineering, 2004. URL [http://www-bioc.rice.edu/bios576/nih\\_bioreactor/NDL\\_Bioreactor%20Page.htm](http://www-bioc.rice.edu/bios576/nih_bioreactor/NDL_Bioreactor%20Page.htm).

## Bibliography

---

- N. S. Satarkar, W. Zhang, R. E. Eitel, and J. Z. Hilt. Magnetic hydrogel nanocomposites as remote controlled microfluidic valves. *Lab on a Chip*, 9(12):1773–1779, 2009.
- V. M. Sbareto and H. J. Sanchez. Analysis of arsenic pollution in groundwater aquifers by X-ray fluorescence. *Appl. Rad. and Iso.*, 54(5):737–740, 2001.
- T. Schnelle, R. Hagedorn, G. Fuhr, S. Fiedler, and T. Müller. Three-dimensional electric field traps for manipulation of cells - Calculation and experimental verification. *Biochimica et Biophysica Acta*, 1157(2):127–140, 1993.
- D. L. Scott, S. Ramanathan, W. Shi, B. P. Rosen, and S. Daunert. Genetically engineered bacteria: electrochemical sensing systems for antimonite and arsenite. *Anal. Chem.*, 69(1):16–20, 1997.
- W. Shi, J. Wu, and B. P. Rosen. Identification of a putative metal binding site in a new family of metalloregulatory proteins. *J. Biol. Chem.*, 269(31):19826–19829, 1994.
- H. J. Shin, H. H. Park, and W. K. Lim. Freeze-dried recombinant bacteria for on-site detection of phenolic compounds by color change. *Journal of Biotechnology*, 119(1):36–43, 2005.
- K. Siegfried, C. Endes, A. F. Md. K. Bhuiyan, A. Kuppardt, J. Mattusch, J. R. van der Meer, A. Chatzinotas, and H. Harms. Field testing of arsenic in groundwater samples of Bangladesh using a test kit based on lyophilized bioreporter bacteria. *Environ. Sci. Technol.*, 46(6):3281–3287, 2012.
- S. Silver and G. Ji. Newer systems for bacterial resistances to toxic heavy metals. *Environ. Health Perspect.*, 102:107–113, 1994.
- M. L. Simpson, G. S. Sayler, B. M. Applegate, S. Ripp, D. E. Nivens, M. J. Paulus, and G. E. Jellison Jr. Bioluminescent-bioreporter integrated circuits form novel whole-cell biosensors. *Trends in Biotechnology*, 16(8):332–338, 1998.
- PL Smedley and D.G Kinniburgh. A review of the source, behaviour and distribution of arsenic in natural waters. *Applied Geochemistry*, 17(5):517–568, 2002.
- Allan H. Smith, Claudia Hopenhayn-Rich, Michael N. Bates, Helen M. Goeden, Irva Hertz-Picciotto, Heather M. Duggan, Rose Wood, Michael J. Kosnett, and Martyn T. Smith. Cancer risks from arsenic in drinking water. *Environ. Health Perspect.*, 97:259–267, 1992.



- C. M. Steinmaus, C. M. George, D. A. Kalman, and A. H. Smith. Evaluation of two new arsenic field test kits capable of detecting arsenic water concentrations close to 10  $\mu\text{g}/\text{l}$ . *Environ. Sci. Technol.*, 40(10):3362–3366, 2006.
- J. Stocker, D. Balluch, M. Gsell, H. Harms, J. S. Feliciano, S. Daunert, K. A. Malik, and J. R. 22 van der Meer. Development of a set of simple bacterial biosensors for quantitative and rapid measurements of arsenite and arsenate in potable waters. *Environ. Sci. Technol*, 37(20):4743–4750, 2003.
- H. A. Stone and S. Kim. Microfluidics: basic issues, applications, and challenges. *AIChE Journal*, 47(6):1250–1254, 2001.
- M. K. Sun, H. L. Sung, and Y. S. Kahp. Cell research with physically modified microfluidic channels: a review. *Lab on a Chip*, 8(7):1015–1023, 2008.
- W. Tan and T. A. Desai. Microfluidic patterning of cellular biopolymer matrices for biomimetic 3-D structures. *Biomedical Microdevices*, 5(3):235–244, 2003.
- H. Tani, K. Maehana, and T. Kamidate. Chip-based bioassay using bacterial sensor strains immobilized in three-dimensional microfluidic network. *Anal. Chem.*, 76(22):6693–6697, 2004.
- S. Tauriainen, M. Karp, W. Chang, and M. Virta. Recombinant luminescent bacteria for measuring bioavailable arsenite and antimonite. *Appl. Environ. Microbiol.*, 63(11):4456–4461, 1997.
- R. Tecon and J. R. van der Meer. Information from single-cell bacterial biosensors: what is it good for? *Current Opinion in Biotechnology*, 17(1):4–10, 2006.
- R. Tecon and J. R. van der Meer. Bacterial biosensors for measuring availability of environmental pollutants. *Sensors*, 8(7):4062–4080, 2008.
- Nikola Tesla. Valvular conduit, 1920.
- M. W. Tibbitt and K. S. Anseth. Hydrogels as extracellular matrix mimics for 3D cell culture. *Biotechnology and Bioengineering*, 103(4):655–663, 2009.
- R. Tombolini, A. Unge, M. E. Davey, F. J. de Bruijn, and J. K. Jansson. Flow cytometric and microscopic analysis of GFP-tagged *Pseudomonas fluorescens* bacteria. *FEMS Microbiol. Ecol.*, 22(1):17–28, 1997.

## Bibliography

---

- P. T. K. Trang, M. Berg, P. H. Viet, N. V. Mui, and J. R. van der Meer. Bacterial bioassay for rapid and accurate analysis of arsenic in highly variable groundwater samples. *Environ. Sci. Technol.*, 39(19):7625–7630, 2005.
- M. A. Unger, H.-P. Chou, T. Thorsen, A. Scherer, and S. R. Quake. Monolithic microfabricated valves and pumps by multilayer soft lithography. *Science*, 288(5463):113–116, 2000.
- P. Vadgama. Microfluidic applications for biosensors. Technical report, Touch Briefings PLC, 2004.
- C. Valsangiacomo. The importance of water in development and cooperation. Technical report, SUPSI, 2010.
- J. R. van der Meer and S. Belkin. Where microbiology meets microengineering: design and applications of reporter bacteria. *Nature Reviews Microbiology*, 8(7):511–522, 2010.
- Jan Roelof van der Meer, David Tropel, and Marco Jaspers. Illuminating the detection chain of bacterial bioreporters. *Environmental Microbiology*, 6(10):1005–1020, 2004.
- X. B. Wang, Y. Huang, J. P. H. Burt, G. H. Markx, and R. Pething. Selective dielectrophoretic confinement of bioparticles in potentiayl energy wells. *J. Appl. Phys.*, 26:1278–1285, 1993.
- D. B. Weibel, W. R. Di Luzio, and G. M. Whitesides. Microfabrication meets microbiology. *Nature Reviews Microbiology*, 5(3):209–218, 2007.
- M. Wells, M. Göch, R. Rigler, H. Harms, T. Lasser, and J. R. van der Meer. Ultrasensitive reporter protein detection in genetically engineered bacteria. *Anal. Chem.*, 77(9):2683–2689, 2005.
- G. M. Whitesides. The origins and the future of microfluidics. *Nature*, 442(7101):368–373, 2006.
- WHO. Diarrhoeal disease, 2009. URL <http://www.who.int/mediacentre/factsheets/fs330/en/index.html>. Fact sheet N°330.
- M. Wiklund, C. Günther, R. Lemor, M. Jäger, G. Fuhr, and H. M. Hertz. Ultrasonic standing wave manipulation technology integrated into a dielectrophoretic chip. *Lab on a Chip*, 6(12):1537–1544, 2006.
- K. D. Wittrup. Course materials for 10.37 chemical and biological reaction engineering, Spring 2007. URL <http://ocw.mit.edu>. Downloaded in September 2012.

- A. Wixforth. Acoustically driven planar microfluidics. *Superlattices and Microstructures*, 33 (5-6):389–396, 2004.
- J. Wu and B. P. Rosen. The ArsR protein is a trans-acting regulatory proteins. *Mol. Microbiol.*, 5 (6):1331–1336, 1991.
- J. Wu and B. P. Rosen. Metalloregulated expression of the ars operon. *J. Biol. Chem.*, 268(1): 52–58, 1993.
- L. Y. Wu, Dino Di Carlo, and L. P. Lee. Microfluidic self-assembly of tumor spheroids for anticancer drug discovery. *Lab on a Chip*, 10(2):197–202, 2008.
- Z. Xua, Jumin Hao and Fasheng Li, and X. Meng. Surface-enhanced Raman spectroscopy of arsenate and arsenite using Ag nanofilm prepared by modified mirror reaction. *Journal of Colloid and Interface Science*, 347(1):90–95, 2010.
- B. Yalcin and S. Otles. Nanobiosensor and food pathogen interaction mechanisms. *Electronic Journal of Environmental, Agricultural and Food Chemistry*, 9(7):1257–1273, 2010.
- C. Yu, S. Mutlu, P. Selvaganapathy, C. H. Mastrangelo, F. Svec, and J. M. J. Fréchet. Flow control valves for analytical microfluidic chips without mechanical parts based on thermally responsive monolithic polymers. *Anal. Chem.*, 75(8):1958–1961, 2003.
- K. Zengler, G. Toledo, M. Rappe, J. Elkins, E. J. Mathur, J. M. Short, and M. Keller. Cultivating the uncultured. *Proc. Natl. Acad. Sci. USA*, 99(24):15681–15686, 2002.
- Z. Zhang, P. Boccazzi, H. G. Choi, G. Perozziello, A. J. Sinskey, and K. F. Jensen. Microchemostat-microbial continuous culture in a polymer-based, instrumented microbioreactor. *Lab on a Chip*, 6(7):906–913, 2006.



# **A Matlab code of the arsenite transport effect model**

```

1 %%%%%%%%%%%%%%%%%%%%%%%%%%%%%%%%%%%%%%%%%%%%%%%%%%%%%%%%%%%%%%%%%%%%%%%%%%
2 % SAMPLE CONCENTRATION + FLOW RATE %
3 %%%%%%%%%%%%%%%%%%%%%%%%%%%%%%%%%%%%%%%%%%%%%%%%%%%%%%%%%%%%%%%%%%%%%%%%%%
4
5 C_solution_ugL=10; %ug/L
6 FlowRate_Lh=0.1e-6; %L/h
7
8 %%%%%%%%%%%%%%%%%%%%%%%%%%%%%%%%%%%%%%%%%%%%%%%%%%%%%%%%%%%%%%%%%%%%%%%%%%
9 % CONSTANTS %
10 %%%%%%%%%%%%%%%%%%%%%%%%%%%%%%%%%%%%%%%%%%%%%%%%%%%%%%%%%%%%%%%%%%%%%%%%%%
11
12 %Geometry parameters
13 Slice_size=5e-6; %m
14 Expansion_factor=1.7; %Factor which takes into account the fact that
due to the applied pressure channels expands and cells are squeezed
15
16 %Influx
17 Uptake_per_cell_max=125; %Maximum uptake rate per cell in
molecules/s (Michaelis-Menten)
18 Km_in=27e6; %3 %Arsenic concentration in molecules/slice at which the
uptake rate is half the maximum (Michaelis-Menten)
19
20 %ArsR and ArsB production rate in 1/s
21 Ratio_pc=10; %Ratio between the number of plasmids DNA and the
chromosomal DNA
22 Production=1/60; %Production rate in 1/s
23 Production_factor=10; %Takes into account the intrinsic difference in
production rate between ArsR and ArsB
24 ArsR_rate=Production*Production_factor;
25 ArsB_rate=Production;
26 ArsB_max=1e3; %Maximum number of ArsB molecules per cell
27
28 %Efflux
29 Out_max=10; %Maximum efflux rate per cell in molecules/s (Michaelis-
Menten)
30 Km_out=5e6; %Arsenic concentration at which the efflux rate is half
the maximum in molecules/cell (Michaelis-Menten)
31
32 %Times
33 Transitory=2; %Transitory period in s during which there is no
productio of EGFP molecules (the arsenite defense mechanism takes time to
be put in place)
34 Time_end=200*60; %Experiment time in s
35
36 %Flow and concentration in channel and slices
37 Na=6.022e23; %Avogadro number
38 Cell_length=2e-6; %m
39 Cell_d=1e-6; %m
40 pi=3; %Pi
41 Cell_volume_m3=(Cell_d/2)^2*pi*Cell_length; %m^3
42 Cell_volume_dm3=Cell_volume_m3*1000; %dm^3
43 Mw=78e6; %ug/mol
44 C_solution_molL=C_solution_ugL/Mw; %mol/L
45 C_solution_molecules_L=C_solution_molL*Na; %molecules/L
46 FlowRate_m3s=FlowRate_Lh/(1000*3600); %m^3/s
47 FlowRate_molecules_h=C_solution_molecules_L*FlowRate_Lh; %molecules/h
48 FlowRate_molecules_s=FlowRate_molecules_h/3600; %molecules/s
49 Cavity_length=250e-6; %m
50 Cavity_width=100e-6*Expansion_factor; %m
51 Cavity_height=20e-6*Expansion_factor; %m
52 Slice_volume_m3=Slice_size*Cavity_height*Cavity_width; %m^3
53 Slice_volume_dm3=Slice_volume_m3*1000; %dm^3
54 Slice_nb=floor(Cavity_length/Slice_size); %Number of slices
55 Cells_per_slice=floor(Slice_volume_m3/Cell_volume_m3); %Cells per

```

```

slice
56 C0_slice_molecules=C_solution_molecules_L*Slice_volume_dm3; %Number
of arsenic molecules per slice in the first slice
57
58 %Reactions parameters
59 Kd1_uM=8.1818e3; %Dissociation constant As-ArsR in uM
60 Kd2_uM=0.33; %Dissociation constant ArsR-DNA in uM
61 Nb_DNA=Ratio_pc+1; %Number of plasmids DNA per cell
62 Molecules_DNA_per_cell_M=Nb_DNA/(Cell_volume_dm3*Na); %Concentration
of DNA molecules in M
63 Molecules_DNA_per_cell_uM=Molecules_DNA_per_cell_M*1e6; %
Concentration of DNA molecules in uM
64 Cst=Kd2_uM/(Kd1_uM*Molecules_DNA_per_cell_uM); %Kd,2/(Kd,1*[DNA]),
Equation 5.8
65
66 %Background signal
67 bg=20; %Factor which divides the total ArsR and ArsB production to
obtain the background production
68
69 %%%%%%%%%%%%%%%%%%%%%%%%%%%%%%%%%%%%%%%%%%%%%%%%%%%%%%%%%%%%%%%%%%%%%%%%%
70 % VARIABLES INITIALIZATION %
71 %%%%%%%%%%%%%%%%%%%%%%%%%%%%%%%%%%%%%%%%%%%%%%%%%%%%%%%%%%%%%%%%%%%%%%%%%
72
73 x=linspace(0,Cavity_length*1e6, Slice_nb); %x-dimension
74
75 %Variables for arsenic influx
76 C_factor=0; %Factor to take into account the local arsenic
concentration
77 As_flux_in=zeros(Slice_nb,Time_end); %Arsenic flux coming to slice n
at each time step
78 Uptake_per_cell_cont=zeros(Slice_nb,Time_end); %Continuous arsenic
uptake per cell at each time step
79 Uptake_per_cell_dis=zeros(Slice_nb,Time_end); %Discrete arsenic
uptake per cells at each time step
80 Resto_Uptake=zeros(Slice_nb,Time_end); %Continuous-discrete
81 Uptake_per_slice=zeros(Slice_nb,Time_end); %Arsenic uptake in the
slice n at each time step
82
83 %Variables describing the arsenic in the cell
84 As_cell=zeros(Slice_nb,Time_end); %Unbound number of arsenic
molecules per cell
85 As_cell_uM=zeros(Slice_nb,Time_end); %Unbound number of arsenic
molecules per cell in uM
86
87 %Variables for GFP production
88 GFP_prod_cont=zeros(Slice_nb,Time_end); %Continuous number of GFP
molecules produced at each time step
89 GFP_prod_dis=zeros(Slice_nb,Time_end); %Discrete number of GFP
molecules produced at each time step
90 Resto_GFP=zeros(Slice_nb,Time_end); %Continuous-discrete
91 GFP_prod_total=zeros(Slice_nb,1); %Total number of GFP molecules
produced per cell
92 GFP_prod_total_slice=zeros(Slice_nb,Time_end); %Total number of GFP
molecules produced per slice
93
94 %Variables for ArsB production
95 ArsB_prod_cont=zeros(Slice_nb,Time_end); %Continuous number of ArsB
molecules produced at each time step
96 ArsB_prod_dis=zeros(Slice_nb,Time_end); %Discrete number of ArsB
molecules produced at each time step
97 Resto_ArsB=zeros(Slice_nb,Time_end); %Continuous-discrete
98 ArsB_prod_total=zeros(Slice_nb,1); %Total number of molecules of ArsB
produced per cell
99

```

```

100 %Variables for arsenic efflux
101 Exit_per_cell_cont=zeros(Slice_nb,Time_end); %Continuous number of
arsenic molecules exiting the cell at each time step
102 Exit_per_cell_dis=zeros(Slice_nb,Time_end); %Discrete number of
arsenic molecules exiting the cell at each time step
103 Resto_Exit=zeros(Slice_nb,Time_end); %Continuous-dicrete
104 Exit_per_slice=zeros(Slice_nb,Time_end); %Number of arsenic molecules
exiting the slice n
105
106 %Variables for the reactions occurring in the cell
107 RatioUnboundBound=zeros(Slice_nb,Time_end); %Ratio unbound/bound
108 TimeRatio=zeros(Slice_nb,Time_end); %Time unbound/time bound
109 UnBound=zeros(Slice_nb,Time_end); %If unbound is 1
110
111 Test=zeros(Slice_nb,Time_end); %Matrix to verify the value of a
variable
112
113 %%%%%%%%%%%%%%%%%%%%%%%%%%%%%%%%%%%%%%%%%%%%%%%%%%%%%%%%%%%%%%%%%%%%%%%%%
114 % START OF THE SIMULATION %
115 %%%%%%%%%%%%%%%%%%%%%%%%%%%%%%%%%%%%%%%%%%%%%%%%%%%%%%%%%%%%%%%%%%%%%%%%%
116
117 %We work with discrete numbers (floor) but in the next time step with
add
118 %the rest from the previous time step
119
120 for i=1:1:Time_end
121
122     for k=1:1:Slice_nb %Space dimension
123
124         if k==1 %The arsenite flux in the first slice is the flux
given by the syringe pump
125             As_flux_in(k,i)=FlowRate_molecules_s;
126         else %The arsenite flux in the next slices is given by
Equation 5.9
127             As_flux_in(k,i)=As_flux_in(k-1,i)-Uptake_per_slice(k-1,i)+
+Exit_per_slice(k-1,i); %The flux to the next slice is the flux to the
previous slice minus the arsenic it has taken plus the arsenic exited
from it
128
129             if As_flux_in(k,i)<0 %The arsenite flux can not be
negative
130                 As_flux_in(k,i)=0;
131             end
132         end
133
134         C_factor=As_flux_in(k,i)/As_flux_in(1,i); %Ratio between the
reference flux in the first slice and the flux in the actual slice
135         C_slice_molecules=C0_slice_molecules*C_factor; %Arsenite
concentration in molecules/slice
136
137         if i>1 %Only after the first time step there is a rest to add
138             Uptake_per_cell_cont(k,i)=
(Uptake_per_cell_max*C_slice_molecules)/(C_slice_molecules+Km_in)+
+Resto_Uptake(k,i-1); %The uptake follows a Michaelis-Menten Kinetics,
Equation 5.1
139         else
140             Uptake_per_cell_cont(k,i)=
(Uptake_per_cell_max*C_slice_molecules)/(C_slice_molecules+Km_in);
141         end
142
143         Uptake_per_cell_dis(k,i)=floor(Uptake_per_cell_cont(k,i));
144         Resto_Uptake(k,i)=Uptake_per_cell_cont(k,i)-
Uptake_per_cell_dis(k,i);
145         Uptake_per_slice(k,i)=Cells_per_slice*(Uptake_per_cell_dis(k,

```



```

i));
146
147     if i>1 %Only after the first time step there is a previous
number of arsenite molecules to add
148         As_cell(k,i)=Uptake_per_cell_dis(k,i)+As_cell(k,i-1); %
The number of arsenic molecules in the cell is the number of uptaken
arsenic molecules plus the number already present
149     else
150         As_cell(k,i)=Uptake_per_cell_dis(k,i);
151     end
152
153     if i>Transitory %Only after the transitory period the
arsenite defense mechanism is put in place
154
155         %The value of RatioUnboundBound corresponds to the ratio
unbound/bound ArsRd to DNA, Equation 5.8
156         %TimeRatio translates RatioUnboundBound(k,i) in a number
of time steps during which there is ArsR, ArsB and EGFP production and
157         %a number of time steps during which there is no
production.
158         %UnBound indicates wheter there is production (=1) or no
production (=0).
159
160         if (TimeRatio(k,i-1)>0) %If the number of time steps with
production or with no production is not over, TimeRatio is decrease by 1
161             TimeRatio(k,i)=TimeRatio(k,i-1)-1;
162             UnBound(k,i)=UnBound(k,i-1);
163             if (TimeRatio(k,i-1)<=1)&&(RatioUnboundBound(k,i)>0)
164                 Resto_GFP(k,i-1)=0;
165                 Resto_ArsB(k,i-1)=0;
166             end
167         end
168
169         if TimeRatio(k,i)==0 %When the time steps with
production/no production are over we reinitialize RatioUnboundBound and
TimeRatio
170             As_cell_uM(k,i)=1e6*As_cell(k,i)./(
Na*Cell_volume_dm3); %As concentration in uM
171             RatioUnboundBound(k,i)=Cst.*As_cell_uM(k,i); %
Equation 5.8
172             %Test(k,i)=RatioUnboundBound(k,i);
173
174             if (RatioUnboundBound(k,i)>=1) %In this case there is
certain number of steps with production and 1 with no production
175                 UnBound(k,i)=1;
176                 TimeRatio(k,i)=round(RatioUnboundBound(k,i)+1);
177             else if (RatioUnboundBound(k,i)<1)&&(RatioUnboundBound
(k,i)>0) %In this case there is certain number of steps with no
production and 1 with production
178                 UnBound(k,i)=0;
179                 TimeRatio(k,i)=round(1./RatioUnboundBound(k,
i)+1);
180             end
181         end
182
183         if RatioUnboundBound(k,i)==0 %In case there are not
arsenite molecules in the cell
184             TimeRatio(k,i)=0;
185         end
186     end
187
188     if (UnBound(k,i)==1)&&(TimeRatio(k,i)>1) %Production
189         GFP_prod_cont(k,i)=ArsR_rate*Ratio_pc+Resto_GFP(k,i-
1);

```

```

190             ArsB_prod_cont(k,i)=ArsB_rate+Resto_ArsB(k,i-1);
191
192             else if (UnBound(k,i)==1)&&(TimeRatio(k,i)==1) %Step with
no production (background production) because we work with a ratio
193                 GFP_prod_cont(k,i)
=ArsR_rate*Ratio_pc/bg+Resto_GFP(k,i-1);
194                 ArsB_prod_cont(k,i)=ArsB_rate/bg+Resto_ArsB(k,i-
1);
195             end
196         end
197
198         if (UnBound(k,i)==0)&&(TimeRatio(k,i)>1) %No production
(background production)
199             GFP_prod_cont(k,i)=ArsR_rate*Ratio_pc/bg+Resto_GFP(k,
i-1);
200             ArsB_prod_cont(k,i)=ArsB_rate/bg+Resto_ArsB(k,i-1);
201
202             else if (UnBound(k,i)==0)&&(TimeRatio(k,i)==1) %Step with
production because we work with a ratio
203                 GFP_prod_cont(k,i)=ArsR_rate*Ratio_pc+Resto_GFP
(k,i-1);
204                 ArsB_prod_cont(k,i)=ArsB_rate+Resto_ArsB(k,i-1);
205             end
206         end
207
208         if TimeRatio(k,i)==0 %When the are not arsenite
molecules in the cell there is only the background production
209             GFP_prod_cont(k,i)=ArsR_rate*Ratio_pc./bg+Resto_GFP
(k,i-1);
210             ArsB_prod_cont(k,i)=ArsB_rate/bg+Resto_ArsB(k,i-1);
211         end
212
213         GFP_prod_dis(k,i)=floor(GFP_prod_cont(k,i));
214         Resto_GFP(k,i)=GFP_prod_cont(k,i)-GFP_prod_dis(k,i);
215         GFP_prod_total(k)=GFP_prod_total(k)+GFP_prod_dis(k,i);
216         GFP_prod_total_slice(k,i)=GFP_prod_total(k).
*Cells_per_slice;
217
218         ArsB_prod_dis(k,i)=floor(ArsB_prod_cont(k,i));
219         Resto_ArsB(k,i)=ArsB_prod_cont(k,i)-ArsB_prod_dis(k,i);
220         ArsB_prod_total(k)=ArsB_prod_total(k)+ArsB_prod_dis(k,i);
221
222         Exit_per_cell_cont(k,i)=ArsB_prod_total(k)/ArsB_max*
(As_cell(k,i)*Out_max)/(As_cell(k,i)+(Km_out))+Resto_Exit(k,i-1); %
Michaelis-Menten kinetic multiplied by the ArsB ratio, Equation 5.3
223         Exit_per_cell_dis(k,i)=floor(Exit_per_cell_cont(k,i));
224         Resto_Exit(k,i)=Exit_per_cell_cont(k,i)-Exit_per_cell_dis
(k,i);
225
226         As_cell(k,i)=As_cell(k,i)-Exit_per_cell_dis(k,i);
227         Exit_per_slice(k,i)=Exit_per_cell_dis(k,i).
*Cells_per_slice;
228
229     end
230 end
231 end
232
233 %%%%%%%%%%%
234 % GRAPHS %
235 %%%%%%%%%%%
236
237 hold on;
238 plot(x,GFP_prod_total_slice(:,200*60), '-o b',x,GFP_prod_total_slice
(:,180*60), '-x b',x,GFP_prod_total_slice(:,160*60), '-* b',x,

```

```

GFP_prod_total_slice(:,140*60), 'o b',x,GFP_prod_total_slice(:,120*60),k
'x b',x,GFP_prod_total_slice(:,100*60), '* b',x,GFP_prod_total_slice(:,k
80*60), '- b');
239 grid on;
240 l=legend('10ug/L 200min','10ug/L 180min','10ug/L 160min','10ug/Lk
140min','10ug/L 120min','10ug/L 100min','10ug/L 80min');
241 title('0.5uL/h');
242 xlabel('distance (um)');
243 ylabel('EGFP per slice');
244
245 % hold on;
246 % plot(x,GFP_prod_total_slice(:,200*60),'r');
247 % grid on;
248 % l=legend('50ug/L 200min');
249 % title('0.5uL/h');
250 % xlabel('distance (um)');
251 % ylabel('EGFP per slice');

```



## **B Curriculum Vitae**

**Nina Buffi**  
Route de Genève 64C  
1028 Préverenges (VD)  
Switzerland



Single  
02.04.1985  
E-mail: [nina.buffi@gmail.com](mailto:nina.buffi@gmail.com)  
Mobile phone: +41 79 673 83 64

## Objectives

Never stop challenging my mind and make a difference in the world.

## Interests

BioMEMS, lab-on-a-chip devices, impact of technologies on society.

## Education

- **Swiss Federal Institute of Technology (EPFL)** Lausanne, Switzerland  
*Ph.D. in Microsystems and Microelectronics*  
– Development of an arsenic whole-cell living biosensor  
*May 2009 - April 2013*
- **University of British Columbia (UBC)** Vancouver, Canada  
*Master Thesis*  
*Sept. 2008 - Mar. 2009*
- **Swiss Federal Institute of Technology (EPFL)** Lausanne, Switzerland  
*Master, Microengineering*  
– Specialization in Biomedical Technologies  
*Sept. 2007 - Mar. 2009*
- **Swiss Federal Institute of Technology (EPFL)** Lausanne, Switzerland  
*Bachelor, Microengineering*  
*Oct. 2004 - July 2007*
- **Liceo Cantonale di Bellinzona** Bellinzona, Switzerland  
*High school diploma, option Latin and ancient Greek*  
*Sept. 2000 - June 2004*

## Work Experiences

- **Doctoral assistant** EPFL, Lausanne  
*Microsystems Laboratory 4 (LMIS 4), Prof. Philippe Renaud*  
*May 2009 - April 2013*  
– Teach practical work sessions “Noise in measurement systems”, correct and grade students reports  
– Supervise Master’s and Bachelor’s students projects
- **Journalist** Perugia, Italy  
*Monthly magazine “Frate Indovino”*  
*Sept. 2011- In progress*  
– Monthly column on the non expected effects of new technologies on society
- **Tennis teacher** Bellinzona, Switzerland  
*Tennis Club Bellinzona*  
*March 2009 - April 2009*

## School Projects

- **On-chip impedance spectroscopy flow cytometry** UBC, Vancouver  
*Microsystems and Nanotechnology group*  
*Sept. 2008 - March. 2009*  
– Development of an on-chip flow cytometer for single cell discrimination based on dielectric spectroscopy

- **DEP sorting and impedance flow cytometry** EPFL, Lausanne  
*Microsystems Laboratory 4 (LMIS 4)* Feb. 2008 - June 2008
  - Sorting and counting of different cells populations using dielectrophoresis (DEP) and impedance spectroscopy
- **Single photon detection under extreme magnetic fields** EPFL, Lausanne  
*Microsystems Laboratory 3 (LMIS 3)* Sept. 2007 - Dec. 2008
  - Influence of static and RF magnetic fields on the detection of single photons using an avalanche photodiode

### Skills

Languages: Italian (mother tongue), French (fluent), English (fluent) and German (basic knowledge)

Microfabrication: Photolithography, soft lithography, lab-on-a-chip fabrication, thin film deposition, dry etching

Applied physics: Microfluidics, dielectrophoresis

Softwares: Matlab, ImageJ, Metaview, Comsol, Illustrator, Clewin, Solidworks, Latex, Office

Programming: C/C++, Assembler

### Sports & Hobbies

Tennis (ex number 24 in Switzerland, trainer certificate), ski (trainer certificate)

Writing, traveling, reading, cinema, pianoforte

### Publications

- D. Merulla, N. Buffi, S. Beggah, F. Truffer, M. Geiser, Ph. Renaud and J. R. van der Meer, *Bioreporters and biosensors for arsenic detection. Biotechnological solutions for a world-wide pollution problem*, Current Opinion in Biotechnology, vol. 24, 2012.
- N. Buffi, D. Merulla, J. Beutier, F. Barbaud, S. Beggah, Ph. Renaud and J. R. van der Meer, *Miniaturized bacterial biosensor system for arsenic detection holds great promise for making integrated measurement device*, Bioengineered Bugs, vol. 2, num. 5, p. 296-298, 2011.
- N. Buffi, D. Merulla, J. Beutier, F. Barbaud, S. Beggah, Ph. Renaud and J. R. van der Meer, *Development of a microfluidics biosensor for agarose-bead immobilized Escherichia coli bioreporter cells for arsenite detection in aqueous samples*, Lab on a Chip, vol. 11, num. 14, p. 2369-2377, 2011.
- G. Mernier, N. Piacentini, R. Tornay, N. Buffi and Ph. Renaud, *Cell viability assessment by flow cytometry using yeast as cell model*, Sensors and Actuators B: Chemical, vol. 154, num. 2, p. 160-163, 2011.

### Conferences and Proceedings

- N. Buffi, D. Merulla, F. Barbaud, S. Beggah, Ph. Renaud and J. R. van der Meer, *Development of a bacterial biosensor for arsenic detection*, the 14th Annual European Conference on Micro&Nanoscale Technologies for the Biosciences, NanoBioTech, Montreux, Switzerland, 2010.
- D. Merulla, N. Buffi, H. van Lintel, Ph. Renaud and J. R. van der Meer, *Development of a bacterial biosensor for arsenite detection*, 14th International Biotechnology Symposium and Exhibition (IBS-2008), Rimini, Italy, 2010.
- G. Mernier, N. Piacentini, R. Tornay, N. Buffi and Ph. Renaud, *Electrical sorting and counting of yeast cells for viability studies*, the 13th Annual European Conference on Micro&Nanoscale Technologies for the Biosciences, NanoBioTech, Montreux, Switzerland, 2009.
- G. Mernier, N. Piacentini, R. Tornay, N. Buffi and Ph. Renaud, *Label-free sorting and counting of yeast cells for viability studies.*, Eurosensors XXIII conference, Lausanne, Switzerland, 2009.